UNIVERSITY OF BIRMINGHAM

Experimental rubber friction modelling and its application in tyre finite element analysis

By

Shahriar Parisouz

A thesis submitted to

The University of Birmingham

For the degree of

Doctor of Philosophy

SCHOOL OF MECHANICAL ENGINEERING

THE UNIVERSITY OF BIRMINGHAM

September 2017

Abstract

Modelling tyre behaviour has been a challenge for many years and even after an extensive research it is almost impossible to predict tyre behaviour only by considering the material properties of its components and the conditions of the environment. Rubber non-linear behaviour, as evidenced by its viscoelasticity and hyper-elasticity, makes tyre modelling a very complicated subject. In addition there have been attempts, over a long period of time, to examine rubber friction and understand its behaviour. Numerous experiments have been conducted to develop tyre friction models, yet still there remain numerous questions and gaps in this field. Therefore, the aim of this research was to develop a model which accurately represents rubber frictional behaviour under different contact pressures and sliding velocities. Since it is difficult to control and measure temperature in the experiments, it was not considered herein, however it is important to note that it considerably affects friction result.

Various experimental facilities have been developed to measure and model rubber and tyre friction and each one has its own benefits and disadvantages. In this research two experimental facilities – pin on disc and rotational pin on disc, have been designed and manufactured to measure rubber friction. The test beds were capable of covering different parameters which affect rubber frictional behaviour. All of the experiments for this study were carried out using one of the facilities. This test rig (rotational pin on disc) was calibrated and a code for processing the data was developed. Various series of tests have been conducted on different surfaces - steel discs to show rubber friction on smooth surfaces and sandpapers to show the results involving asperities. A friction model dependent on major parameters of the system (i.e. velocity and contact pressure) was generated.

Finite Element Analysis (FEA) is one of the most common methods used in tyre simulations, and in this kind of modelling, constant friction coefficient (i.e. Coulomb's law) is normally

used but it is well known that this can lead to inaccuracies. It is expected that better accuracy of tyre behaviour under dynamic conditions can be modelled by importing the rubber friction model obtained from the experiments into a commercial FEA package ABAQUS.

Experimentally obtained friction values were used to model a tyre and simulate cornering. A 3D tyre model was developed and the friction coefficients were employed in three models: rubber/steel, sandpaper grit 120 and sandpaper grit 400. The tyre was modelled in free rolling and then in steering. The forces in cornering were evaluated and the effect of the friction coefficients was assessed. It was shown that with constant friction coefficient, cornering stiffness increases with increasing normal load. However, in the proposed friction models cornering stiffness increases with normal load up to a peak, after which it starts to decrease. This is in accordance with experimental evidence. In conclusion, considering the results of cornering stiffness, it is suggested to use the generated friction models when a tyre is simulated in FEA.

Acknowledgments

Firstly I would like to express my appreciation to my supervisor Dr. O. A. Olatunbosun for all of his help and support. I witnessed during my studies he treated all of his students like a family member and words cannot describe how to acknowledge all the things he has done for me. He always helped me with patience and wanted me to improve in my life and studies. I know all his concern was to help me and guide me better in my studies and I sincerely appreciate all he did.

I would like to send my gratitude to my co-supervisor Dr. M. Saadat for his support especially during the period that I could not see any achievements and could not find a way to go forward, he motivated me to finish my research and I am very thankful to him. Also I like to appreciate Dr. K. D. Dearn for all of his supports and guidance during my project, I was always welcome to go to him and ask for help and I had his unconditional supports. Moreover I would like to thank Dr. R. Hood for his support and advices.

I would like to say thanks to University Of Birmingham for this opportunity, especially the staff in mechanical engineering and mostly to the technicians: Mr. C. Hingley, P. Thonrton, L. Gauntlett and J. Garrod.

I would like to extend my gratitude to my colleagues Mohammad Behroozi, Samaneh Arabi, Adebola Ougunoiki, Ammar Kubba, Hamad Aldhuafiri, Chongfeng Wei and Abdul-waheed Adnan.

Also I would like to say thanks to all of my friends who helped me during my studies: Jelena Sostare, Aydin Sabouri, Maria Del Carmen Bogarra Macias, Salman Saeidlou, Jose Martin Herreros Arellano, Isaline Lefort, Carolina Eleonora Lavecchia, Seyed Arash Nassirpour Oskouei, Chongming Wang, Omid Doustdar, Nasim Mahmoudi, Alessandro Abena and

Catalin Pruncu. I would like to especially gratitude one of my friends who supported me in the most difficult time of my studies Kiyarash Rahbar, it was not possible to carry on without his support and I always thank him for this.

Finally I like to give my appreciation to my parents for their supports and helps, it is very difficult to gratitude what they have done and I hope to compensate it one day.

Table of Contents

1. Introduction

This chapter features a brief description of the study that has been carried out. In the first part of this section the background and importance of the research is explained and in the second part, thesis structure is described.

1.1. Background and motivation

Tyre: "A thick rubber ring often filled with air that is fitted around the outer edge of the wheel of a vehicle, allowing the vehicle to stick to the road surface and to travel over the ground more easily" [1].

The above-mentioned sentence, quoted from Cambridge dictionary, is an excellent example that expresses the significance of tyres. The tyre is one of the most important parts of a vehicle that tolerates all the forces and gives the vehicle transportation ability. All the contact that the tyre makes with the pavement is almost equal to a shoe size of normal human being, although this ratio is not same for their weights.

It is important to note that more than half of the transportations in the world are conducted via vehicles that move on rubber tyres, therefore tyre behaviour plays a significant role in vehicle dynamics [2]. Improving vehicle quality is one of the greatest challenges for engineers and in order to succeed it is necessary to provide more accurate vehicle simulations. Since tyres are amongst the most important parts of a vehicle, tyre modelling plays a crucial role in this process. There are three different ways to model a tyre: analytical, numerical and empirical. All these models have been used to predict tyre behaviour although each of them has their own deficiencies. Furthermore, none of approaches modelled friction realistically.

The current research encompasses two fields: tribology and vehicle dynamics; the first part describes the frictional behaviour of rubber and the second part characterizes the effect of friction on tyre and vehicle.

Tribology is defined as a study of surfaces in motion and it focuses on friction, wear and lubrication. The term “tribology”, is relatively new and it was introduced by a British physicist and engineer D. Tabor [3]. In science though this field is not novel, it has been known from the old times; some wall drawings from ancient Egypt show that a lubricant (most likely water or vegetable oil) was used to simplify the transportation of a statue(Figure 1-1; [4]).

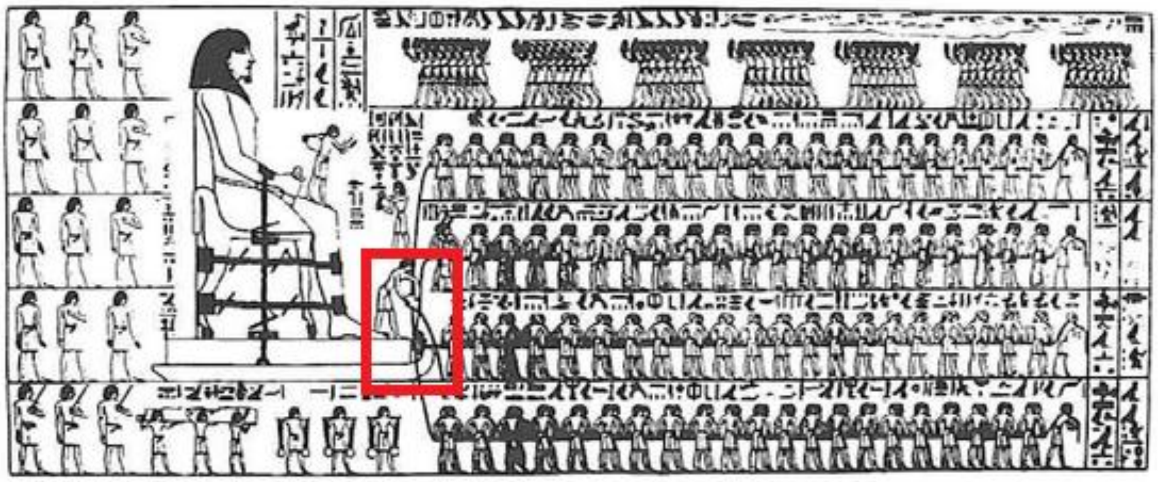

Figure 1-1 Probably one of the first tribologist of history, adding a lubricant to smooth transportation of statute of Ti [4]

The movement of a tyre starts with sticking of the tyre to the road and the reason for the movement is friction. Friction is defined as the resistance to motion whether it is sliding or rolling. The most well-known formula, which describes this phenomenon, is Amontons-Coulomb’s law, which predicts that friction is equal to the division of the tangential force by normal force and it is called the friction coefficient. It is important to note that friction coefficient is not a material property, it is a property of the system [5]; different circumstances in a condition provide different friction coefficients. Apart from Coulomb’s law there are other friction theories such as Lugre, Dahl, switching, etc., which cover more effective system parameters in their formulas [6].

Rubber, which is the main component of the tyre, is an elastomer. This material does not follow the most well-known friction model i.e. Coulomb's law, since there are different parameters that affect the friction coefficient than the ones considered in Coulomb's law. In this research the attempts to model rubber friction and tyre frictions are discussed in detail. Researchers have tried to apply different general friction models to rubber (example [7]), use experimental results (example [8]) or provide new formulas (example [9]) to model rubber frictional behaviour, but all of them have some shortcomings that will be discussed in detail.

1.2. Objectives and scope

The aim of the current study is to develop a friction model for rubber, dependant on different parameters (i.e. contact pressure and slip) and then apply it on a tyre to improve the prediction in vehicle simulation.

For this purpose an experimental device has been designed to measure rubber friction force, the calculation for this rig has been based on normal force on a tyre. This rig was designed considering other experimental facilities; it is capable to measure friction for the materials, in which relative motion is an effective parameters. There are other frictional rigs that measure friction and slip (the most famous one is known as LAT 100 or Grosch's abrader rig), but they require test specimens in shapes of rings or similar geometries to a tyre. The designed rig tests rubber samples extracted from a tyre tread and measures slip in different speed ranges (low speed or high speed) by considering the effect of the contact pressure. Several experiments were conducted against surfaces with different roughness, measuring friction force dependant on speed and contact pressure.

The outputs of this rig have been processed and friction function was obtained and a friction model based on these results was developed.

A series of results were imported as a look up table into FEA package (i.e. ABAQUS) and it was applied in tyre modelling. Tyre behaviour in cornering was simulated and the FEA results between the experimental friction models and constant friction coefficients were compared. In this diagram the importance of the friction modelling in vehicle simulations is illustrated.

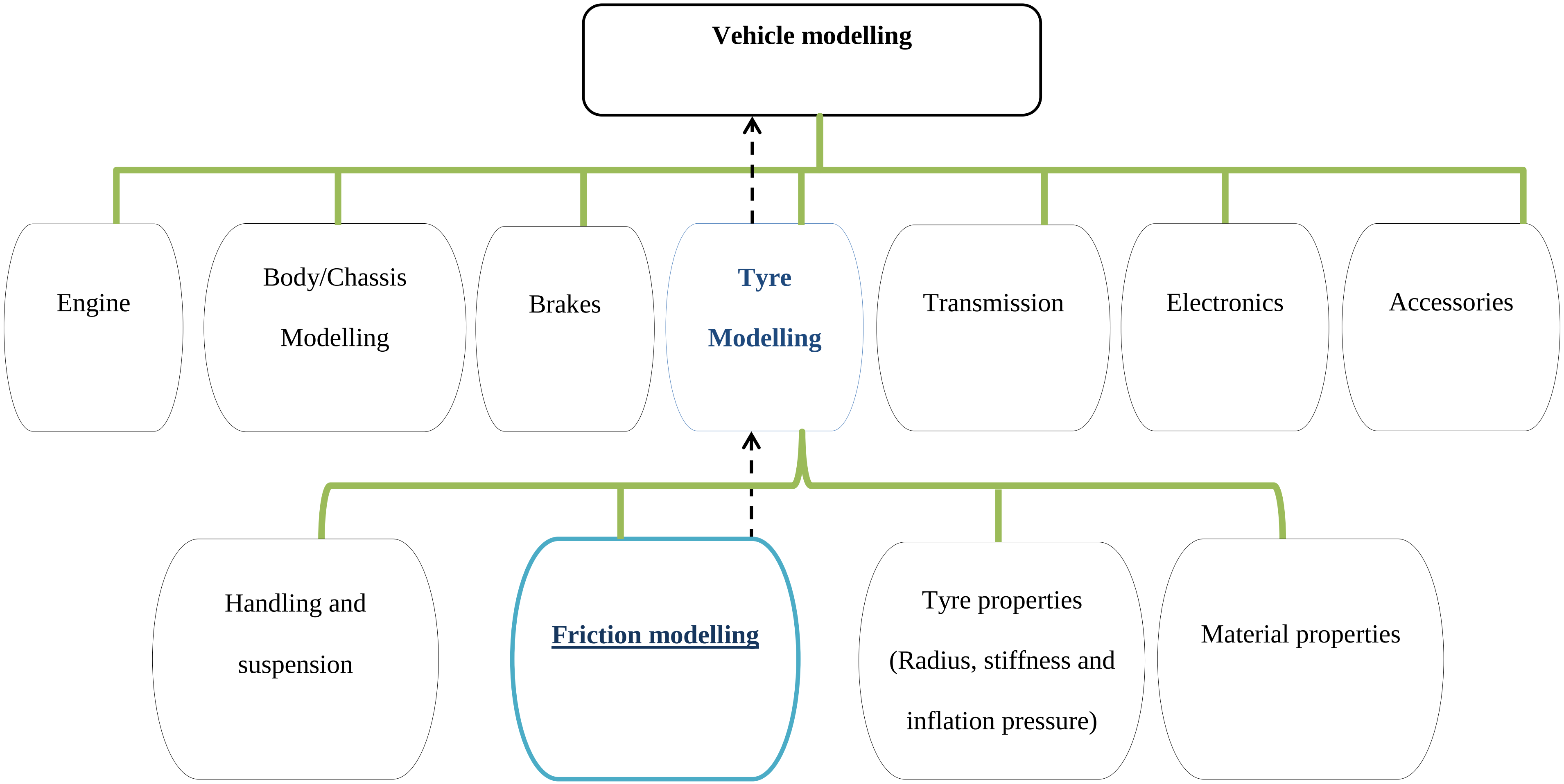

Figure 1-2 A diagram to show rubber friction modelling effect on vehicle modelling

1.3.Thesis outline

In this chapter the background and the aim of the project was established, the problem was briefly explained and the method for the solution was discussed.

In Chapter 2, the previous researches on rubber/tyre friction modelling are reviewed. Initially the early studies that investigated rubber friction dependence on different parameters are discussed in detail, and then tests on dry and lubricated surfaces are reviewed. The friction models for rubber friction are explained and their advantages and disadvantages are compared. Similar to rubber friction, the friction models for tyre are mentioned and discussed. For both rubber and tyre friction modelling a case study is described. These studies applied the friction models in daily application and the results were reviewed.

Chapter 3 features the description of the experimental facility. The background of the tribometers is shown and the development of the current facility is justified. In addition, the design of the tribometer is presented and calculations for requirements are elucidated. Finally, the calibration of the rig is shown and the initial steps for conducting a test are explained.

In chapter 4 the experimental methodology is fully described, all the conditions in which tests has been carried out are explained and an example for each of the test are demonstrated. The initial results are briefly described and the result post processing was shown.

In chapter 5 the experimental results are discussed and the trend in the variation is explained. Results are compared and a friction model with linear regression is provided, this model shows rubber friction dependency on contact pressure and normal load.

In chapter 6, the a FEA model for a tyre is developed and the obtained friction coefficients are applied on a tyre, a brief description of tyre FEA modelling was shown and the results from these simulations are compared with tyre simulations of constant friction coefficient.

In chapter 7 the conclusion and the future work of the research is explained and described. All the outcomes from different stages of the study are explained and the gaps, which can be addressed in further studies, are briefly described

2. Literature survey

2.1. Introduction

Friction is a subject of considerable importance on a day-to-day basis, and its sufficiency or deficiency has a noticeable influence on human life. A phenomenon that affects everyday activities, it has been under investigations since the old times. Such phenomena exist in various aspects of life from taking steps to more complicated phenomena like designing load transmissions. Generally, friction is defined as the resistance to sliding or rolling of an object. Optimising the friction could reduce fuel consumption considerably as well as economical saving, which are known as main engineering concerns. It is obvious friction deficiency or sufficiency between two surfaces leads into a waste of power and cause problems in any system [10].

In this chapter the general definition of friction is reviewed, then the application of this definition to the behaviour of elastomers, especially rubber is described in detail. In addition, the theories about rubber friction and various methods of measuring it are discussed. Since the ultimate application of this research is concentrated on tyre modelling, the implementation of rubber friction theories in tyre modelling is comprehensively investigated.

2.2. Friction overview

Friction in general is defined as the resistance to motion, as it is shown in Figure 2-1. It is evident from this figure that, for a solid body with weight of "W" moving towards a direction (right in Figure 2-1) whether sliding or rolling, there always exist a resistance force opposite to the motion direction (left in Figure 2-1) proportional to the normal weight which is known as the friction force. Figure 2-1 details the definition of such force in a free body diagram for sliding and rolling.

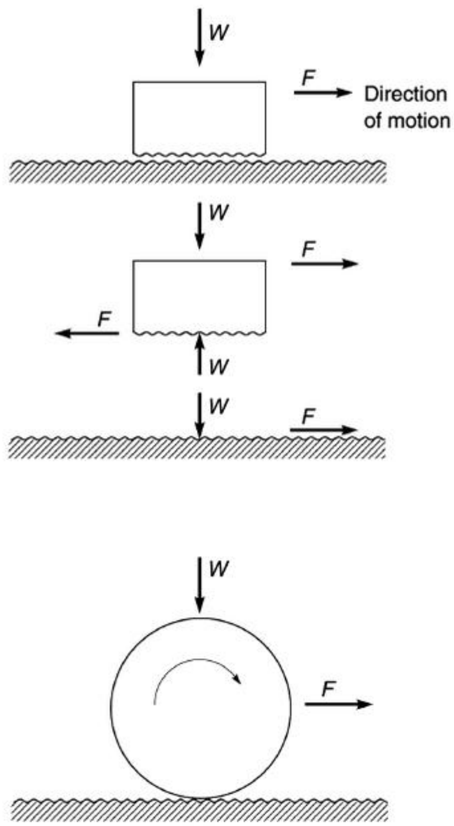

Figure 2-1 Friction is resistance to motion for sliding and rolling, in this figure an object is shown in both sliding and rolling and in the picture in the middle the free body diagram is demonstrated [11]

2.2.1. Coulomb friction

Da Vinci, Amontons and "Coulomb" were the pioneers of research on friction [12]. The preliminary laws of friction were defined by Amontons as follows [12]:

I. The frictional force is directly proportional to the applied normal load

II. The frictional force is independent of the apparent area of contact

Following Atonmons, Coulomb is well known for defining a mathematical formula for friction including the friction coefficient as well as expanding the "Amontons" statements with two additional laws which are shown as below:

III. Static friction coefficient is greater than kinetic friction coefficient

IV. Friction coefficient is independent of the sliding velocity

According to "Coulomb", the formulas for friction coefficient are defined as follows:

$$\mu_s = F_s/W \quad \text{Equation 2-1}$$

$$\mu_k = F_k/W \quad \text{Equation 2-2}$$

Where μ_s and μ_k are the friction coefficient for static and kinetic phases respectively while F_s and F_k are the frictional force in static and kinetic conditions correspondingly and W is the normal load.

Later experiments exhibited discrepancies that violated the "Coulomb" friction statements [12]. For example, Figure 2-2 shows that there could be variation in kinetic friction coefficient (μ_k) with increasing the sliding velocity (v). In this figure, it was shown that friction coefficient has changed against sliding velocity for different operating conditions. It has been seen for some materials that there is no significant difference in static and kinetic friction coefficients (Figure 2-2 (a)). Although it is common to expect that friction coefficient is less in kinetic phase than the static one (Figure 2-2 (b)), it was shown that in some case this rule was not observed (Figure 2-2 (c)). Moreover, the kinetic friction coefficient can have a fluctuating behaviour as it is depicted in

Figure 2-2 (d) in presence of a viscous lubricant. Consequently, only the first Amontons statement (I) as well as Equation 2-1 and Equation 2-2 from “Coulomb” were accepted by the researchers as will be discussed in the following sections.

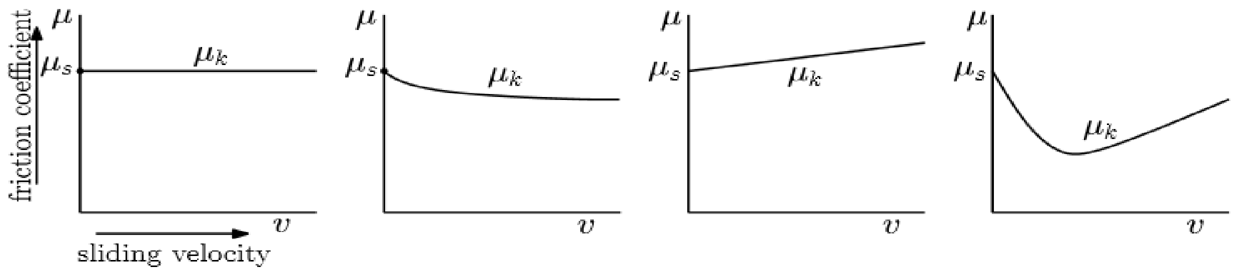

Figure 2-2 Friction vs. sliding velocity [13]

2.2.2. Elastomers friction

In 1929 it was discovered that classical laws of friction do not apply to all materials [14]. Later it was found that the second law of friction (statement II) is only applicable to the materials that have definite yield strength. Afterwards, Moore et al. [12] concluded that the third law of friction (statement III) is not valid for elastomer materials and the forth law (statement IV) is not valid for any type materials.

Sliding velocity and load dependency of friction coefficient was considered by many researchers like Roth, Thirion, and Deny and many results have been obtained [15].

Roth, Driscoll and Holt [15] were the first researchers who reported experiments on elastomer friction and their findings were the basis for future tests and investigations. Their experiments are divided into two parts because they were done with two years gap period, the first part was a general investigation and in a large variety of conditions and the second part was about more specific areas. In the experiments three rubber discs were tested against glass with different degrees of roughness. They found out that rubber friction coefficient increases with sliding velocity and surface smoothness and on the other hand it decreases with load variations, surface roughness and use of lubricants, also it should be mentioned that it was not possible to measure friction coefficient at high speed because of vibration. Eventually it was mentioned that friction coefficient is independent of size of the specimen.

Denny [16] made large-scale investigation on nine different kinds of rubber, and his research was focused on the effect of contact pressure on adhesion, these experiments involved dynamic tests and wet surfaces. The Contact areas were varying between 0.08-100 cm^2 and the maximum load was 50 Kg.

Following such studies it was reported that for lubricated elastomer (rubber-like) material the following conclusions can be drawn:

- Coefficient of sliding friction decreased with increasing contact pressure, and the slope for this decrease is more effective for rough surfaces.
- Surface roughness makes various changes in friction coefficient, the asperities affect the wear and the adhesion and it causes changes in the friction coefficient.

2.2.3. Rubber friction

Rubber is latex from a tree called "*Hevea brasiliensis*" which native Indians in America used to make playing balls [17]. This material is categorised as an elastomer and its properties were surprising for people as in bouncing ball. Day by day this material is utilised in industry for different types of products such as O-rings, wiper-blades, seals and tyres and its benefits and applications could not be denied [17].

2.2.3.1. *Rubber friction theories*

The Coloumb's laws of friction (Equation 2-1 and Equation 2-2) are not applicable to rubber-like materials due to their low elastic modulus and the high internal friction. There are different parameters that affect the rubber friction force such as adhesion, viscosity and cohesion as shown by Equation 2-3 [18].

$$F = F_{Adhesion} + F_{Hystersis} + F_{Viscous} + F_{cohesion} \quad \text{Equation 2-3}$$

Where $F_{Adhesion}$ is from adhesion kinetics and the intermolecular bond between rubber and the contact surface. $F_{Hystersis}$ also known as $F_{Deformation}$ is the friction caused by the deformation of the rubber specimen. When a layer of lubricant is added to the contact of rubber and the surface, the effect of $F_{Viscous}$ becomes apparent which is due to the existence of shear of rubber with the lubricant. This layer should be sufficient that it does not allow direct contact between rubber and the interface. $F_{cohesion}$, which also known as F_{Wear} is the energy loss of the small particles that has been detached from the rubber. Apart from these parameters, there are other factors that affect the rubber friction which are listed in Table 2-1 [10].

Table 2-1 Affective categories in rubber friction [10]

	Category	Factor
1	Material properties	Stiffness and elasticity
2	Contact geometry	Contact area; apparent or real
3	Surface asperity	Shapes and varieties of the roughness
4	Relative motion	Velocity, acceleration
5	Applied forces	Contact pressure and changes in the forces
6	Temperature	Effects on material properties
7	Lubrication	Film thickness, and effects on the motion
8	Stiffness and vibrations	Stick-slip, Schallamach waves
9	Wear	Abrasion

For example, material properties significantly influence stiffness and elasticity of the system whether, when there is relative motion, velocity and acceleration should be considered. Furthermore, when surfaces with different textures are in contact, shapes and roughness should be taken into account.

Overall, it can be concluded that, rubber-like materials have complicated behaviour that cannot be explained by simple Coloumb law. Accordingly, for such material more complex formulation that includes the aforementioned parameters is required as will be explained in the following sections.

2.2.3.1.1. *Dry rubber friction*

As it was mentioned earlier, many factors like surface asperities and adhesion are effective on rubber friction; therefore testing this material in systems where there is dry contact between surfaces is necessary to highlight the effect of parameters listed in Table 2-1.

Grosch has done various tests on natural rubber against smooth and coarse surfaces in dry condition [19]; the obtained result was a master curve which is presented in Figure 2-3. The experiments were conducted at a range of different operating conditions (i.e. temperature and sliding speed) against three kinds of surfaces such as silicon carbide, smooth surface and glass. The master curve was achieved by transforming all the data using Williams-Landel-Ferry (WLF) equation [20] into a single curve. WLF transform enables shifting a curve for different temperatures using Equation 2-4.

$$\text{Log aT } = \frac{-8.86(T - Ts)}{T - Ts + 101.6} \qquad \textbf{Equation 2-4}$$

Where T (^oC) is the temperature that rubber is in use, T_s (^oC) is the reference temperature, which is also known as 50 ^oC more than T_g (where T_g is the glass transition temperature), a_T presents a shift factor to overlap different curves [20].

Figure 2-3 shows that with increasing sliding velocity, friction coefficient increases and after reaching a peak point it starts to decrease. It should be mentioned that each surface has its own master curve and different surfaces demonstrate different behaviours. It was concluded that rubber friction occurs because of two reasons; adhesion of the surface and rubber deformation, as it is demonstrated by Equation 2-5[19].

Equation 2-5

$$F = F_{Adhesion} + \mathrm{F_{Hystersis}}$$

This was a basic idea for many years and many subsequent researchers made attempts to characterise rubber friction based on this idea, though during the next decades, the idea was changed.

It is worth mentioning that it was revealed in a private conversation [21] that Grosch, used abraded rubber to avoid the heavy stick-slip motion. This is why other researchers did not obtain this curve and therefore achieved different results.

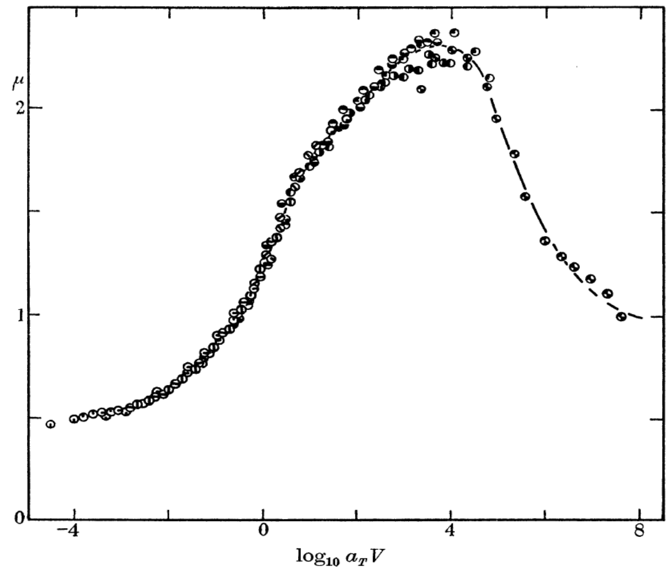

Figure 2-3 Grosch master curve for glass [19]

In this research, it was found that the velocity of the maximum friction (V_s) increases as the glass-transition temperature decreases. It was explained where the frequencies at which the loss modulus (E'') and the loss factor ($\tan \emptyset$) have similar manner in their maximums. It was discovered, the velocities of maximum friction agree with the maximum of $\tan \emptyset$, therefore a formula was derived to show the relation between the maximum friction velocity over the maximum loss frequency ($f_{E''}$, which loss modulus is maximum) is equal to constant value, this formula is shown in equation Equation 2-6:

$$\frac{V_s}{f_{E''}} = \lambda = 6 \times 10^{-7} \text{ cm}$$ Equation 2-6

Generally, dry rubber friction studies are divided into two categories: molecular and macroscopic [22]. In molecular theories, the basic assumption is that bonds form on the contact patch during sliding, get strained and then break. Despite several definitions, it was commonly agreed that in macroscopic theories, small bonds that are formed contain some energy and this energy absorbed by the material forms a new bond when the previous one is broken.

Schallamach [23] investigated the dry rubber friction based Grosch master curve (Figure 2-3) using molecular approach. It was reported that by increasing the speed, the strength in the bond between rubber and the contact patch was increased. However it led to a reduction in number of bonds.

Bartenev [24] explained rubber as a viscous flow liquid; he shows that friction increases when the speed is increased, but on the other side the area of contact has significantly decreased. It was stated that the cause of friction is molecular adhesion due to forces acting on the actual contact area. These results were obtained from testing rubber against hard smooth surfaces (Polished steel) for different normal pressures varying from 1 to 200 kg/cm^2. It was mentioned that for the small load regions, Coulomb's law is still valid and another friction theory that is known as Thirion's model (which will be explained and discussed in section 2.3.2) is valid for larger loads.

Savkoor [25] investigated the dry rubber friction using macroscopic approach, it was assumed rubber adhered to surface with domains, that each domain has a number of bonds. Each bond could sustain a small force, which he assumed to be a shear force that is equal to breakage of a bond and producing of another bond, this adhesion was considered as a time-dependent process and dependency of rubber on visco-elastic properties were discussed.

Bulgin, Hubbard and Walters [26] expressed that when rubber is adhered to the slide track, it would get elongated and when it detaches from the surface, some of the energy returns back to the rubber sample and the energy loss depends on the rubber hardness.

Ludema and Tabor [27] believed that the bond between rubber and the contact surface is so strong that when they get separated a very thin layer of rubber around 10nm remains on the surface, although later, it was underlined that it only occurred at high speeds and there was no evidence to prove this theory at low sliding speeds.

Finally, Kummer [22] made a combination of molecular and macroscopic theories and declared that adhesion is caused by electrostatic attraction between the surfaces. It was discussed that adhesion is mostly generated in dry conditions and hysteresis is for when the track is wet, since the pressure is not enough to break the lubricant film. It was mentioned that adhesional term of the friction would decrease with increasing with load, while the hysteresis part would increase. This theory is a very important idea which was used by researchers because of its completeness to expand their new ideas.

One of the most important characteristic of dry friction phenomenon that was addressed by Schallamach is that when rubber slides on a smooth surface because of adhesion, rubber starts to buckle and produces detachment waves which are called “Schallamach waves”. This happens because of low elasticity of rubber and it is mostly obvious when the rubber is sliding on a smooth hard surface [12]. Figure 4 presents the appearance of the Schallamach waves in detail.

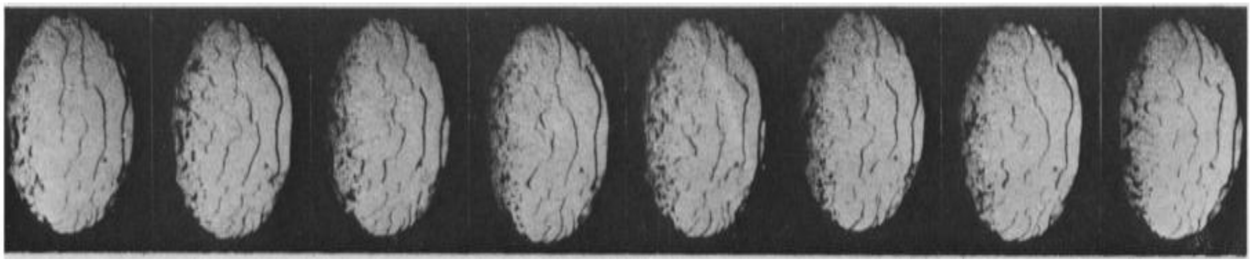

Figure 2-4 Eight frames of sliding rubber against Perspex showing Schallamach waves [23]

Many researches have performed studies to understand Schallamach waves and obtain a better understating of this phenomenon. There are calculations to measure tangential force F and the energy dissipation (r(v)) of the waves, and the formulations are shown in Equation 2-7 and Equation 2-8 [28]:

$$F = \frac{\gamma\omega}{\lambda v} \qquad \text{Equation 2-7}$$

$$\mathrm{r}(v) = \frac{Fv}{nA} \qquad \text{Equation 2-8}$$

Where γ is dependent to the surface energy, ω is the wave velocity, v is the sliding velocity, and λ is the spacing between two gaps, n is number of waves and A is the contact area [29].

2.2.3.1.2. *Lubricated rubber friction*

Lubrication is one of the factors that affect rubber friction, as it was summarised in Table 2-1, the viscosity of the lubricant has direct effect on the system and it is necessary to study lubricated friction together with its indirect effects on the other factors such as surface asperities and adhesion. The following summarizes the main efforts and researches on lubricated rubber friction.

Roth, Drsicoll and Holt [15] were one of the first scientists to use their laboratory for lubricated tests on rubber. Water, Caster oil, wet soap, tale and graphite were used as a lubricant and the experimental equipment was the same as explained in section 2.2.3.1.1. They showed the result is dependent on thickness of the lubricant, sliding speed and contact pressure.

Denny [16] showed that friction for lubricated rubber decreased while increasing the contact pressure and for smooth surfaces had higher rate of variation. Later investigation by Deny showed that if the rubber specimen remains under pressure for a long period of time, the lubricant would run out of the contact patch and the results resembled dry friction.

Greenwood and Tabor [30] made discussions by carrying out experiments about existence of a friction component that only appears between rubber and rough surfaces (especially metallic materials), where relatively large deformations are produced. This component becomes obvious when there is low adhesion and the surfaces are well lubricated. In their research hard spheres and cones were slid on rubber surfaces. It was found that for spheres the sliding friction is almost the same as the rolling friction. The main conclusion was that in conditions that rubber and hard materials are in contact the friction from the deformation is dominant to other effective factors of friction and it would be more significant when the rubber has low Young's modulus.

Denny [31] conducted experiments to show that lubricants like mixture of water and alcohol can reduce the friction; it should be considered that if a surface is hydrophobic or hydrophilic, there would be difference in the result of the experiments. It was shown that increasing the speed and the viscosity of a lubricant decreased the friction coefficient and then after reaching a steady-state and it increased again. Furthermore, high viscosity of a lubricant produced resistance against the specimen and the viscous shear influenced the friction coefficient.

In later studies Moore [32] declared that the elastohydrodynamic force from lubricants to the specimen lifts up the latter, which reduces the adhesion and produces a gap between the surface asperities and the rubber contact area. This feature resulted in decrease of the friction force.

Analogous to “Schallamach waves” described in section 2.3.1.1 for dry conditions, these waves were observed in sliding rubber with a lubricant (i.e. lubricated friction) and are known as “wet Schallamach waves” that the detachment waves were water [33] [34].

Table 2-2 summarizes the theories about dry and lubricated rubber friction as following:

Table 2-2 Rubber friction theories

No.	Author[Ref]	Description
1	Roth, Driscoll and Holt [15]	Made experiments on rubber by sliding against glass in two different rectangular sizes and presented µ versus $F_{N,}$ Total friction force was presented as sum of friction from hysteresis and µ multiplied by normal force. $F_T = F_{Hs} + \mu_A F_N$ Also for contacts with lubrications, it was shown that the friction is dependent on film thickness and viscosity.
2	Thirion [35]	Same experiments as Roth, Driscoll and Holt were carried out for rectangular specimen sliding against glass. There are some contrasts with Their results and it is known because Roth et al experiments covered higher range of pressure (22 K) than Thirions (13 kg)
3	Schallamach [36]	Carried out experiments on three kind of rubber (soft, medium and hard) against glass, the justifications of this research were based on molecular approaches and the effective factors on rubber friction were considered as hysteresis and adhesion (where it was explained as the Van der Waals bond). Also one, a rubber phenomenon known as "Schallamach waves" has been described.
4	Bartenev et al. [24]	Carried out an experiment on soft, medium and hard vulcanized rubber against polish steel in 23 ^{O}C. This study considered rubber in macroscopic approach and described rubber as a viscous flow and explained that by increasing sliding speed; the area of contact would decrease but number of the bonds between rubber and the surface would increase.
5	Savkoor [25]	Explained rubber friction by Macroscopic approach, by assuming the adhesion to a surface with number of domains that each domain has number of bonds, each bond contain a small force that is known as the shear force and this force would sustain in breakage of bond and creation of another one.
6	Bulgin et al. [26]	Explained that the when a bond is broken, the energy return back to the rubber sample and this loss depends on rubber hardness.
7	Ludema et al. [27]	Investigates showed that the bond between rubber and the surface is so strong that when they are separated a thin layer of rubber would remain on the surface, this phenomenon was visible in high speed experiments.
8	Kummer [22]	Combined both molecular and macroscopic theories and explained the adhesion because of electrostatics. Also it was mentioned adhesion is common in dry friction and hysteresis is the cause of friction in wet surfaces.
9	Deny [16] [31]	Conducted experiments for lubricated friction for different contact pressures and it was found that rubber friction under pressure is related to time, since staying under pressure for a long time, provide result similar to dry contact pressure.
10	Greenwood et al. [30]	Tested rubber in different shapes such as spheres and cones against rough surfaces, and consider results for large deformations.
11	Moore et al. [12]	Explained that elastohydrodynamic force from the lubricant lifts the specimen up and reduce the adhesion between rubber the surface.

2.2.3.2. *Experimental studies on rubber friction*

As it was mentioned earlier Coloumb friction law is not applicable on rubber and therefore, experimental study of rubber is vital to investigate its dependency on different parameters (refer to Table 2-1). This section summarizes the most important researches about rubber friction tests and their applications are discussed as well as the theories to replace Coloumb law.

Schallamach [37], defined a new theory for dynamic rubber friction; the basis of such theory is the adhesion of the molecular bond between rubber and track. The Grosch's tests [19] were re-conducted and the developed theory was validated based on such results using Grosch's master curve [19]. It was mentioned that any rubber friction theory should show that WLF transform (Equation 2-4) is applicable on it. It was tried to demonstrate the effect of temperature on the bonding process. Moreover, it was expressed that the static rubber friction may also originate from more bonds, which have been created because of rubber resting on the track. It is easy to observe this feature from the adhesion of rubber to a surface that had been in contact for a long time.

Michel Barquins [38] conducted experiments on rubber-like materials to obtain a better understanding of dry friction and its relation to rolling friction and wear. This study was mainly concerned about monitoring and visualizing the adhesion and kinetics, rolling friction, static friction, friction in low and high sliding speed and wear in the contact area; "Schallamach waves" theory was visible in these experiments (as it is shown in Figure 2-5). For this purpose, different rigid punches (sphere, cylinder, cone, flat-ended cone, flat ended sphere, rounded sphere and rounded cone) were used and each of their effects was shown individually.

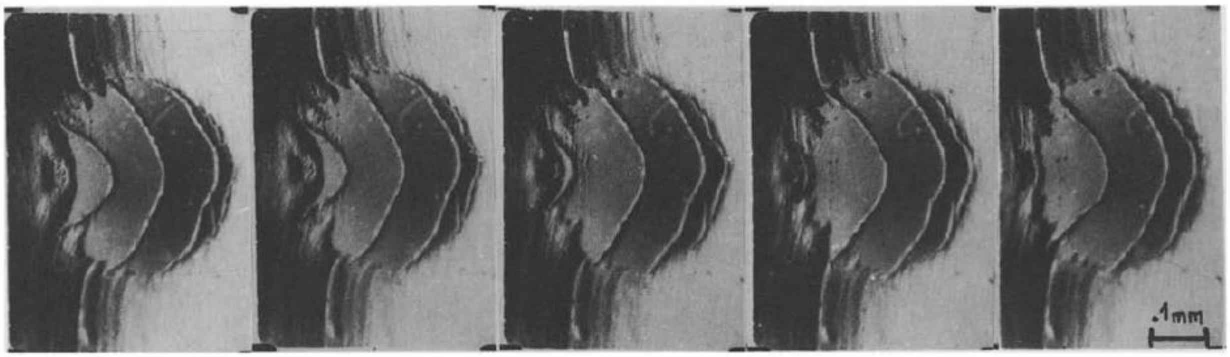

Figure 2-5 Appearance of schallamach waves on sliding a rigid sphere on smooth surface of rubber [23]

In 1975 Briggs and Briscoe [39] performed experiments on rubber against glass surface and recorded the frictional force, velocity and frequency of the waves. In these experiments "Schallamach waves" were observed and they were expressed as key phenomenon which happened when rubber slid on a smooth surface. It was concluded that the main energy loss in sliding of rubber was due to the adhesion, though, the energy loss for peeling of rubber in contact area was also considered.

Persson [40] discussed the effects of an external force on friction, which led to stick and slip. A relationship between drift velocity and the external force was proposed and it was shown that for a large range of sliding velocities the ratio of F_k/F_s was equal to $\frac{1}{2}$. In addition, it was declared that for the ratio of μ_k/μ_s the same value was applicable. F_k and F_s are the frictional forces for kinetic and static conditions and μ_k and μ_s are the friction coefficients.

There exists one interesting feature that was common in all the aforementioned experimental studies (refs [15] to [41]) (all based on rubber sliding) which concluded that by increasing the normal load the friction coefficient decreases and underlined the load dependency of rubber friction. Figure 2-6 demonstrates the summary of the results.

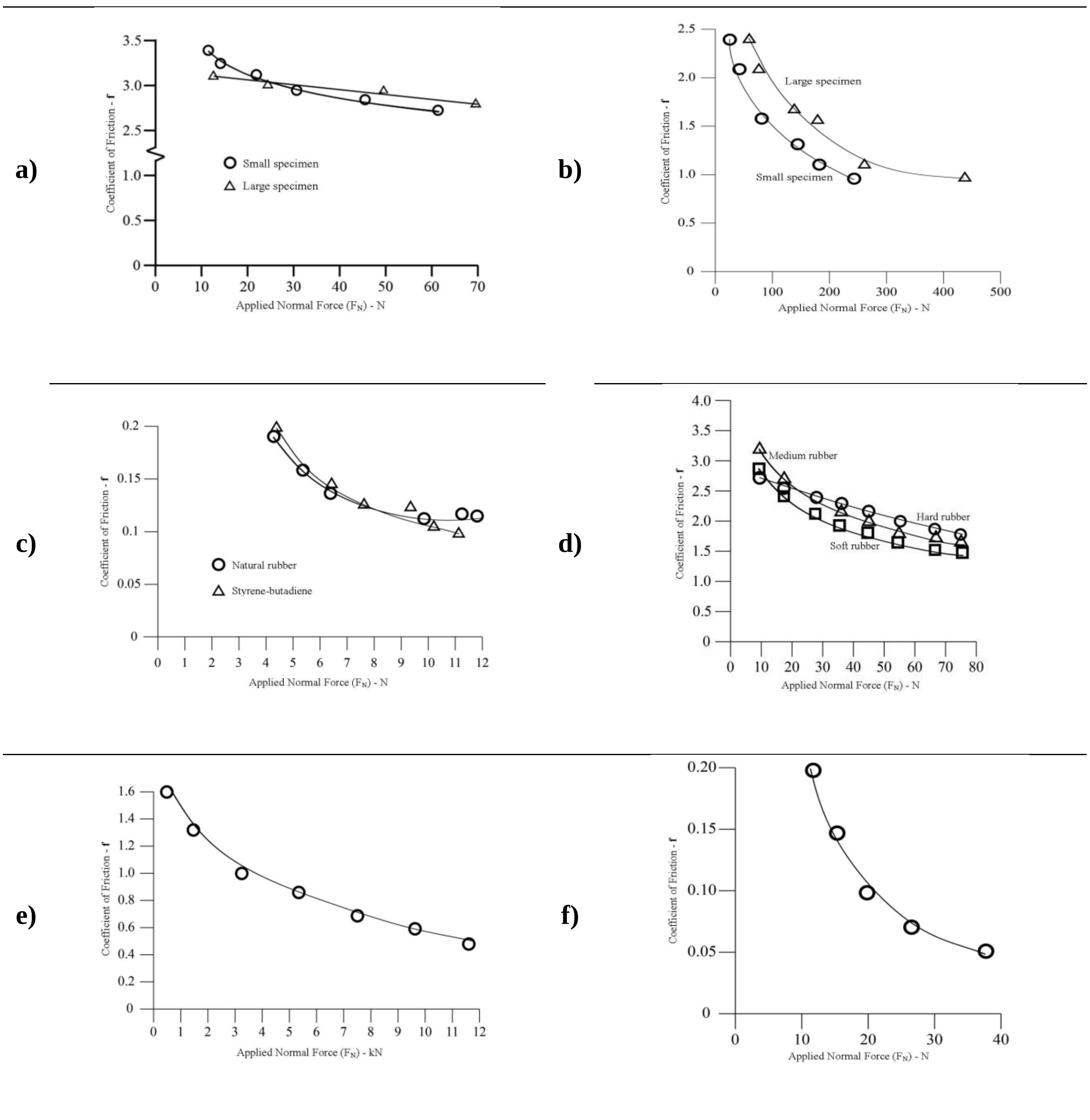

g)

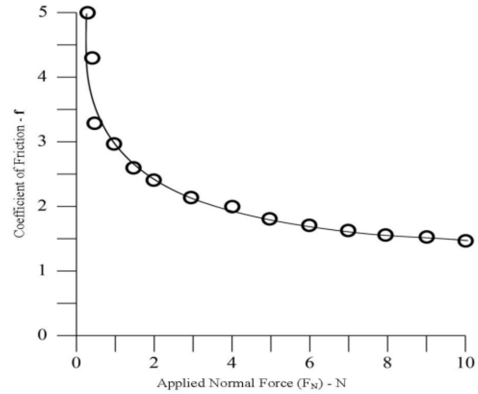

Figure 2-6 Friction coefficient vs contact pressure. a) Rubber against smooth glass [15] b) Rubber against smooth glass [35] c) Rubber against smooth ice [42] d) Rubber specimens with different stiffness against smooth glass [36] e. Rubber from aircraft tyre against concrete [43] f) Steel pin against soapy rubber [44] g. steel pin against dry flat rubber [41]

In a recent research [45], waste rubber powder was combined with polypropylene discs and was tested for friction by using a pin on disc tribometer. In the tests discs were made of mixture of polypropylene and rubber wastes. A copper pin was tested against different discs in which different amount of rubber waste (from 0% to 40% at 10% increment) were used as presented in Figure 2-7. Figure 2-8 shows the results of experiments for friction coefficient for different pins against sliding velocity. As it is evident, the higher the amount of rubber powders the higher the friction coefficient is and it is an evidence for bulk frictional property of this material. The authors concluded that the higher measured friction coefficient in the experiments can be attributed to two factors: Firstly, rubber remained as semi-solid and could not be vulcanized even at high temperature, secondly, due to the layers of rubber waste, a higher friction coefficient was produced, because of the bulk property of the rubber which is known as the internal friction [45].

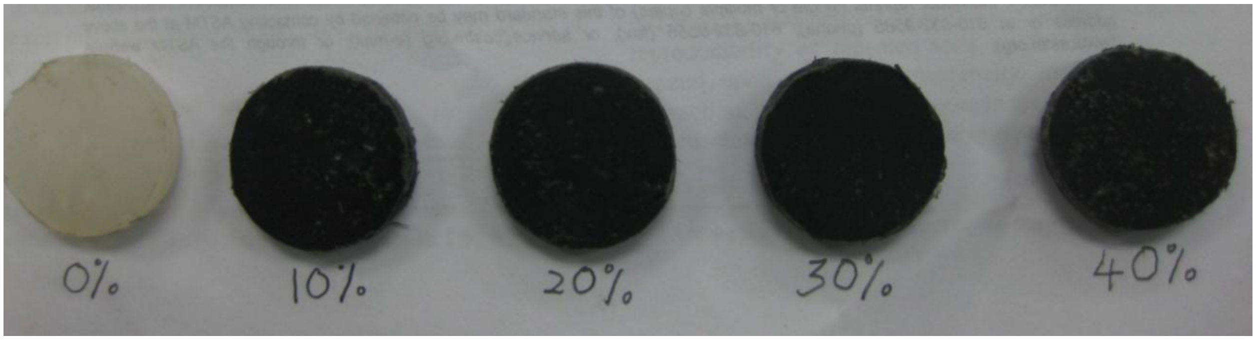

Figure 2-7 Polypropylene disc with different rubber wastes [45]

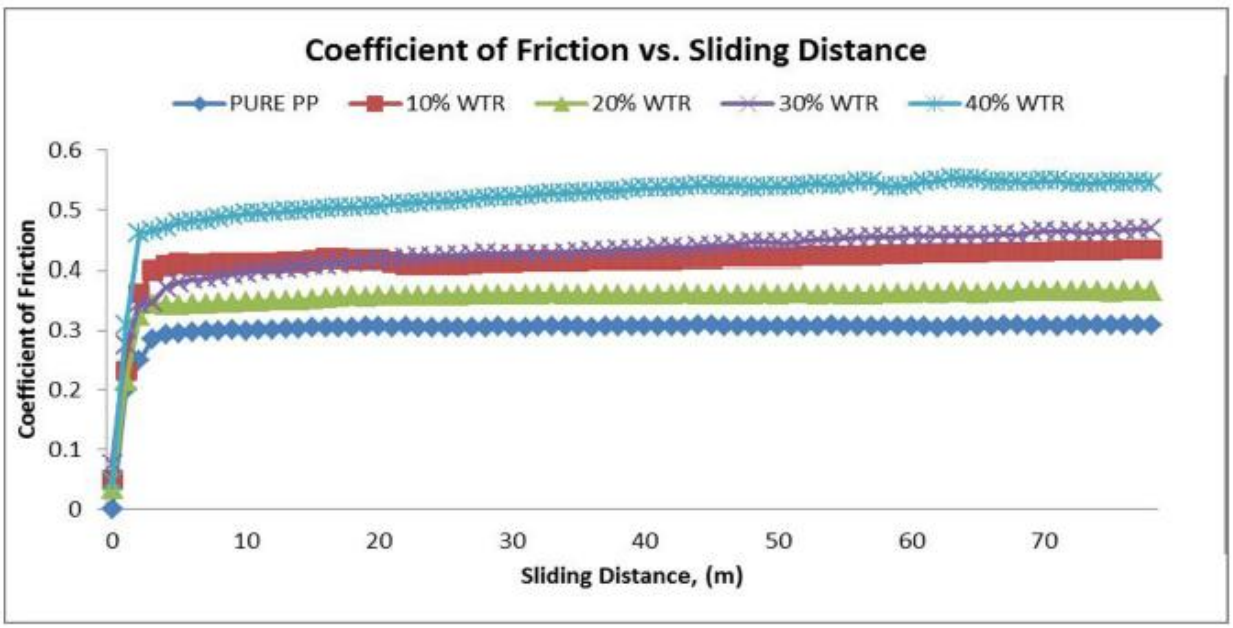

Figure 2-8 Friction coefficient vs sliding distance for different polypropylene discs [45]

In an investigation by Xu et al [46] the effect of surface roughness for dry and lubricated surfaces was considered, two kinds of samples i.e. textured and non-textured were tested. The test apparatus was the pin on disc tribometer, which is illustrated in Figure 2-9. The radius of the pin was 8.5 mm the sliding velocity was varying between 0.004-1 m/s and the normal load was between 1-3 N.

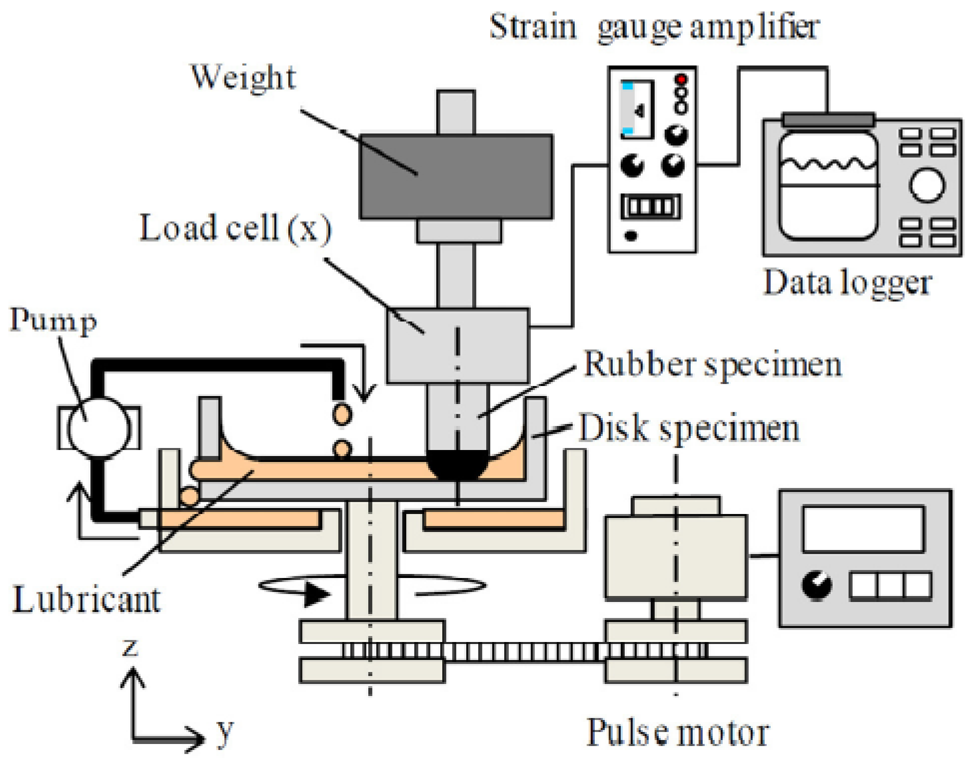

Figure 2-9 Experimental setup for friction measurement [46]

It was concluded that in dry conditions friction coefficient for textured specimens were lower than non-textured samples, this agrees with the fact that in dry conditions adhesion has the most effect on friction. In lubricated conditions, friction coefficient of textured samples was higher at low speeds (less than 0.1 m/s), but this value decreased and became less than plain samples, when the velocity exceeded 0.1 m/s [46].

In a research by Mofidi et al [47], rubber friction on apparent smooth glass with lubrication was investigated. It was aimed to show that short-wavelength roughness, which cannot be spotted by naked eye, has noticeable effect on rubber friction. The experiments were carried out for two different kinds of samples (i.e. aged and none-aged rubber, (acronitrile butadiene Rubber, (NBR), the aged samples were resting in different fluids at the temperature of 125 ^{o}C for a week), the samples were sliding against a steel cylinder (D=1.5 cm and L= 2.2 cm) with different kinds of lubricants. Figure 2-10 shows the experimental apparatus. It is notable that the cylinder slides against the samples in two ways; parallel and perpendicular.

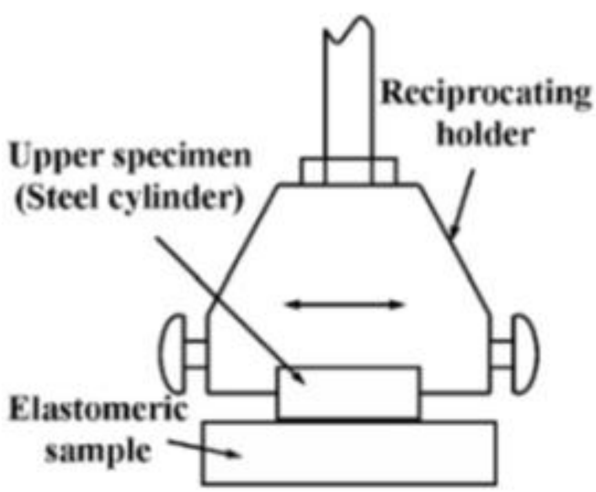

Figure 2-10 Mofidi et al experimental setup, as it was described the samples were moving in both parallel and perpendicular directions [47]

In Figure 2-11 a series of result from the experiment is shown for aged and non-aged sample.

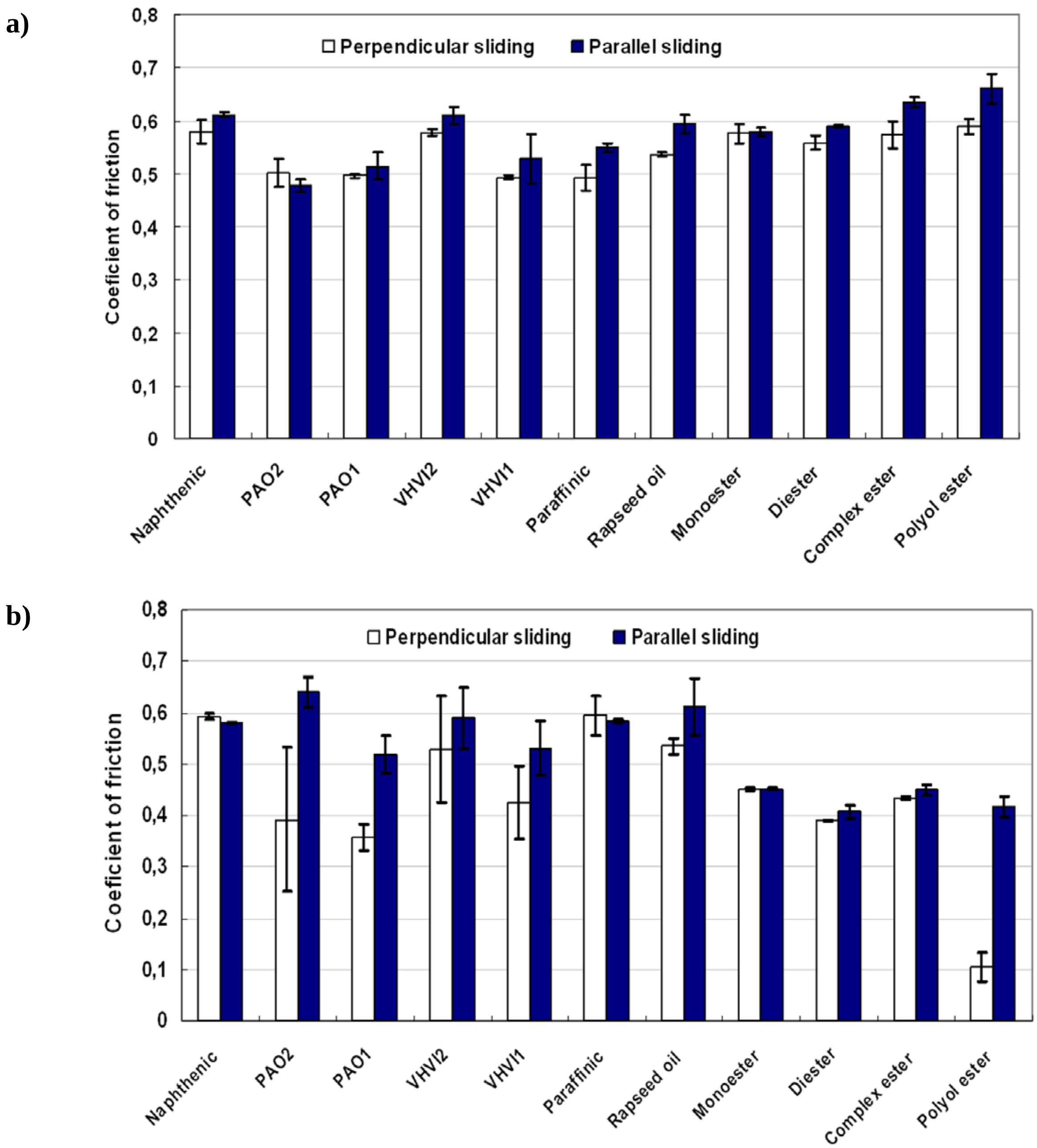

Figure 2-11 Friction measurement for non-aged a) and aged b) samples for normal load of 100N [47]

It was presented that rubber time-dependant deformations against hard surfaces has the greatest effect on rubber frictional properties. Also for surfaces that seem to be smooth by the look, asperities have obvious effect on friction coefficient. This research presented experimental theories to be applied on rubber seals in future studies, therefore it was explained that for rubber seals, lubricant will squeeze out of the contact after some time and the result would be similar to unlubricated surface. This subject has been mentioned by Denny [31], which earlier has been discussed in section 2.3.1.2. Also the effect of the roughness on rubber or the counter-surface and the result on friction was discussed. It was explained that roughness on the counter-surface has a share in friction, but when the rubber surface is not smooth and is abraded, there is a chance that it decreases the sliding friction because of trapping lubricant; this might also be valid when there is roughness on both surfaces.

2.2.3.3. *Rubber Unified theories*

As it was discussed in section 2.2.3.2, rubber friction coefficient cannot be measured by Coloumb-Amonton's friction law (Equations 1 & 2), therefore, extensive efforts have been made to find new methods of predicting the friction coefficient. This section is a comprehensive discussion about different models for predicting the friction coefficient.

One of the primary models that was suggested by Thirion [35] and formulated on the empirical basis, relates the inverse of friction coefficient and its dependency on normal pressure, as shown in Equation 2-9:

$$\frac{1}{\mu} = b + c(P_N)$$

Equation 2-9

Where c and b are constants obtained from the inverse curve of friction coefficient against normal pressure, b is the intersect of the inverse curve with y-axis and c is the slope of the linear part of the curve (L-H line). Figure 2-12 clarifies this concept with definition of all parameters.

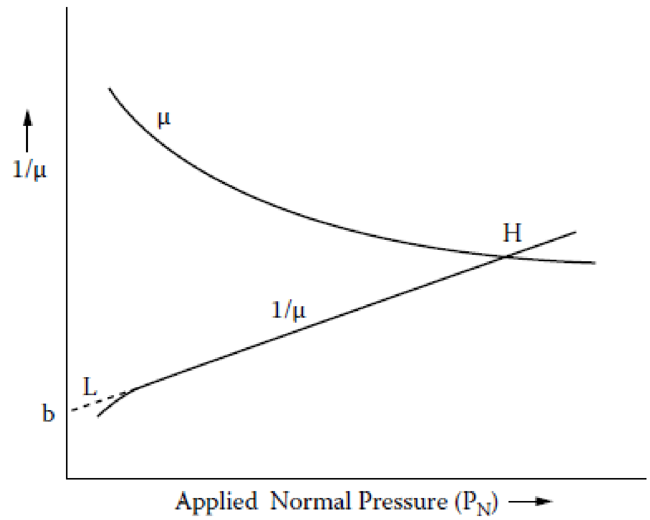

Figure 2-12 Inverse of friction by Thirion, friction coefficient against applied normal load [35]

Schallamach [36] underlined the dependency of adhesional rubber friction (μ_A) on contact area by conducting experiments while employing Hertz contact theory [48]. The obtained model is shown via Equation 2-10:

$$\mu_A = c_A {F_N}^{-1/3} \quad \textbf{Equation 2-10}$$

Where C_A is an experimental parameter and F_N is the normal load.

Denny [16] further developed Thirion's model by including the stress (σ) and compression modulus (E_v) in his model as it is shown by Equation 2-11:

$$\frac{1}{\mu} = a(1 + b\left(\frac{\sigma}{E_v}\right))$$ Equation 2-11

Such model was based on the fact that with increasing normal stress the friction coefficient decreases and explains their inverse relationship. The author stated that a depends on the experimental conditions with the suggested range of 1 to 8, while b was set equal to 15 in all cases [16]. It should be mentioned that this formula is only valid for hard rubbers, since the stress would be the same as contact pressure on contact area and it would change in the material because of internal friction and bulk properties of the material [35].

Another friction model [49] known as exponential friction model shows the dependency of friction on velocity by considering two phases of static and dynamic friction; this model is shown in Equation 2-12:

$$\mu = \mu_s + (\mu_D - \mu_s)e\hat{}(-\gamma V^{\delta})$$ Equation 2-12

In this model μ_s is static friction coefficient, $\mu_D$is the dynamic friction coefficient, V is the sliding velocity, δ and γ are constants [49].

As it was mentioned in section 2.2.3.1, Grosch's master curve obtained from experiments [19] was employed as a reference by many scientists and researchers for experiments validation. Savkoor [25] obtained a friction model based on this curve as formulated by Equation 2-13 and Equation 2-14:

$$\mu(v) = \mu_s + (\mu_m - \mu_s)exp\left\{-h^2\log^2\left(\frac{v}{V_{peak}}\right)\right\}$$ Equation 2-13

$$\mu(p) = \mu_0(\frac{P}{E})^n$$ Equation 2-14

Where μ_s is a static friction coefficient, μ_m is the maximum of the curve, h is the difference of maximum and minimum velocities that shows the width of the speed range, E is the elastic modulus and μ_0 and n are obtained empirically [25].

This friction model was divided into two parts, the first shows the dependency of friction on velocity (that was shown in Equation 2-13) and second demonstrates the dependency of friction coefficient on pressure (Equation 2-14).

In 2009, a research [50] proposed a new explanation about rubber hysteresis sliding friction on rough surfaces shaped like cylinder, wedge, sphere and cone. The model was based on the slope on the peak of the contact line and the contact length as formulated by Equation 2-15:

$$\mu_{tot} = \frac{F_{tot}}{F_y} = \frac{1 + P_a}{P_0} - (\frac{P_f}{P_0})(\frac{1 - \pi\Delta^2}{\lambda_1^2})$$ Equation 2-15

Where Δ is the contact radius, P_a is the atmospheric pressure, P_0 is the external pressure, λ is the length of the contact.

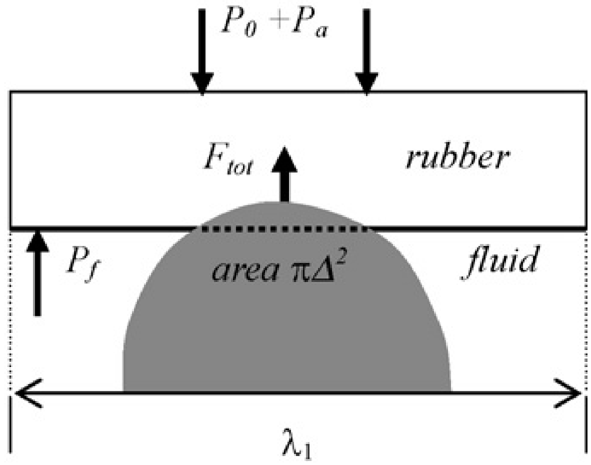

Figure 2-13 Contact of rubber against a surface over a peak [50]

In this study it was discovered that friction for a single peak was same as for a uniform array of identical peaks while the contact length does not change with sliding speed [50].

Another model that shows the dependency of friction coefficient on velocity and pressure was developed by Nackenhorst [13] and is shown in Equation 2-16:

$$\mu(v,p) = c_1 \left[\frac{p}{c_2}\right]^{c_3} + c_4 \ln\frac{v}{c_5} - c_6 \ln\frac{v}{c_7} \qquad \text{Equation 2-16}$$

Where c_1 to c_7 are determined by experiments. The major drawback of this model is the numerous numbers of constant coefficients that are required to be determined experimentally and without any physical background.

Dorsch [9] proposed a model for rubber friction, as a function of pressure and velocity using a quadratic equation. It was stated that two experimental facilities were used in their experiment to measure the friction coefficient. One of them was Grosch abrader, which was used for abrasion tests. The other test facility was a linear friction tester and tangential force was measured, while the pin was accelerating then running at a constant speed for the length of 0.2 m and finally deceleration. Figure 14 shows the schematic of both facilities.

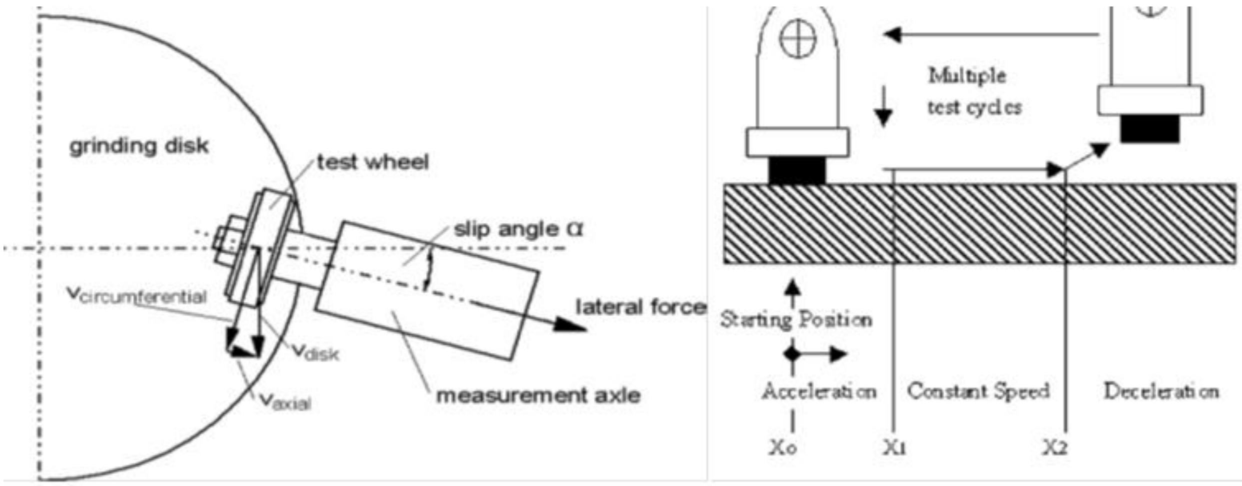

Figure 2-14 Grosch abrader rig (left) and linear friction tester (right) [37]

From the data obtained from experiments a model was derived as shown in Equation 2-17:

$$\mu = c_0 p + c_1 p^2 + C_2 v_s + c_3 p^2 + c_4 v_s + c_5 v_s^2 \qquad \text{Equation 2-17}$$

Where c_1 to c_5 are constants, p and vs are pressure and sliding velocity, respectively. Figure 2-15 shows the experimental results overlaid on the model prediction results (Equation 2-17) for comparison. As it is evident, such model is a strong function of contact pressure, while it is not significantly affected by the slip velocity.

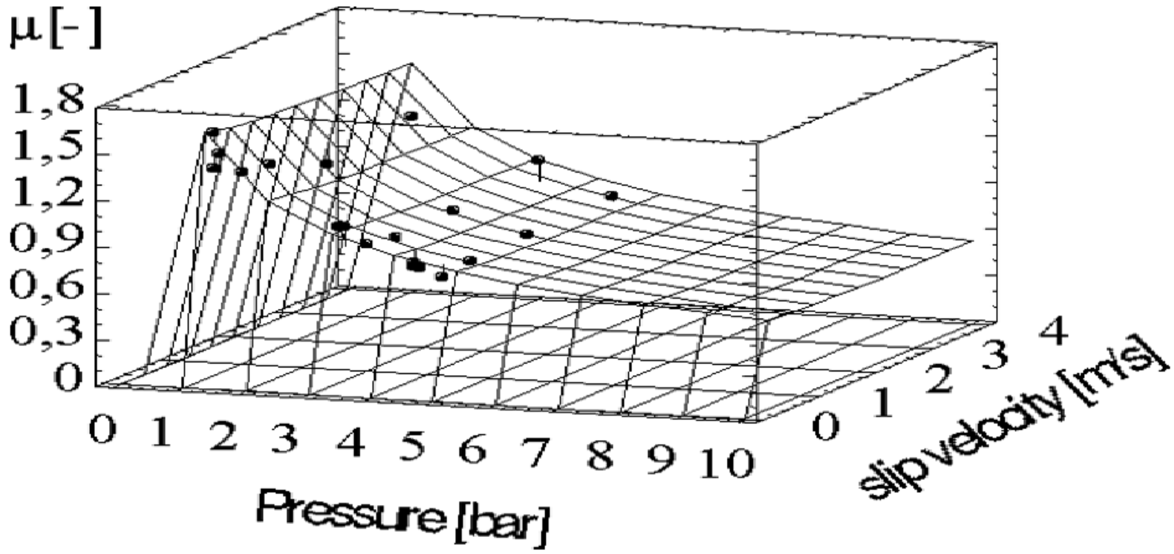

Figure 2-15 Dorsch frictional function [9]

The friction model obtained by the experimental data (Figure 2-15) was implemented into a finite element analysis (FEA) package (i.e. Abaqus) by writing a subroutine. The numerical results from the FEA were compared against the experimental study of a tyre (as will be explained in section 2.3.2) for validation. It was stated by Dorsch [9] that the rubber friction is a function of temperature, though the temperature variable was omitted because of complexity. Although their approach presents a method for measuring rubber friction coefficient against pressure and slip velocity, there are some unclear parameters in the experiments, especially that there is no change in friction coefficient against the slip velocity.

In 2006, Park [51] proposed a model that improved the deficiencies of the Coulumb law (Equation 2-1 and Equation 2-2) and exponential friction model (Equation 2-12) that included the changes in rubber friction and the effect of pressure, as shown by Equation 2-18:

$$\mu = (P/Po) - n\,f(\log(aTv))$$ **Equation 2-18**

Where $f(\log(a_T v))$, is a master curve, P is the contact pressure, P_o is the reference contact pressure and n depends on the road surface and is equal to 1/9 and 1/3 for rough and smooth surfaces respectively. It was stated that P_o is equal to 1.5×10^5 Pa, because rubber friction is independent of pressure close to this value [51].

The improved friction model was implemented to Abaqus/Explicit FEA package by writing the VFRIC subroutine (i.e. a subroutine to define frictional behaviour between two surfaces, where Coulomb law is restrictive [52]), which was able to calculate the friction coefficient by using Equation 2-18, frictional energy by the dot product of frictional force and slip increment and the cornering force was obtained by the software. The results for cornering force, cornering moment and frictional energy were predicted for different torque values and were compared with the tyre tests and Coulomb friction coefficient with constant values of 1 and 2. Figure 2-16 and Figure 2-17 demonstrate sample results from this study for cornering force and cornering moment against slip angle and frictional energy against time, respectively. Notably, the comparison for frictional energy has not been validated with empirical results. It can be concluded from all the results that the developed model predicted experimental values with better accuracy compared to the Coloumb law [51].

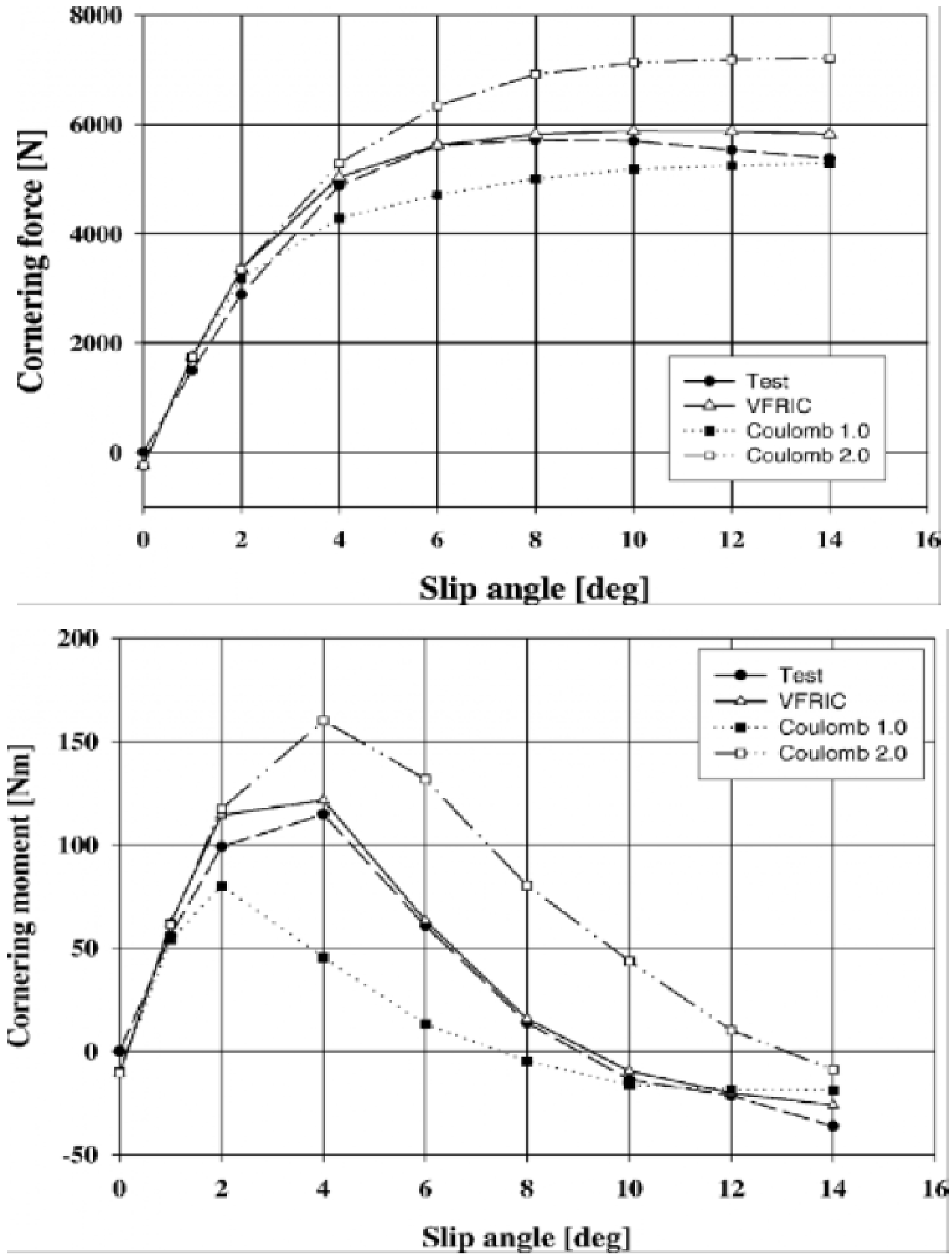

Figure 2-16 Cornering force (top) and cornering moment (bottom) against slip angle for the speed of 65 km/h [51]

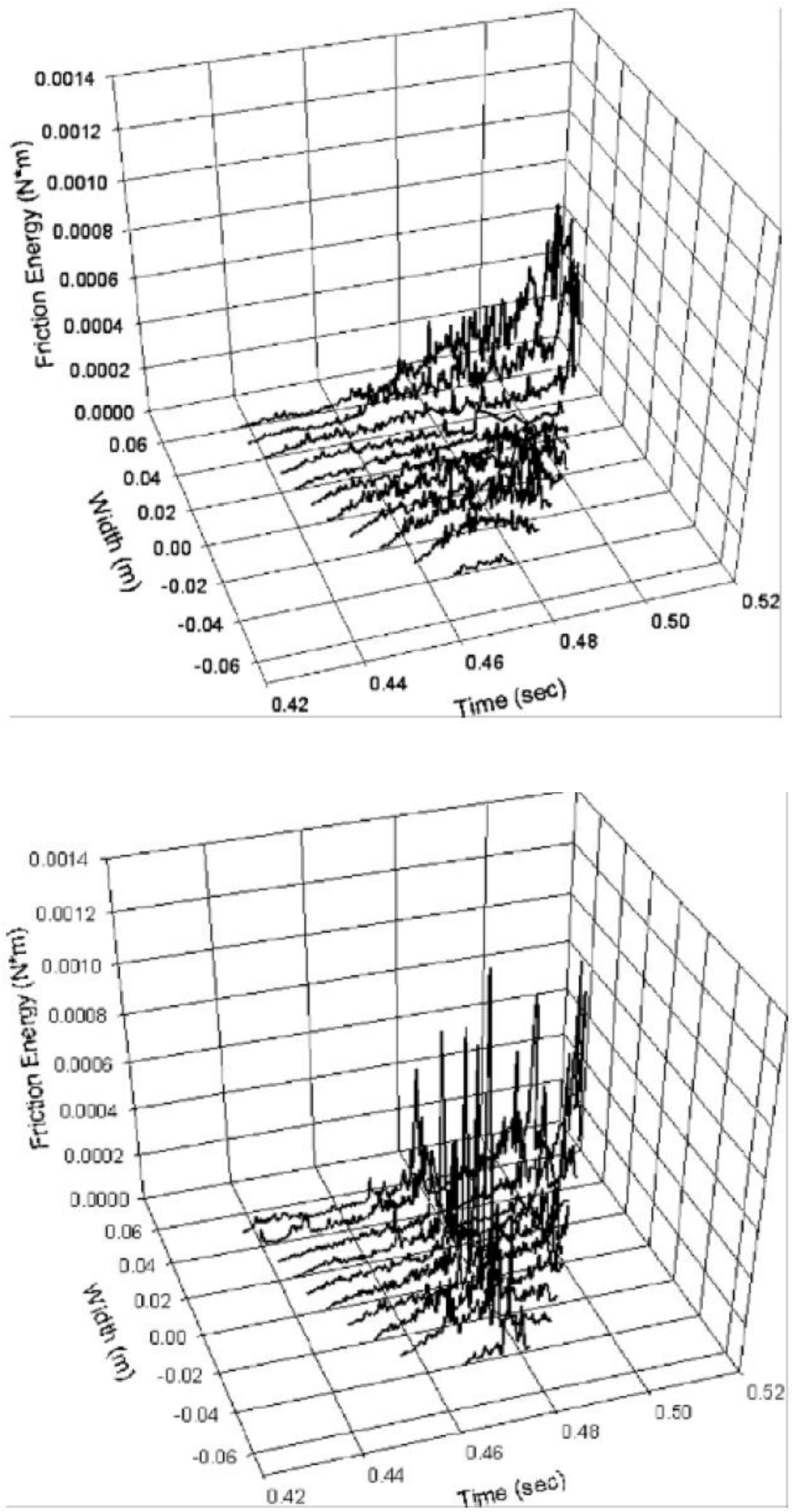

Figure 2-17 Frictional energy distribution for constant Coulomb law (top) and the obtained model (bottom) with slip angle of 6^{o} [51]

In 2011, a model was proposed by Huemer [53] obtained from sliding friction on ice and concrete as it is presented by Equation 2-19:

$$\mu(v,p) = \frac{\alpha|p|^{n-1} + \beta}{a + \frac{b}{|v|^{1/m}} + \frac{c}{|v|^{2/m}}}$$ Equation 2-19

Where *p* and *v* are the contact pressure and the sliding velocity. In this model *α*, *β* and *n* are the contact pressure dependant parameters and *a*, *b*, *c* and *m* are dependent on the sliding velocity [53].

Heinrich [54], divided the friction coefficient into adhesion and hysteresis; this was due to the fact that for elastomer materials kinetic friction on dry and wet tracks is dependent on these two terms. Equation 2-20 shows hysteresis component of the friction coefficient model.

$$\mu_{\text{hysteresis}} = \frac{F_{\text{hysteresis}}}{F_N} = \frac{1}{2(2\pi)^2}\frac{\delta_t}{pv}\int_{\omega\, min}^{\omega\, max} d\omega\omega G''(\omega)S(\omega)$$ Equation 2-20

Where δ_t is the thickness of rubber, p is the normal pressure, v is the sliding velocity, G'' is the shear modulus and *S* is a parameter to express the surface texture in terms of a power function. *ω* is the excitation frequency and it depends on the surface roughness, as it is shown in Equation 2-21 [54]:

$$\omega = 2\pi\varsigma$$ Equation 2-21

Where ς shows the surface roughness for horizontal cut-off roughness. The maximum frequency can be obtained by Equation 2-22 [54]:

$$\omega_{max} = 2\pi v / \varsigma_{min}$$ **Equation 2-22**

The adhesional term of the friction coefficient model is shown by Equation 2-23 [54]:

$$\mu_{Adhesion} = \frac{F_{Adhesion}}{F_N} = \frac{\sigma_\tau}{p}\,\frac{A}{A_0}$$ **Equation 2-23**

Where σ_τ is the shear stress in the real contact area, A is the real contact area and A_0 is the nominal contact area.

Although this research seems to differentiate the adhesional and hysteresis parts of rubber friction and expresses each of them separately, it should be noted that, to find the friction coefficient based on this model, several parameters have to be calculated. Although these parameters can be measured from experimental testing, it is an exhaustive procedure for daily engineering applications.

Wriggers and Reinelt [55] suggested a model in multi scale for rough surfaces, as it was stated since, the main purpose of rubber friction is tyre analysis and tyres are mostly in contact with asphalt, therefore sandpapers were used for experiments to present a similar condition. This model is formulated by Equation 2-24:

$$\mu(v, p) = \left(\frac{2v\overline{v}}{v^2 + \overline{v}^2}\right)^c \mu_{max}$$ **Equation 2-24**

Where $\overline{v}$ and μ_{max} are the corresponding coordinates of the maximum point on their experimental curve and c is a scaling factor to broaden the range of sliding velocity.

Two individual functions were defined based on the experimental data to predict $\overline{v}$ and μ_{max} without performing the experiments and were obtained based on various normal pressure values as are described by Equation 2-25 and Equation 2-26, respectively.

$$\mu_{max} = \frac{b}{P_N} \tan^{-1}(d\, P_N) \qquad \text{Equation 2-25}$$

$$\overline{v} = a\, P_N \qquad \text{Equation 2-26}$$

Where all four constants a, b, c & d are obtained by nonlinear least-square algorithm [55], though, no range or values are given for these constants.

It was highlighted in this study that the multi-scale functionality of the proposed model (Equation 2-24) is a difficulty due to the lack of computer resources.

Figure 2-18 shows an example of his numerical analysis, the dots show the result of finite element calculation and solid lines are from the functions. Eventually, it was stated by Wrigers et al, that this is an appropriate model to predict the hysteresis of bulk material, but its functionality for different scale is an unknown and changes in surfaces changes the properties and may cause problems in the calculations [55].

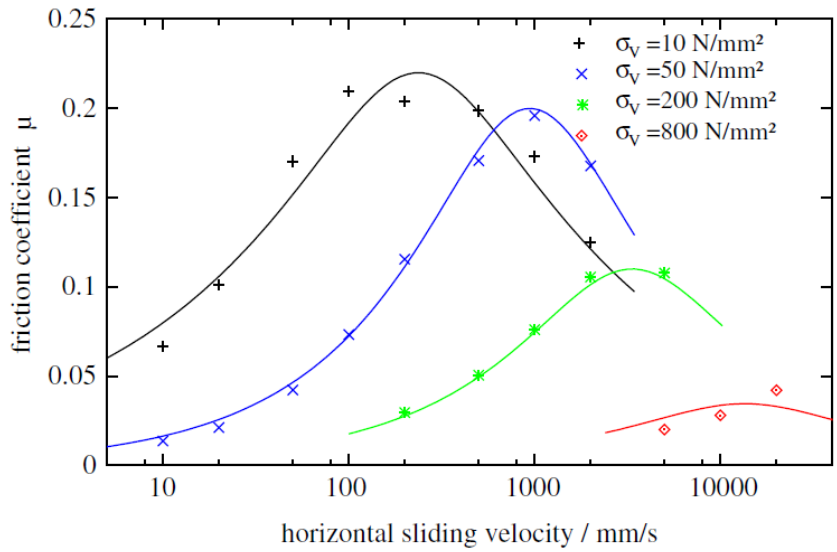

Figure 2-18 Different range of friction coefficient of Wriggers et al. [55]

Persson [56] found out that a large fraction of rubber friction is because of energy dissipation in bulk property of rubber, which is known as internal friction based on his previous experimental studies on rubber against hard, rough surfaces ([57] and [58]). A friction coefficient was derived from complex calculations as it is shown by Equation 2-27:

$$\mu \approx \frac{1}{2}\int \mathrm{dq}\ \mathrm{q}^3\, C(q)P(q)cos\,\emptyset) \times \int_0^{2\pi} d\emptyset \cos\emptyset Im\frac{E(qv\cos\emptyset)}{(1-v^2)\sigma_0}$$

Equation 2-27

Where $C(q)$and $P(q)$ depends on the value of q and q is dimensional vector, h is the height of surface asperity, v is the sliding velocity, E is young's modulus and σ is the stress of rubber, ∅ is the angle between the direction of velocity and the asperities, which is either zero or $\frac{\pi}{2}$, H is self-affine fractal surfaces found from both surface texture. Moreover there a scaling factor of ς with the value between zero and one and ς defines the contact of rubber over the road on the counter-surface, which is variable between zero and infinity. This value is used when there are randomly rough asperities, and the model gets more complicated. Figure 2-19 clarifies the definition of ς, in which λ is the length of asperity and L is the total length of contact.

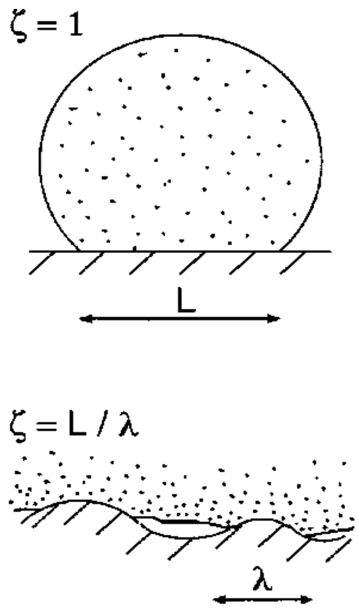

Figure 2-19 ς**, the contact of rubber and the road [56]**

One of the findings in this research was that for typical pressures between a tyre and road the rubber makes an apparent contact with 5% of the road. It was mentioned in this study that tyre producers prefer to provide rubber compounds with lower rolling resistance and higher sliding friction coefficient, while reducing wear. A better understating of friction eases the design of the products that contains rubber-like material (such as tyre and wiper blades) and makes it much more convenient [56].

Table 2-3 represents all of the rubber friction formulas that have been discussed above.

Table 2-3 Rubber unified theories

No	Author [Ref]	Model	Advantages	Drawbacks	Remarks
1	Thirion[35]	$\frac{1}{\mu} = b + c(P_N)$	Simplicity	It is essential to deliver experiments to obtain this model	One of the first friction models which shows the dependency of friction coefficient on contact pressure
2	Schallamach [36]	$\mu_A = c_A F_N{}^{-1/3}$	Demonstrate adhesional coefficient of friction	It is a coefficient of adhesional term of friction and must not to be confused with friction coefficient	Based on Hertz contact theory
3	Denny [16]	$\frac{1}{\mu} = a(1 + b\left(\frac{\sigma}{E_v}\right))$	Simplicity of the model, including some material properties, also a range for the unknowns	Dependency of friction on velocity is not shown	This model is developed based on Thirion's model
4	Li Chun Bo [49]	$\mu = \mu_s + (\mu_D - \mu_s)e\hat{}(-\gamma V^{\delta})$	Distinguish dynamic friction from static friction	Does not show the effect of pressure on rubber friction	---

5	Savkoor [25]	$\mu(p) = \mu_0(\frac{P}{E})^n$ $\mu(v) = \mu_s + (\mu_m - \mu_s) exp\left\{-h^2 \log^2\left(\frac{v}{V_{peak}}\right)\right\}$	Shows the friction coefficient for velocity and pressure	The model separated the friction for both pressure and velocity; it is confusing to obtain a value for friction coefficient for different conditions.	The term dependant on velocity is similar to exponential model (No. 4)
6	Pinnington [50]	$\mu_{tot} = \frac{F_{tot}}{F_y} = \frac{1 + P_a}{P_0} - (\frac{P_f}{P_0})(\frac{1 - \pi\Delta^2}{\lambda_1^2})$	Measure friction based on surface roughness and simplicity	Generalised a surface only on one peak without considering the rest of the contact patch and does not include velocity	---
7	Persson [56]	$\mu \approx \frac{1}{2}\int \mathrm{dq}\ \mathrm{q}^3\, C(q)P(q)cos\,\emptyset) \times \int_0^{2\pi} d\emptyset \cos\emptyset Im \frac{E(qv\cos\emptyset)}{(1-v^2)\sigma_0}$	A complete model that takes into account surface roughness	Complexity, too many constants and difficult to be practised on daily basis in engineering applications	---

2.3.3.1 Summary

In this section (2.2.3.3), the theories about dry and lubricated rubber friction were discussed and some of the test measurements about rubber friction were explained. It was shown that rubber friction is dependent on different parameters such as velocity, pressure and temperature. There were many attempts to model rubber friction coefficient in a way to consider the changes in all the effective variables (as shown in Table 2-2 and Table 2-3). The abovementioned models clearly have problems and inaccuracies in their predictions, as it was discussed previously. Although the final purpose of rubber friction modelling generally is to develop a model for tyre applications, these models were obtained from sliding rubber and the effect of slip is completely neglected. Generally, researchers find difficulties to accurately simulate the real behaviour because of the presence of non-linear constants (summarised in Table 2-3) and also the dependency on pressure, velocity and slip is challenging to express in one single model. In the next section these effects on tyre and related experiments will be explained.

2.2.3.4. *Case of study: Rubber unified theories application*

In an investigation carried out by Bielsa et al [59], experimental measurements of rubber friction were performed. The data were obtained from sliding of rubber on metal surfaces. In a tribometer (i.e. Phoenix tribology PLINT TE 77), flat on flats and flat on cylinder were examined, the rubber sample chosen for this purpose was 751IRHD (EPDM type) and the material for counter-surface was 6262-T9 aluminium alloy. Figure 2-20 shows the contact and tribometer in details.

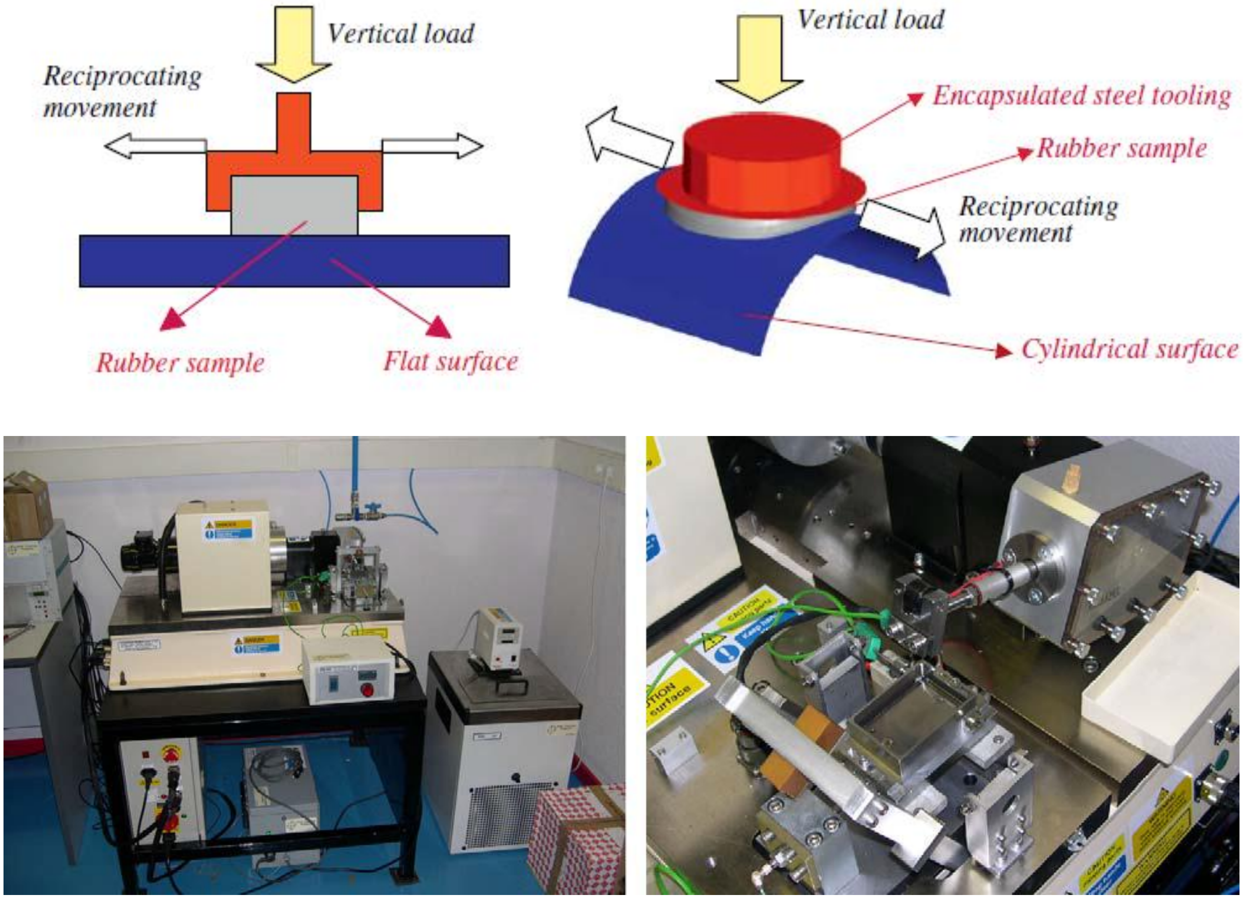

Figure 2-20 Flat on flat and flat on cylinder contacts in TE77 tribometer [59]

Six different loads varying between 100 to 660 N were applied on the samples and the experiments were delivered at room temperature, as it was stated the data were collected with a high frequency of 1 kHz, which explained it was high enough for this measurement. The data obtained from this setup is presented in Figure 2-21.

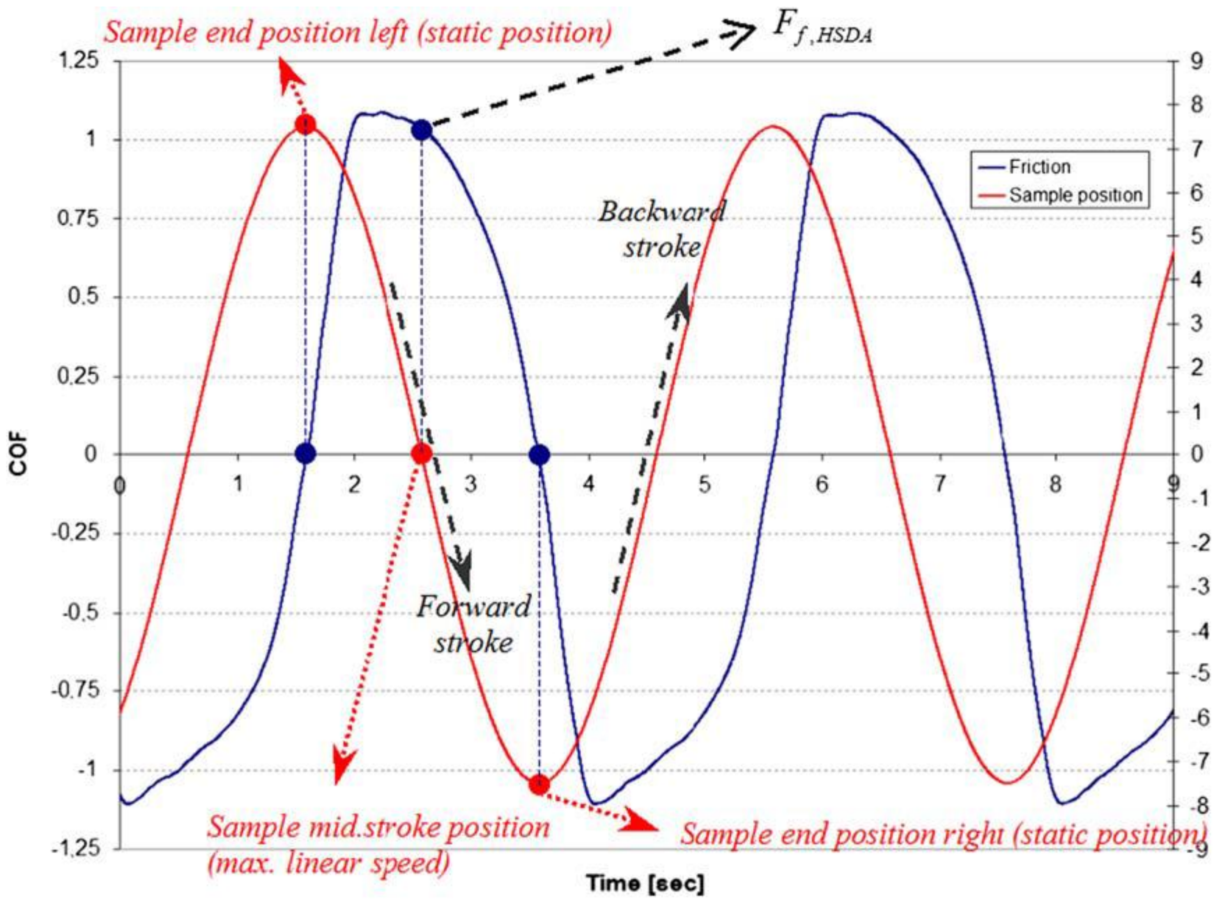

Figure 2-21 Friction coefficient obtained from flat on cylinder [59]

The movement of the sample and measured friction coefficient is illustrated by the authors, meanwhile this procedure was modelled in Abaqus and the area of contact was obtained from the analysis and based on this information a model was developed that is shown in Equation 2-28.

$$F_f = \sum_i \mu\left(P_i^k\right). P_i^k. A_i \quad \text{Equation 2-28}$$

Where F_f is the friction force obtained from experiments, A_i and P_i^k are respectively the contact area and contact pressure for each node extracted from FEA and k shows the number of normal forces on the specimens, which in this case is 6.

The result of this model was compared to another two developed models from unified theories that were discussed in section 31. For this purpose, Thirion's and Schallamach's models (Equation 2-9 and Equation 2-10 respectively) were selected. There was some modification on Thirion's model which has not been explained clearly. Finally, comparison of the friction coefficient against pressure was illustrated, which is shown in Figure 2-22.

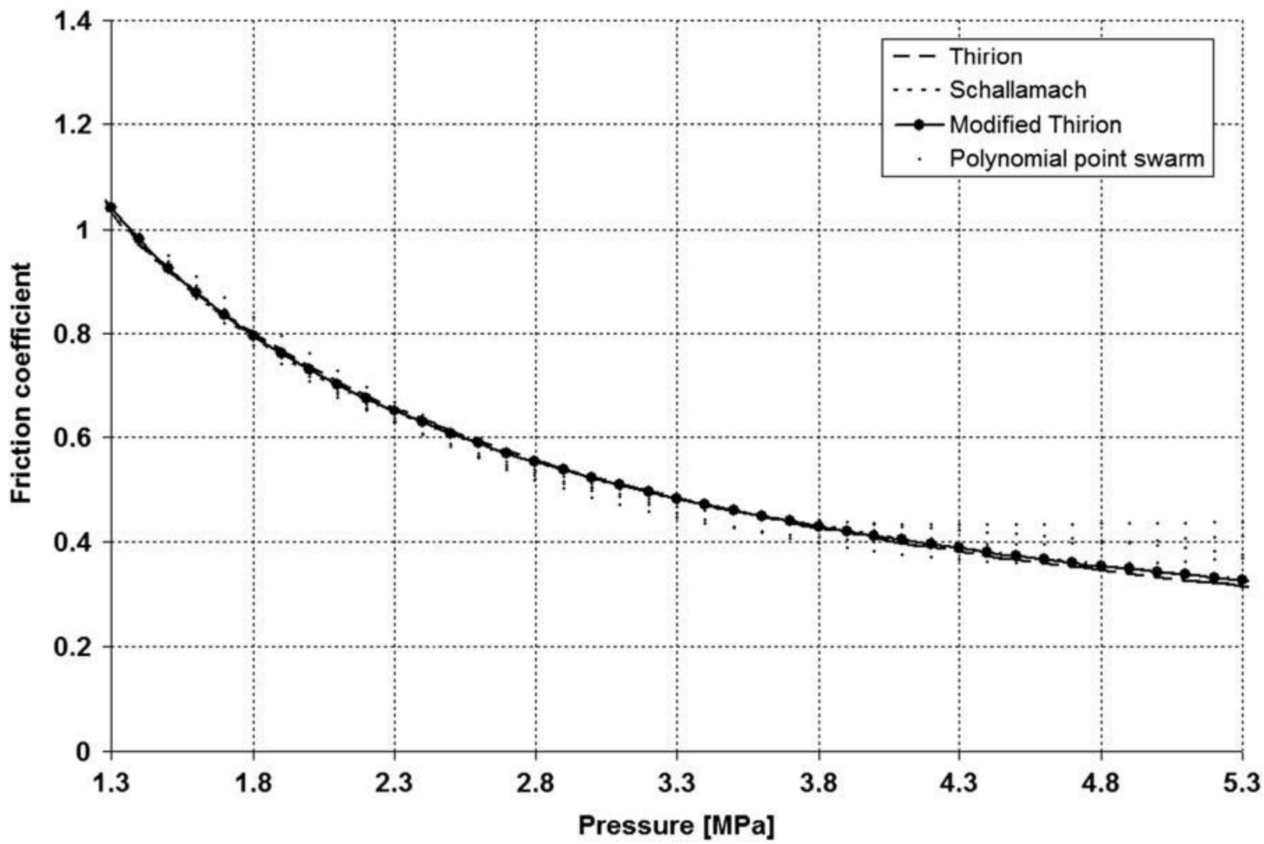

Figure 2-22 Bielsa et al, friction results [59]

It is presented that the models are very similar and they follow each other closely. By this outcome, it was concluded that the model has been approved successfully and the pressure dependency of the friction was shown. The importance of this study is mainly in developing and applying mentioned unified friction theories (section 2.2.3.3), which is something rare in rubber analysis and mostly industries prefer to use empirical results in their analysis. Although this research applied the models for laboratory purposes and it was not used in practical industrial problem, but this could be a sample to use rubber friction models in FEA packages and deliver more efficient and simplified models that cover different effective aspects on industrial consumption of rubber-like materials.

2.3. Tyre Friction

In this section the frictional properties of a tyre and its dependency on different parameters as well as experimental studies on tyres will be discussed in detail.

The first pneumatic tyre production started in 1888 by Dunlop. The pneumatic tyre that is in use nowadays has a lot of differences and improvements from the original one. During this period, many materials have been changed or have been enforced to change in order to improve the strength and durability [18]. Figure 2-23 presents a detailed cross section of a modern tyre in used for typical vehicular application.

Figure 2-23 Tyre cross section [60]

Table 2-4 shows a brief explanation of tyre compounds that has been shown in Figure 2-23:

Table 2-4 Tyre components

Tyre component	Explanation
Abrasion gum strip	A layer of rubber between the body plies and wheel rim
Bead filler (Apex)	To fill the void between the bead and the inner body plies
Sidewall	To protect the plies from impact and abrasion side wall rubber are provided
Plies	Rubber coated brass plated steel cords
Belts	Two steel belts are placed between the ply and the treads opposite to each other
Belts Wedges	Fatigue resistant material that has been placed between the belts
Shoulder	Small parts between the belts and plies
Tread	This part made of rubber that provides grip or traction for the vehicle, which has pattern on it for different reasons such as driving liquids out of the way
Subtread/ Undertread	Layer of rubbers with lower hysteresis to improve the rolling resistance or stability

As it is evident, the majority of the tyre's material is made out of rubber, especially for the tyre tread and there is a necessity for the thorough understanding of its frictional behaviour to further improve vehicle numerical modelling and simulation.

2.3.1. Tyre properties

As it was mentioned in section 2.2.3, Kummer [22] developed a combination of molecular and macroscopic theories of rubber friction to conclude that the main reason for rubber friction was adhesion and hysteresis. In Kummer's research [61], the requirement of tyre manufacturing has been discussed and summarized as following:

- Proper value of friction for transmission
- Safety for cases like getting puncture, tread separation or bursting.
- Correct cornering characteristics
- Driving qualities as in case of suspension
- Tread life endurance
- Low rolling resistance and heat generation
- Controlled noise
- Strong to aging problem
- Control of dimensions

Kummer [11] explained the history of tyre friction experimental studies and examples of friction tests for different tyres against different quality of pavements were demonstrated. Friction coefficient with different friction testers were summarized, as it is presented in Figure 2-24 [61].

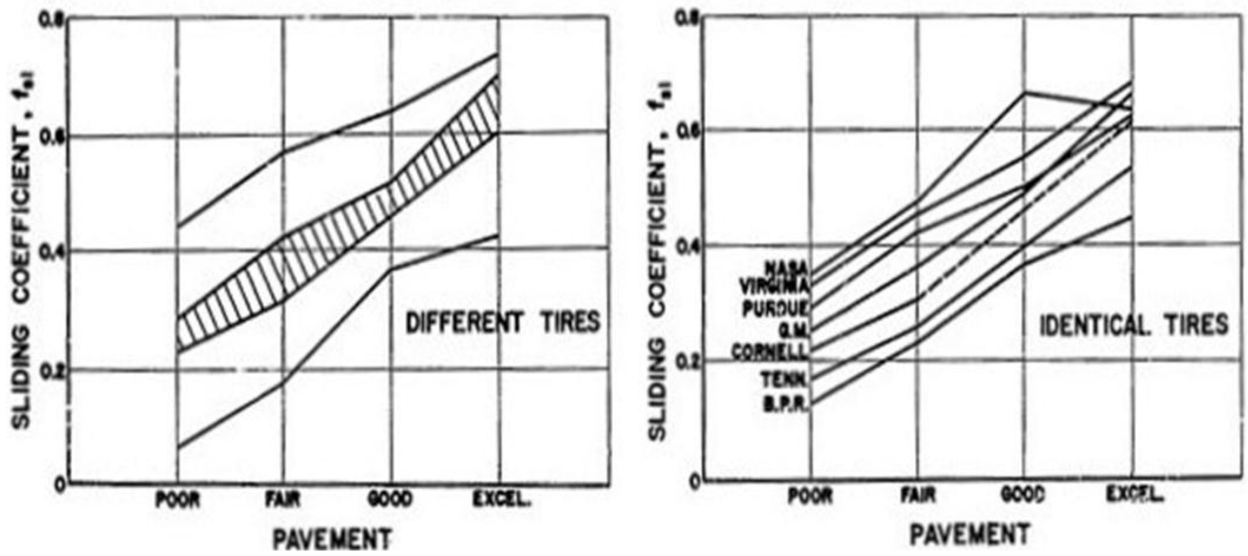

Figure 2-24 Friction coefficient of different tyres (old technology) against different pavements (left), different friction testers for same tyres [35]

The definitions of friction coefficient for tyres were classified into different categories as summarized by Kummer [61] as below:

- At rest
- Starting to skid
- Sidewise sliding (drifting)
- Forward sliding, when the wheel is locked

It was stated that the main drawback of these classifications was that they were loosely defined and the correct parameters for experiment are neither reported or measured [61].

To define friction more precisely, Kummer explained the difference between coefficient of road friction and actual coefficient of friction. Road friction coefficient is obtained by considering the amount of the static normal load on a tyre while the actual friction coefficient is the result of the actual normal load on the rubber specimens/contact patch; as in driving the normal load on the tyres would be different due to the changes in suspension [61]. The terminology that was used in Kummer's definition of friction is listed as following:

- **Critical coefficient of friction**: The maximum friction coefficient.
- **Creep** is the condition that the rubber elements move with a velocity greater than 1inch/sec and is also known as sliding.
- **Skidding** is known as the movement of a vehicle in an uncontrollable motion.
- **Disturbance** is same as the contact patch, which is the part of tyre that is in contact with the road.
- **Apparent pressure** is equal to the normal load divided by the apparent contact area.
- **Gross contact area** is the apparent area of smooth tyre in contact with a smooth road contact area.
- **Net contact area** is the contact of the treaded tyre with a smooth surface.

In addition, effective factors on coefficient of road friction were summarized by Kummer [61] for tyre and vehicle as in Table 2-5.

Table 2-5 Effective factors of friction coefficient by Kummer

Tyre	vehicle
Size and shape	Power train
Tread design	Suspension system
Carcass	Body design

According to Kummer [61], the maximum friction coefficient, obtained on a sliding rubber sample in tests, can only be applied to a tyre when it is locked without rolling. It was also stated that the friction coefficient decreases with increasing pressure. It was described that the friction coefficient for specific slip or slip angle can be smaller for heavier load tyres. One of the findings about the tyre friction shows that after running a tyre, friction coefficient between the tyre and the road was increased, though, it was expected that the rise in temperature increases the inflation pressure and consequently decreases the friction. The increase in the friction coefficient is known to occur because of the changes of the adhesion and hysteresis. It was observed that the adhesion decreased and the hysteresis increased by increasing the inflation pressure [61].

2.3.2. Tyre friction modelling

As it is mentioned in section 2.3.1 Rubber is the main element of a tyre, therefore Amontons-Coulomb friction law is not applicable in tyre friction modelling. In section 2.3.2, Friction models for rubber were considered and discussed in details, in this section, tyre friction models are discussed and explained.

One of the most common semi-empirical models in tyre modelling, known as magic formula, was developed by Pacejka in 1993 [62]. The general form of the formula is shown in Equation 2-29:

$$F(x) = D.Sin\{C.arc\,tan[B.x - E(B.x - arc\,tan(B.x)\,)]\} \quad \text{Equation 2-29}$$

where F is the friction function and x is the slip, B is the factor of stiffness, D is the peak value of the curve, C is the shape factor and E is the curvature value.

To simplify working with this model, two formulas for calculation of C and E are provided, that could be found in the literature [62].

In 1994, Germann [63] claimed that the coefficients in Pacejka's model had been obtained by nonlinear optimization therefore, a polynomial approach was suggested to model the friction as it is shown in Equation 2-29 [63]:

$$\mu = a_0 + a_1 s + a_2 s^2$$ Equation 2-30

In Figure 2-25, the empirical results and results from Pacejka's model and polynomial model from Germann are compared.

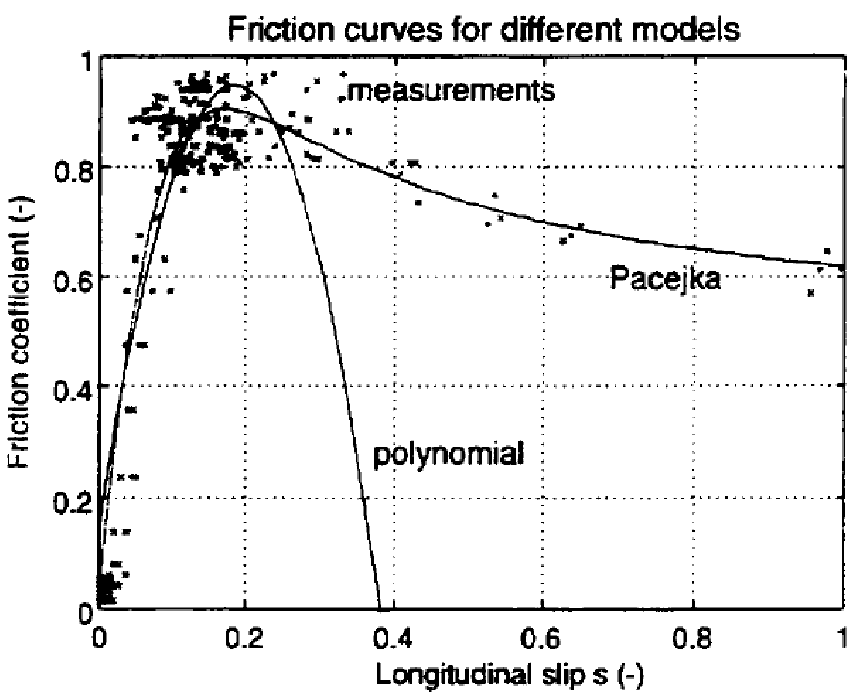

Figure 2-25 Comparison of Pacejkas model, polynomial model and the measurements [63]

As it is shown in Figure 2-25, Pacejka's model is applicable for a wider range of longitudinal slips (up to 1) with reasonable accuracy, while the polynomial model proposed by Germann is suitable for a limited range of slip up to-0.3. Despite the simplicity of the Germann's model and its validity for a range of operating conditions, such model may overlook the complexity of pure sliding in a vehicle and therefore unable to predict the friction for slips more than 0.3.

Burckhardt [64] proposed a friction model dependant on slip (s) and velocity (v) as formulated by Equation 2-31.

$$F(s,v) = (c_1(1 - e^{-c_2 s}) - c_3 s)e^{-c4v}$$

Equation 2-31

Where c_1 to c_4 are constants obtained from the experiments.

Kiencke and Daiss [65] modified the friction model developed by Burckhardt [64] to make it independent from velocity as it is shown in Equation 2-32:

$$F(s) = K_s \frac{s}{c_1 s^2 + c_2 s + 1}$$

Equation 2-32

Where K_s is the slope of the friction force against slip in linear phase and c_1 to c_2 are constants obtained from the experiments.

Another model proposed by Burckhardt [66], followed the same approach as Kiencke and Daiss [65] to remove the dependency of friction model from the velocity with the aim of simplicity. Equation 2-33 shows the mathematical formula for this model:

$$F(s) = c_1(1 - e^{-c_2 s}) - c_3 s$$

Equation 2-33

Where c_1 to c_3 are constants obtained from the experiments.

All models reviewed in this section are disadvantageous as they are formulated in nonlinear form and hence cannot be used for on-line identification. Burckhardt [66] made an effort to further modify the previously developed models (Equation 2-31 and Equation 2-33) for simplicity and ease of implementation. Equation 2-34 shows this model.

$$F(s) = c_1\sqrt{s} - c_2 s$$

Equation 2-34

In 1997 an investigation by Gustafsson [67], assumed that friction force properties, at low slip (no value is given for the range of slip; based on Figure 2-25 this value was about 0.15, and it is necessary to consider that the slope is exaggerated) depends on road condition and a friction model was developed based on this concept as formulated by Equation 2-35:

$$\mathrm{S(t)} = \mu(\mathrm{t})\left({}^{1/k}_{\ \delta}\right) + \mathrm{e(t)}$$

Equation 2-35

Where k is the slope of friction function in low slip area that is known as the longitudinal stiffness, δ is a curve fitting constant and t represents the time since k and δ are time dependant. Although it is expected to develop friction coefficient as the function of slope, this model is backward with two highlighted advantages. Firstly, k and δ are separated and based on what has been stated as the multiplication of k and δ ($k\times\delta$), which is less meaningful; also it avoids using the noisy slip measurement in their analysis. It should be explained that this model is only valid for linear phase of the friction and the reason for changing the order of the equation was due to the regression analysis method used in this study.

Gert Heinrich [40] built a model for rubber friction based on tread deformation, tyre energy dissipation in the contact area (μC) and the viscoelastic energy dissipation-(μD) as formulated by Equation 2-36 and Equation 2-37:

$$\mu \ \equiv \frac{Fx}{Fn} = \mu C + \mu D$$ Equation 2-36

Where F_x and F_n are axial and normal loads respectively and μ_D is obtained by Equation 2-37:

$$\mu_D = \frac{\Delta E_{diss}}{F_N l}$$ Equation 2-37

Where ΔE_{diss} is the longitudinal friction force over the contact length because of dynamic tread element deformation. It was shown that friction coefficient was less sensitive to μ_D and therefore the model was simplified as shown by Equation 2-38:

$$\mu \approx \mu_c(1 + \frac{\pi \sigma_0 h \mu_c}{L} j''(\sigma_0, \omega, T)$$ Equation 2-38

Where σ is the stress, h is the tread height, L is the length of footprint, and j'' is a function of shear modulus dependant on the frequency (ω) and T is the temperature. The result shows the effect of load dependency of the hysteresis friction coefficient over rough surfaces and demonstrates the effects of the height distributions of different roads. It was stated that the relation between the normal load and the real contact area and the surface texture require further discussion.

Table 2-6 presents the reviewed tyre friction modelling studies with a brief discussion about each of them.

Table 2-6 Tyre friction modelling

No.	Author [Ref]	Model	Advantages	Drawbacks	Remarks
1	Pacejka [62]	$F(x) = D.Sin\{C.arc\,tan[B.x - E(B.x - arc\,tan(B.x))]\}$	Most common tyre model that could applied for different applications	Too complicated and there is a need to perform many experiments to obtain the model	This model is applicable for different tyre forces
2	Germann [63]	$\mu = a_0 + a_1 s + a_2 s^2$	simplicity	Only cover the range of slip less than 0.3	---
3	Burckhardt [64]	$F(s,v) = (c_1(1 - e^{-c_2 s}) - c_3 s)e^{-c4v}$	Shows the effect of slip	Dependant on velocity, and does show the effect of pressure, nonlinear constants	---
4	Kiencke and Daiss [65]	$F(s) = K_s \dfrac{s}{c_1 s^2 + c_2 s + 1}$	Include *K* which is the stiffness although this value is dependent on different variables and dependency on slip	Does not show the effect of pressure, nonlinear constants	---
5	Burckhardt [66]	$F(s) = c_1(1 - e^{-c_2 s}) - c_3 s$	Simpler model than No. 3	Does not show the effect of pressure, nonlinear constants	---

6	Burckhardt [66]	$F(s) = c_1\sqrt{s} - c_2 s$	The most simple model	Does not show the effect of pressure, nonlinear constants	---
7	Gustafsson [67]	$\mathrm{S(t)} = \mu(\mathrm{t})\,(\frac{1/k}{\delta}) + \mathrm{e(t)}$	Includes K (Stiffness, although the problems form No.5 is in here too) and can consider error from the noise	Complicated calculation that makes it really difficult to understand and apply on any system, slip is a function of μ, although it is counted as advantages by the writer but it does not make much sense	The model is backward, slip is function of friction coefficient
8	Gert Heinrich [54]	$\mu \approx \mu_c(1 + \frac{\pi\sigma_0 h \mu_c}{L} j''(\sigma_0, \omega, T)$	Shows the effect of temperature, pressure, shear and angular velocity	No hysteresis friction coefficient	Although this model seems to be complete model, still there are some doubts about the effect of hysteresis on rubber friction coefficient

2.3.3. Case study: experimental friction analysis for tyre application

In 2011, Korunovic [8] carried out experimental study and FEA modelling of tyre on a drum test. The experiments were performed under steady-state conditions for measuring the braking force and cornering force. Figure 2-26 presents the schematic of their experimental facility for friction measurement including the linear friction tester and the specimen.

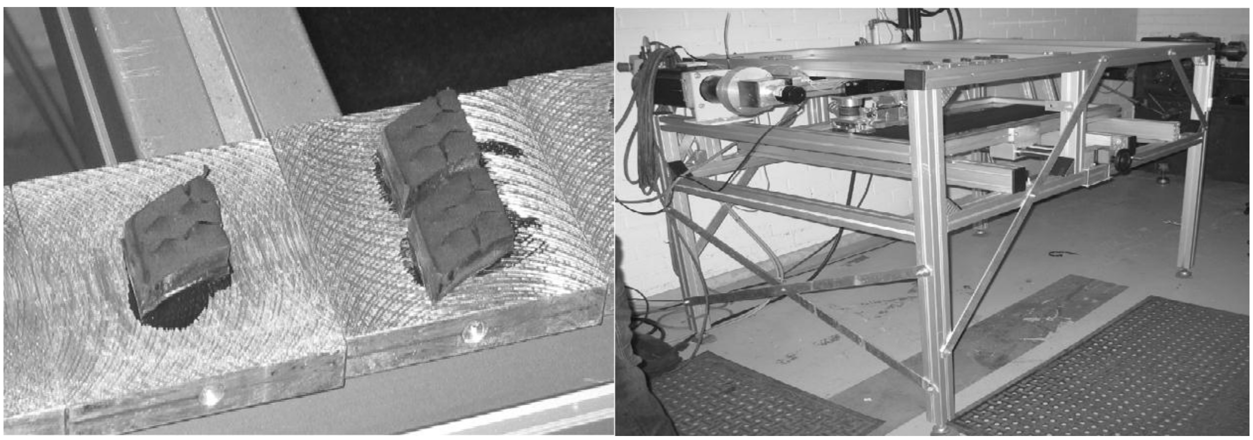

Figure 2-26 Tyre samples and linear friction tester [8]

Friction coefficient was measured by the linear tester against sliding velocity and contact pressure. A surface was fitted to the experimental results as shown by Figure 2-27.

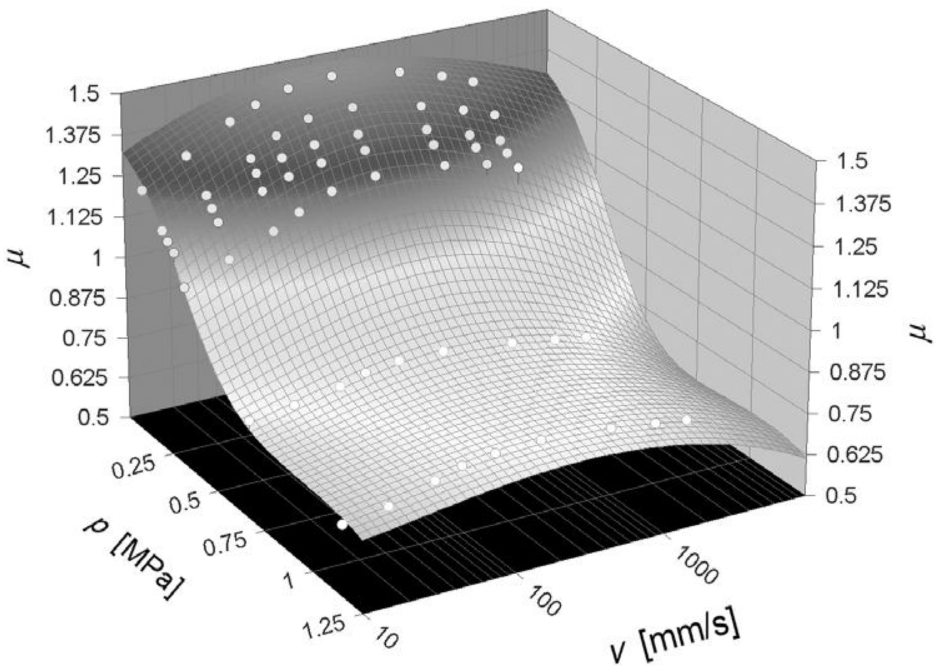

Figure 2-27 Friction coefficient vs pressure and sliding velocity [41] [8]

The experimental results were compared against the FEA results both with constant friction coefficient as well as calibrated friction coefficient, as it is illustrated in Figure 2-28 [8]. As it is evident, the FEA results are in a good agreement with the experimental data, though, the results are only limited to sliding friction coefficient and are not necessary valid for simulating rolling tyre with different slips.

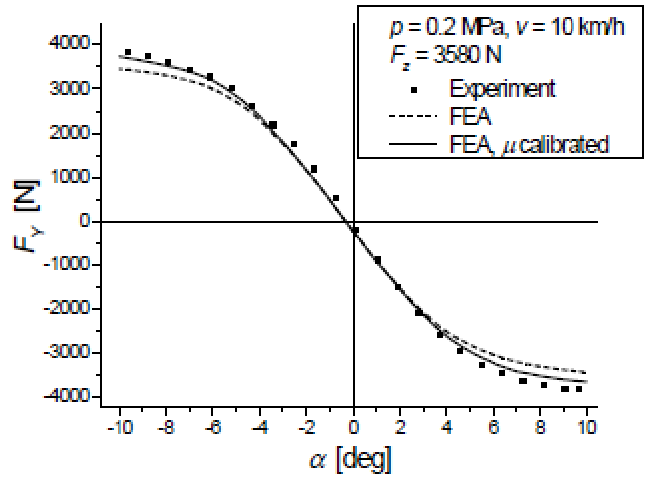

Figure 2-28 Experimental and FEA of the side force [8]

2.4. Summary and conclusions

To sum up, this chapter is divided in two parts as rubber friction and tyre friction theories and modelling studies. In the former, a brief description on rubber friction theories and effective parameters on this phenomenon were discussed, then mathematical and experimental frictional models were described and the efforts in trying to apply rubber friction coefficient in different conditions were explained. In the latter part, tyre properties and the importance of rubber on its frictional behaviour were described. It was shown that several researchers tried to develop new models for friction coefficient whether it is based on mathematical models or obtained by experimental studies.

Because of the complex nature of rubber friction attributed to the large number of parameters involved and the changes in those characteristics that depend on compression and velocity, none of the developed models are able to predict or represent an accurate behaviour of rubber. Therefore, several assumptions were taken into account to simplify them. Moreover, achieving the friction coefficient in these models often requires conducting several experiments. Besides, some of the proposed models for the prediction of rubber friction involved several constants (i.e. surface morphology) and hence implementation of such models could be prohibitive in terms of functionality for industrial applications. In addition, some models were limited only for some certain surface asperities and cannot be extended for various surface types.

The complexity that was inherent within the rubber friction got more complicated when applied for predicting tyre behaviour. This is due to additional critical factors that affect tyre friction such as slip and tyre stiffness. Therefore, it is aimed to provide a friction model to cover the effective parameters (such as material property, pressure, temperature, velocity, surface asperities and slip) on tyre friction for vehicle modelling. Furthermore, developing majority of the reviewed models required numerous time-consuming and costly experiments with several coefficients without any physical background. Moreover, some of the developed models were applicable only to a narrow range of slip or to limited number of operating conditions. All these deficiencies make the reviewed tyre modelling ineffective and expensive for industrial purposes. In addition, there is lack of published studies that investigated the implementation of the tyre friction models into FEA packages (i.e. ABAQUS) to replace the constant friction coefficient (Coulomb law) for further improvement in predicting tyre behaviour in various driving conditions.

Therefore, it is required to design an experimental facility to measure rubber friction dependent on effective parameters (i.e Contact pressure, velocity). Moreover experiments against different surfaces (smooth, fine and rough) in different conditions such normal loads and velocities have to be carried out. A friction model based on the experimental outcomes has to proposed and then the friction coefficients has to be applied on a tyre in FEA packages and the results between the obtained friction and model and constant friction coefficient (Coulomb law) has to be compared.

3. Experimental Facility

3.1.Introduction

In the literature review that was presented in chapter 2, the dependency of rubber friction on different parameters was described. It was explained that several studies, in which rubber friction was measured have employed diverse analysis methods and developed various models.

In order to cover the parameters that affect rubber friction, several friction tribometers have been developed. In general, the purpose of rubber friction measurements is to apply them in tyre modelling and provide a system that simulates an environment similar to a rolling tyre. This process is not straightforward; therefore many of the experimental facilities that have been used did not provide valid results. In this research it was intended to describe different test beds for friction measurements and explain the design and the apparatus of the experimental facilities.

3.2.Background

In this section a brief description of rubber friction experimental facilities is presented. Figure 3-1 shows different test rigs for measurement of elastomers. In the illustrated models, by changing the speed of counter-surface and the samples, different longitudinal slips are calculated. Based on the force sensors, which are in use for the experiments, force or friction coefficient against slip is obtained [68].

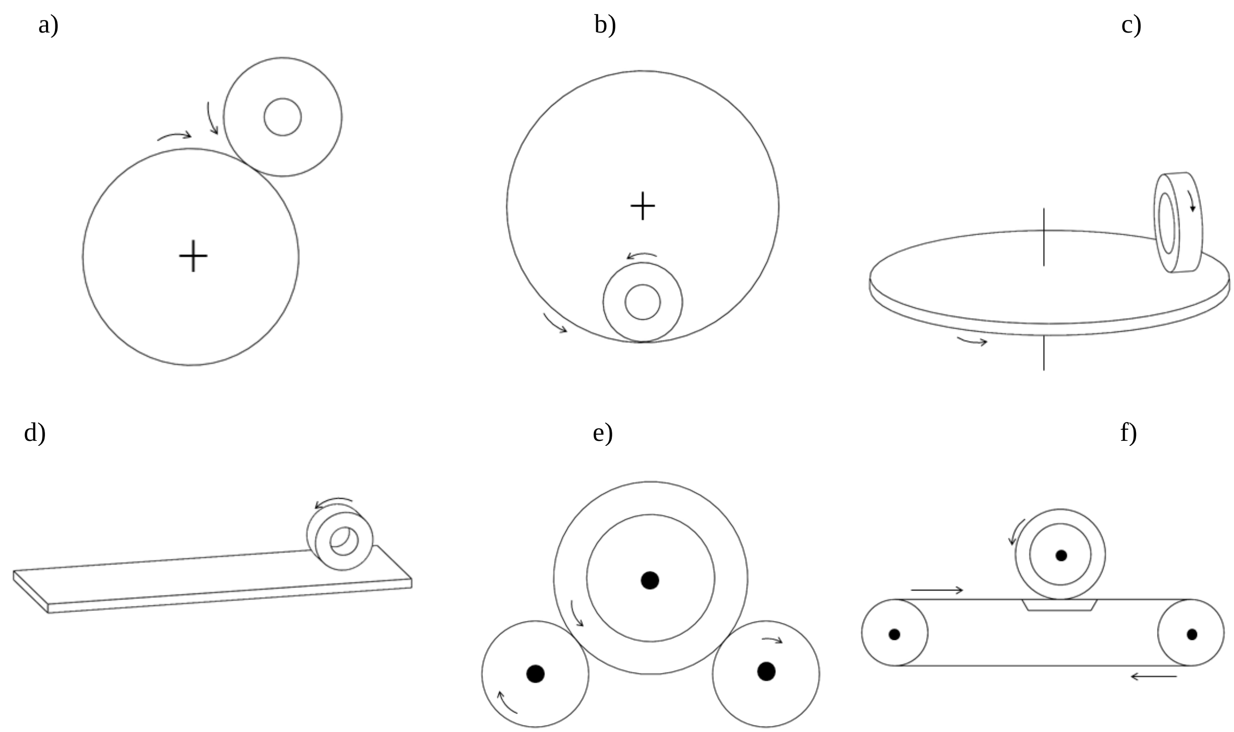

Figure 3-1 Friction tribomoters for elastomers, adopted from [68]

Tyre friction is modelled with two methods:

- Modelling rubber friction and its application on tyre dynamics; this modelling is based on empirical results, as they were revised in Table 2-3
- Analysing and testing a tyre, and expanding model for the applications (refer to Table 2-6)

It is essential to add that different test benches are used for this purpose and the goal is not only to model friction, but also to observe rubber/tyre behaviour [8, 9, 23, 46, 47, 59, 69-72].

Both methods have their own advantages and drawbacks; experiments on rubber specimens in different conditions show friction dependency on different parameters and since test could be carried out in controlled environment, monitoring the effect of the parameter is easier than when the experiments are conducted on a tyre. Although tyre experiments are more realistic and includes the tyre behaviours, controlling the test environment is not as convenient as the rubber experiments.

Also it is known that friction coefficient is not a material property and it is a way to describe a system [73], therefore, there are factors (e.g. tread and other materials used in a tyre) that influence the friction force and it cannot be measured easily with testing rubber samples. Thus, conducting experiments on tyres against different surfaces with lubrication and obtaining different contact pressures and slip velocities is challenging.

3.3.Description of the test rigs

Two experimental setups were manufactured and examined to deliver the results for this study: 1) a common pin on disc tribometer and 2) a rotating pin on rotating disc. The first rig did not provide expected results; therefore a second rig was designed and manufactured to overcome the initial problems. In this chapter the apparatus of both test beds is described and the deficiencies of the first rig are discussed.

3.3.1. Pin on disc tribometer

The first experimental facility, which has been designed and produced for this research was a pin on disc tribometer. The design for this rig was based upon pin on disc standard [14], meaning that in this apparatus a pin is in contact with rotating disc, the normal load is applied on the pin by adding weights on top of the arm that carried the pin, and the speed on the disc is controlled via a speed controller. Two strain gauges were mounted on a steel plate; one end of this plate was fixed and the other end is attached to the carrying arm, therefore it acts like a cantilever beam and by measuring the deflection of this plate, using the strain gauges, the amount of friction force is measured. In Figure 3-2, the 3D design of the rig using SolidWorks is shown and the in Figure 3-3 the manufactured rig is presented.

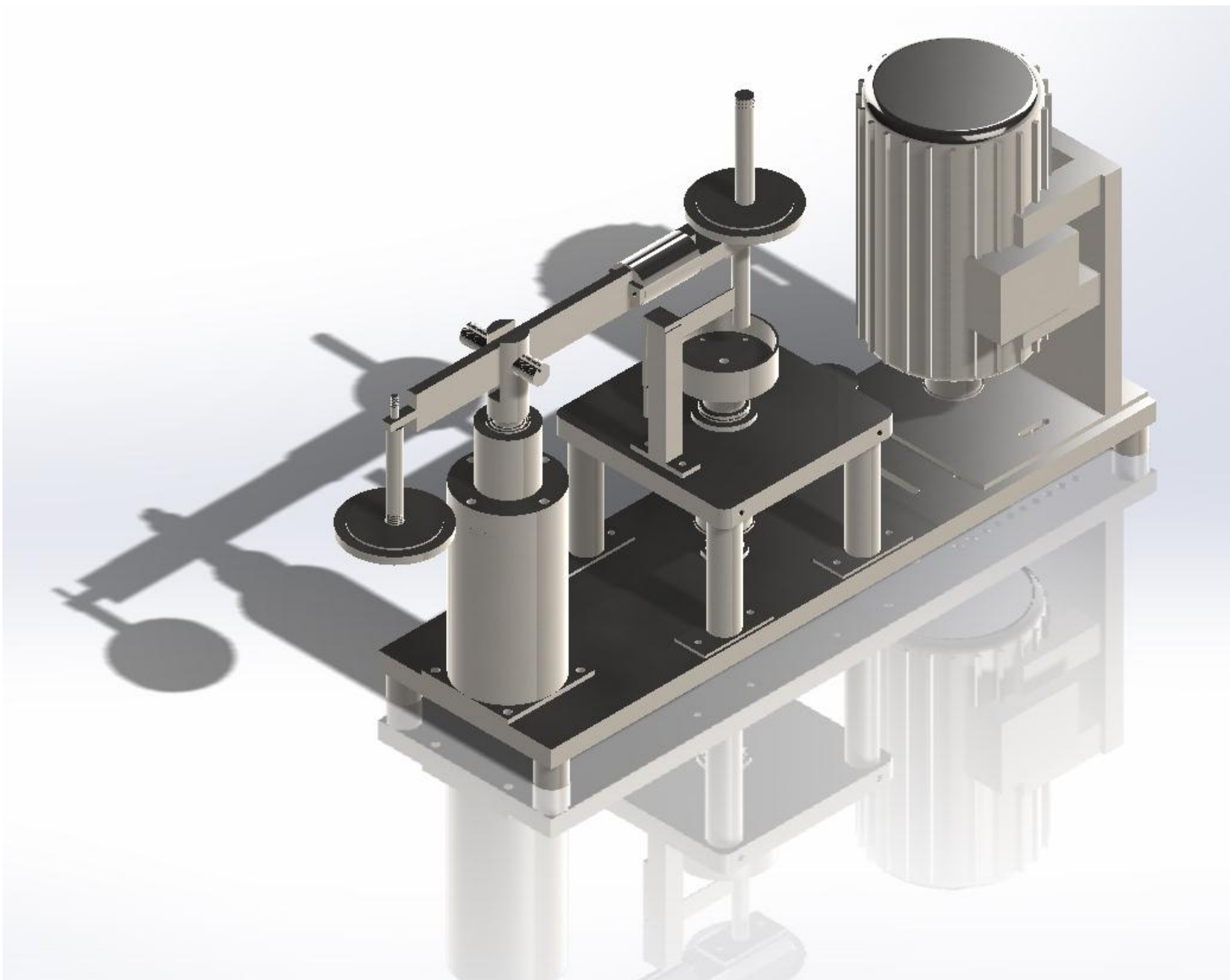

Figure 3-2 Pin on disc 3D design

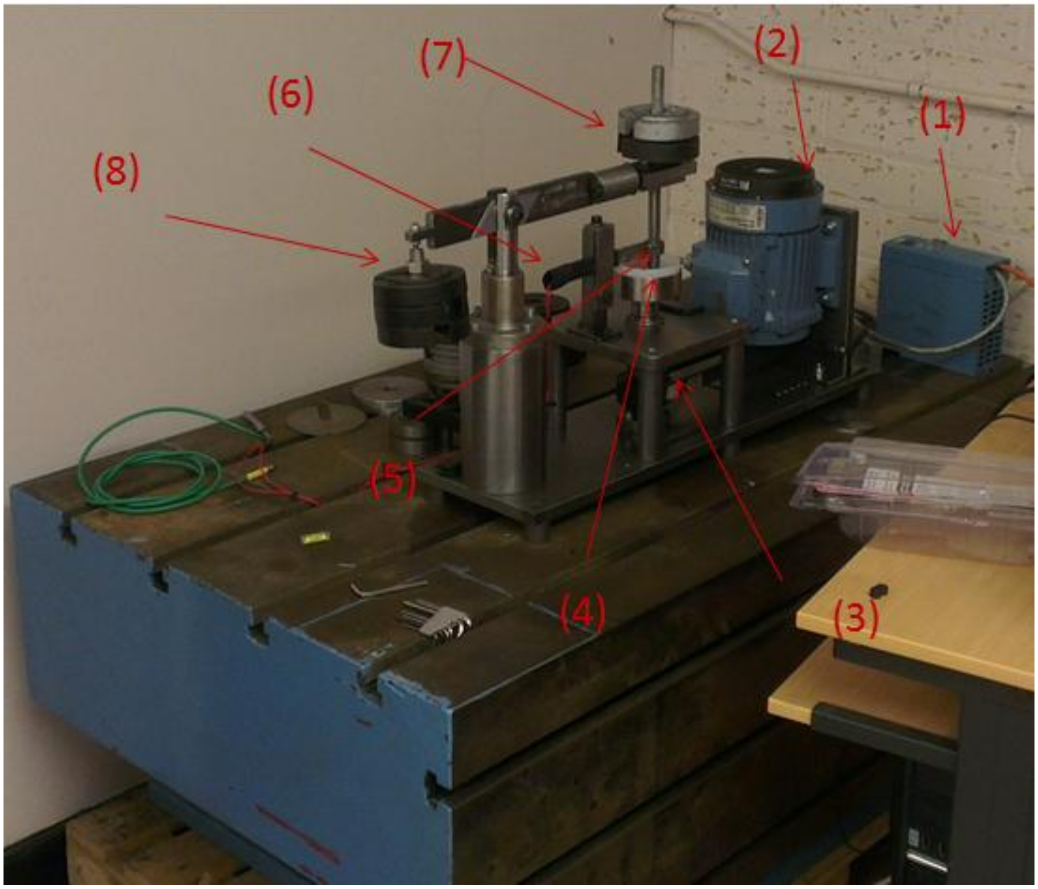

Figure 3-3 Pin on disc tribometer

In Figure 3-3, the components has been numbered and the numbers are described in Table 3-1

Table 3-1 Pin on disc components

Number	Component
1)	Motor controller
2)	Motor
3)	Drive belt and pulley
4)	Disc and lubricant container
5)	Pin
6)	Strain gauges
7)	Normal load
8)	Balance weight

3.3.1.1. *Pin on disc test rig design procedure*

In order to select the motor and the normal weight applied on the pin, a calculation was made based on a force equivalent to a quarter of the weight of a vehicle on the tyre contact patch (Footprint), then the amount of contact pressure was related to the pin samples and the results are shown in Table 3-2.

Table 3-2 Pin on disc load specification

	Tyre	Test specimen (D=9 mm)
Footprint (mm^2)	16500	63.62
Load (N)	3000	11.45
Contact Pressure (MPa)	0.18	0.18

Table 3-2 shows that the amount of normal load for the experiment is 11.45 N. To cover a higher range of normal loads to show a safety factor of 2.4 was considered; therefore the amount of maximum normal load would be 27.99 N, which is equal to 2.86 Kg.

In tyre simulations friction coefficient is estimated to be around 0.9 and 1, and in the current study, by examining rubber samples against smooth surfaces, higher friction than the expected value was obtained. Therefore, for further calculations and selection of facilities, friction coefficient of 1 was employed. The distance between the centres of the pin and rotating disc was approximately 4 cm, therefore it was assumed that the torque generated between the disc and the pin is roughly 1.12 N.m. Furthermore, this value was used as a guidance for selecting the motor.

Table 3-3 Pin on disc specification-2

Maximum Normal F(N) (Safety factor=2.4)	27.99
Max μ	1.00
Tangential Force(N)	27.99
Avg. Radius(m)	0.040
Torque(N.m)	1.12

In order to obtain the result from strain gauges, it was necessary to perform their calibration; in the next section this process is explained.

3.3.1.2. *Strain gauges calibration*

The output of the strain gauges had to be converted to force to show the amount of the friction force. For this purpose the gauges were calibrated using weights. The steel slide with the strain gauges on it, was located on a bench in a similar condition to the way it is mounted on the rig. Then weights, in 100 grams increments, were hung from the slide and the strain value was recorded. After finding strain for several loads a relation between the strain and force was obtained and it was used for the experiments. Figure 3-4a show the steel slide while mounted on the rig and Figure 3-4b shows the strain gauges on it during calibration.

a)

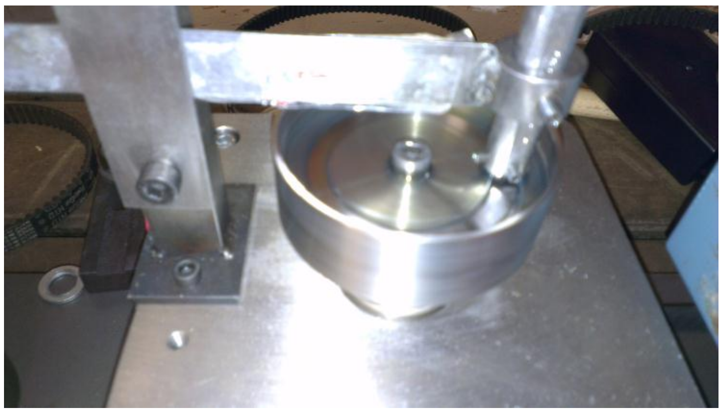

b)

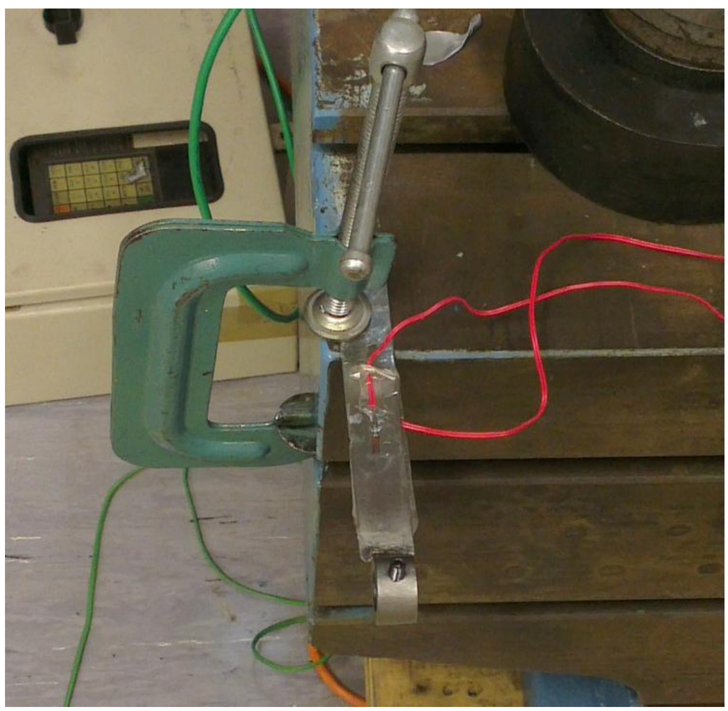

Figure 3-4 a) Strain gauges on the rig b) strain gauges during calibration

3.3.1.3. *Deficiencies of the rig*

It was explained in details in chapter 2 that tyre friction depends on various parameters, and slip ratio is one of the most significant factors in determining tyre friction. The first pin on disc friction tribometer developed was unable to provide an appropriate friction model for tyres. In order to understand this deficiency it is necessary to grasp the concept of the slip ratio. The formula for the slip ratio is shown in Equation 3-1.

$$slip\ ratio = \frac{|r\omega - V|}{Max(r\omega, V)} \qquad \text{Equation 3-1}$$

Where r is the radius of the tyre, ω is the rotational velocity and V is the linear velocity of a vehicle.

3.3.1.4. *Limitations*

In this experimental facility, the pin represents the tyre and disc represents the vehicle; since the pin is fixed, and it does not have any velocity, it makes the formula equivalent to velocity of the disc divided by the same value, which is equal to 1, meaning that friction coefficient obtained from this facility is the skidding friction coefficient. Therefore, it was decided to design and manufacture a new facility to allow the pin and disc to rotate at the same time with different speeds for obtaining friction coefficients in a range of slip velocities ($r\omega - V$).

3.3.2. Rotary pin on disc tribometer

This new setup is derived from the apparatus of an imposed pin-on-disc tribometer [74] and is modified to cover the requirements for the current project. In the imposed pin on disc, the pin and the disc rotate around their own axes. The schematic of the setup is illustrated in Figure 3-1-b.

The general design of the tribometer is similar to the aforementioned rig, but in this experimental bed both pin and disc rotate around the same axis. The justification for this change and outcome of the test is shown in the next section. Moreover, the contact area of the pin was increased in order to make a better contact with counter surface than in a standard pin-on-disc tribometer [75]; the radius of the pin varies between 3 mm to 10 mm, and since for elastomers small specimens do not show the bulk properties of the material and bonds form easier when the contact area is greater, in this rig the radius of the pin was selected to be 10 mm. In this setup it is possible to examine one or two pins against a rotating counter-surface. Both the disc and the pins are rotating with two separate motors and speed controllers; therefore by providing different speeds various slip velocities are achieved.

In this experimental setup the motor rotates the shaft via a drive belt and the shaft is connected to the disc. A torque sensor is mounted on the shaft and measures the rotary torque of the shaft. When the disc is rotating with no contact with the pin, the sensor records a value caused by internal friction of the rig (bearings and etc.). On the other hand when the disc is in contact with pins the friction causes changes to the torque reading and the difference between this reading and initial value of the torque is the result of the friction force; in Equation 3-2 this value is more rigorously defined. The detailed procedure for the obtaining the parameters in this equation is described in the following sections.

$$Torque_{Friction} = torque\ Reading\ - Internal\ torque \qquad \text{Equation 3-2}$$

Equation 3-2 is the main calculation for friction measurement in this facility; it will be modified in 3.3.4, where the rig calibration has been assessed.

The pins, mounted on two locations above the disc, are rotated by the second motor; the shaft which rotates the pins is connected to the motor through a plate and a spline coupling. The plate carries the weights for providing different normal load ranges. When the normal load is applied on the pins, the weights push the pins down to keep them in contact with the rotating disc, in order to keep the contacts between the pins and counter surface, as the pins are abraded. There are four linear bearings mounted on the plate to move the whole part vertically towards to the disc. To prevent the weight of the component from affecting the normal load (such as the plate, bearings, spline hub) four springs are placed under this plate; the location of the springs could be adjusted dependant on the size of the pins.

Figure 3-5 shows the design of the test bed, and Figure 3-6 a & b, show the experimental setup with components in details.

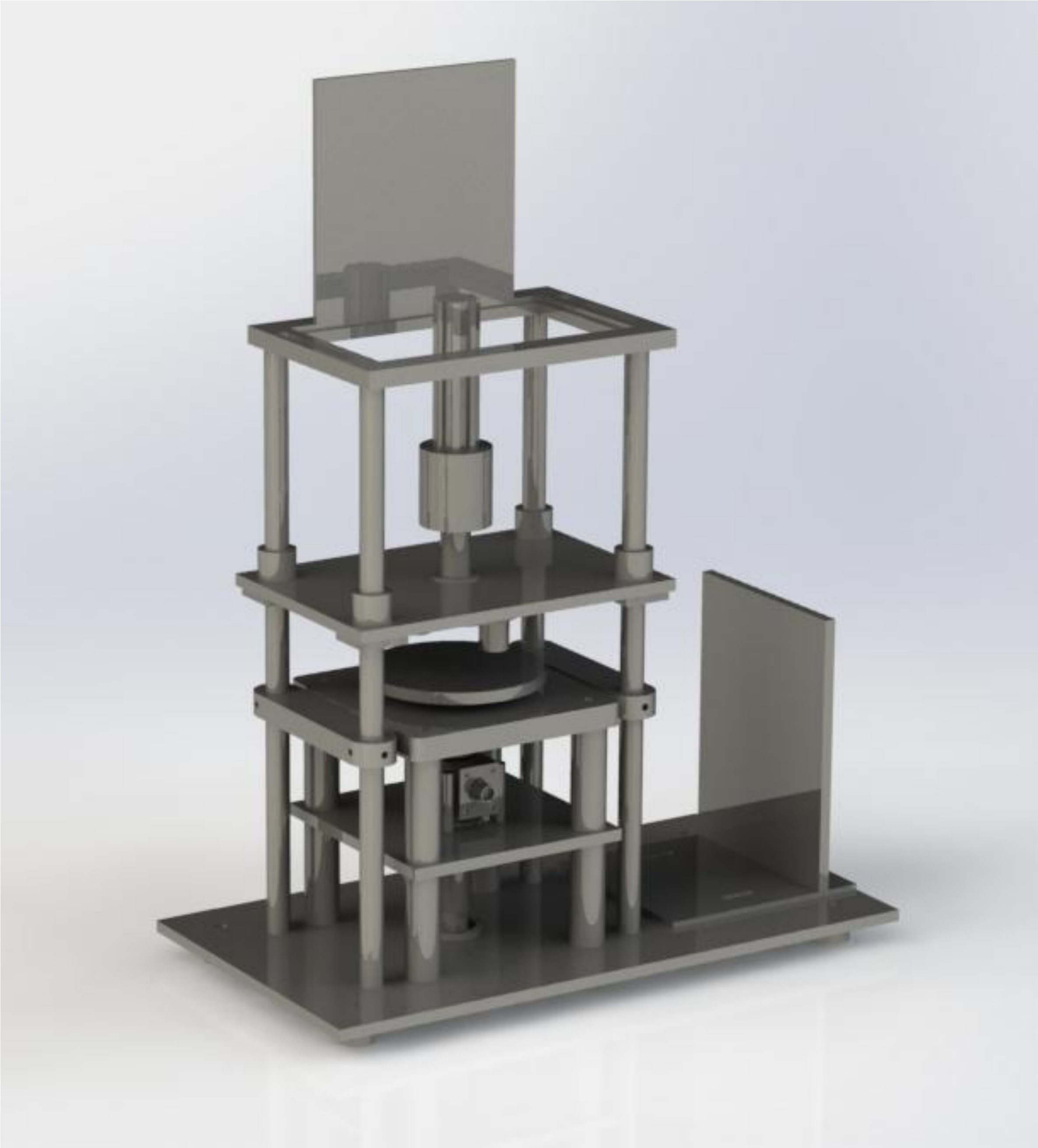

Figure 3-5 Rotary pin on disc

a)

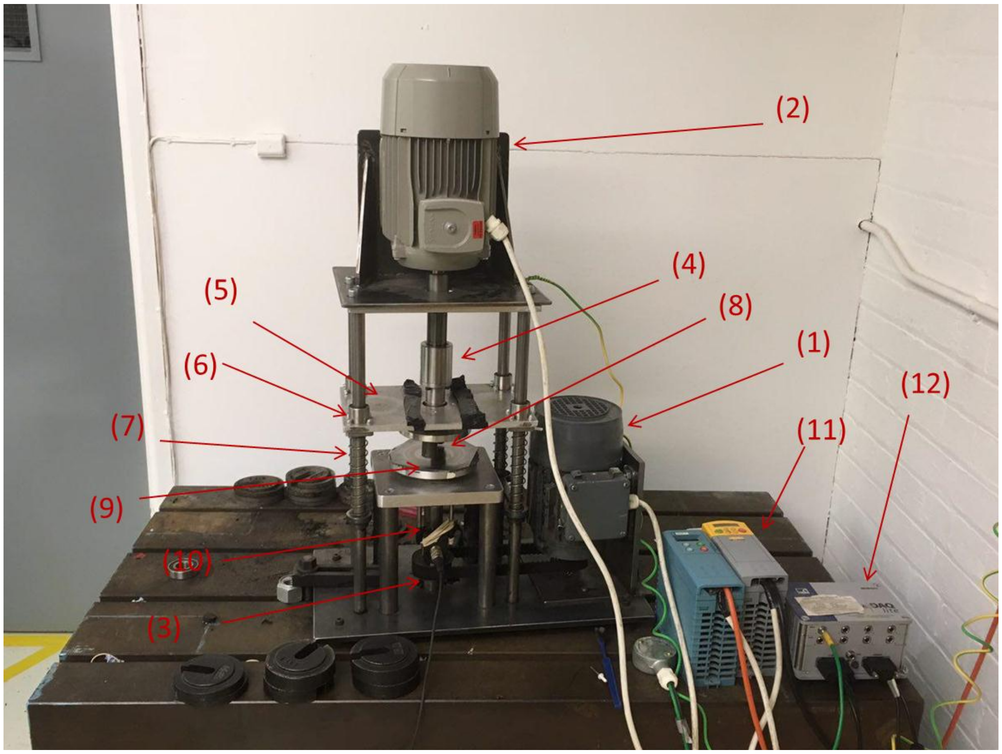

b)

Figure 3-6 a &b) Rig apparatus

In Figure 3-6-a, the components of the rig are numbered and their description is as follows:

Number	Component
1)	Motor 1-Drives the disc
2)	Motor 2-Drives the pins
3)	Drive belt and pulley
4)	Spline coupling (shaft & hub)
5)	Weight plate
6)	Linear bearings
7)	Springs
8)	Pin holders
9)	Disc
10)	Torque sensor
11)	Motor controllers
12)	Data logger

3.3.2.1. *Calculation of specifications*

Selection of the motors and the sensor was based on calculation for tyre modelling. The amount of normal pressure on the pins was calculated from the amount of the normal load on the contact patch of a tyre.

Table 3-4 Normal pressure calculation

Parameters	Tyre	Test specimen (D=20 mm)
Footprint(mm^2)	16500.00	314.16
Load(N)	3000.00	57.12
Contact Pressure (Mpa)	0.18	0.18

As it shown in Table 3-4 the footprint for the tyre selected for the analysis was 16500 mm^2 and the normal load of a quarter of a vehicle was 3000 N, therefore contact pressure was calculated considering those values. As discussed earlier the radius of the pin is equal to 10 mm, consequently it makes the normal load on the pin equal to 57.12 N. This was a general guideline for further calculations, which are explained below.

In order to cover all ranges of data in the study, a safety factor of 2 was introduced into experimental results (This means the facility were capable to measure the friction force, two times higher than the value for a vehicle). Also it was assumed that the maximum friction coefficient for a tyre would be equal to 1 (according to literature this value is applicable for rubber against sandpaper, and higher values could be obtained when rubber is in contact with smooth surfaces such as glass), therefore the amount of tangential force was calculated and this value served as a basis for obtaining the amount of torque. The calculation is shown in Table 3-5. It is important to add that the average radius is the distance between the pin and the centre of the drive shaft.

Table 3-5 Torque calculation

Safety factor	2.00
Maximum Normal F(N)	114.24
Max µ	1.00
Tangential Force(N)	114.24
Avg. Radius(m)	0.040
Torque(N*m)	4.57

3.3.2.2. *Motors*

There are two motors mounted in this rig, Motor 1 (Brook Crompton/200175), which drives the disc to rotate with maximum torque of 4.5 N.m and Motor 2(Siemens/iec en 60043), which rotates the pins and provides maximum torque of 10 N.m.

3.3.2.3. *Drive controller*

As it was mentioned earlier the velocity of the motors is controlled by two inverter drives (Parker AC650, 1.5 kw), which control the motor input voltage frequency, and this provides the ability to control the motor output (i.e. velocity) by changing the voltage. The controllers have a digital display and in order to find the velocity of the disc and the pins a laser-tacho meter was used. It is necessary to consider that inverters do not keep the velocity constant and during the experiments the velocity varies dependant on the load and contacts.

3.3.2.4. *Laser tachometer*

The rotational velocity of the motors was measured by a laser tachometer (CT6/LSR). The tachometer shows the rotational speed of the components, which is controlled by the inverter drive.

3.3.2.5. *Torque sensor*

Calculation of the amount of friction force was conducted by measurement of the torque by a torque sensor; the rotary torque sensor is located on the shaft, which is driving the disc. Rotary torque sensors measure the torque along the shaft by considering the torsion on each end of the main shaft of the sensors.

A series of tests was carried out to calibrate the rig; these tests show the amount of initial torque caused by internal friction of the rig and moment of inertia of the disc. This subject is discussed in the rig calibration (3.3.4) in detail.

The torque sensor chosen for this experimental setup was a Futek (TRS300, shaft to shaft), which can tolerate maximum torque of 10 N.m and maximum speed on 3000 RPM. It was calibrated by the manufacturer and the values for torque and voltage was presented in the calibration certificate.

3.3.2.6. *Data acquisition*

The sensor was connected by a data acquisition system (i.e. Somat eDAQlite) to a computer, and all output data was recorded during the experiment. The data logger supports different strain gauges and bridges; there is specific software (i.e Somat Test Control Environment, TCE) for operation, which has the ability to convert the voltage from the torque sensor into torque based on the calibration of the sensors.

3.3.2.7. *Slip measurement*

It was mentioned earlier that in this facility, it was aimed to measure rubber friction against slip velocity; the formula for the value was shown in Equation 3-1. As it was explained this facility was developed based on an imposed pin on disc rotation, Equation 3-3 shows the formula to calculate the slip ratio in such facilities:

$$slip\ ratio = \frac{|(r_{Pin} \times \omega_{Pin}) - (R_{Disc} \times \omega_{Disc})|}{Max(r_{Pin} \times \omega_{Pin}, R_{Disc} \times \omega_{Disc})}$$ Equation 3-3

To apply this formula on the rig, Equation 3-4 was generated, in this formula the velocity of the pin and disc in this facility was replaced and then the radius was omitted from the equation, therefore the formula will be the difference of the velocities of the pin and disc divided by maximum velocity:

$$slip\ ratio = \frac{|\omega_{Pin} - \omega_{Disc}|}{Max(\omega_{Pin}, \omega_{Disc})}$$ Equation 3-4

3.3.2.7.1. *Difference of imposed pin rotation and rotary pin*

It was explained earlier that the initial rig was modified from the imposed pin on disc tribometer (Figure 3-1 b), which included the pin rotational direction change for the utilized tribometer. The reason behind this modification was to introduce the slip measurement into the system. While in imposed pin on disc tribometer the rotational velocity is constant for the whole pin, the velocity for centre of the pin (where r = 0) is zero, therefore the slip in the centre is also equal to zero. In rotary pin on disc tribometer, the whole pin is rotating around the main axis and for slip measurement the difference between the pin centre to the disc centre is used. Figure 3-7 shows the schematic of the contact area of the both facilities.

a)

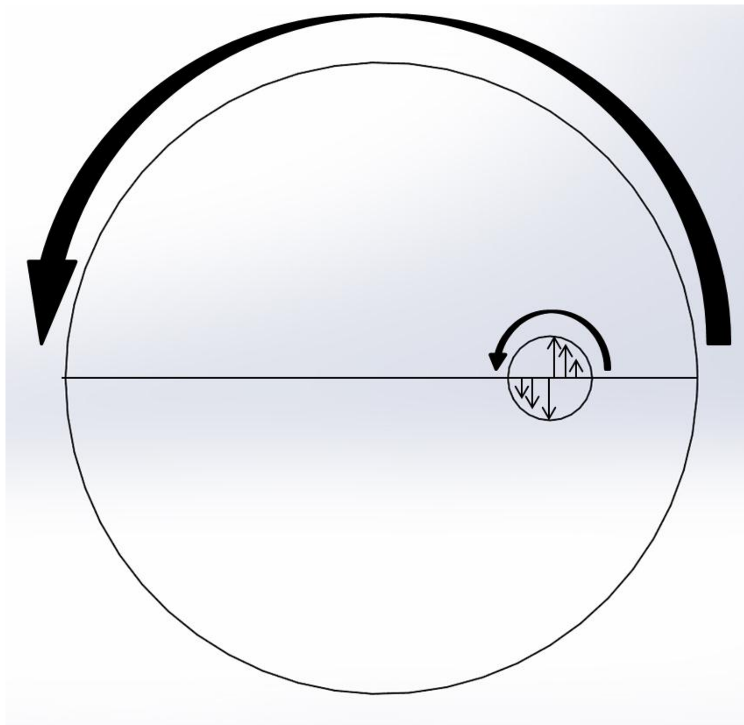

b)

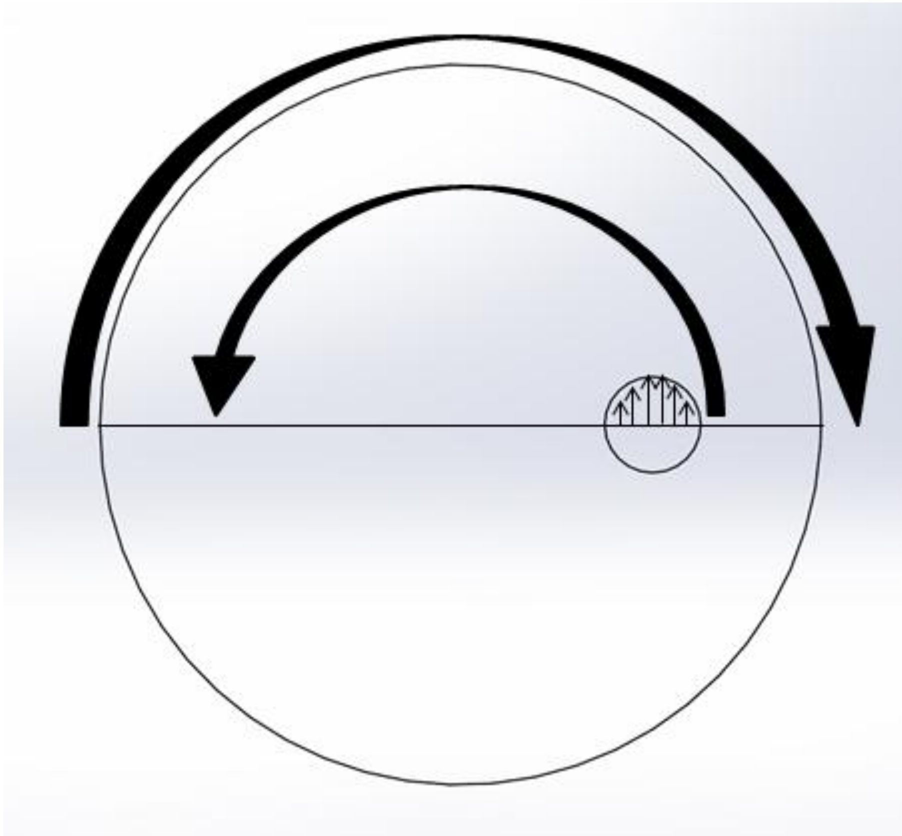

Figure 3-7 Rotation and shear forces for two cases of a) Imposed pin on disc vs. b) rotary pin on disc

3.3.3. Result processing

In general, the result from the sensor has high amount of noise, which makes raw result hard to interpret and therefore renders it unusable. There are three main reasons for the high amount of noise in this facility (as explained below in details); the first two reasons can be attributed to a modification of the manufactured rig and original design (as there were some changes in the setup to make it operational).

- Shaft alignments: Although all the facility compartments were machined with high accuracy, it is hard to avoid the miss-alignment of the shafts, especially when there are several components attached to each other.
- Rig vibration: The rig was going through vibration especially in a specific range of speed for one of the motors, as it was reaching its natural frequency. There were attempts to fix several points of the rig to the plinth with clamps and the performance was improved although it was not removed completely.
- Electrical noise: There was an electrical noise on sensor coming from power cable, this noise was temporary and its interference was detected in some of the experiments.

To remove the noise from the results, a low-pass filter was applied to the raw data using MATLAB. Low-pass filter was considered appropriate for these data after applying fast Fourier transform (FFT) on the collected data which showed the frequency content of the measured signals and noise. Figure 3-8 shows an example for one of the series which has been recorded, FFT was applied on it and then the processed data was shown, this process is described in detail in next sections.

a)

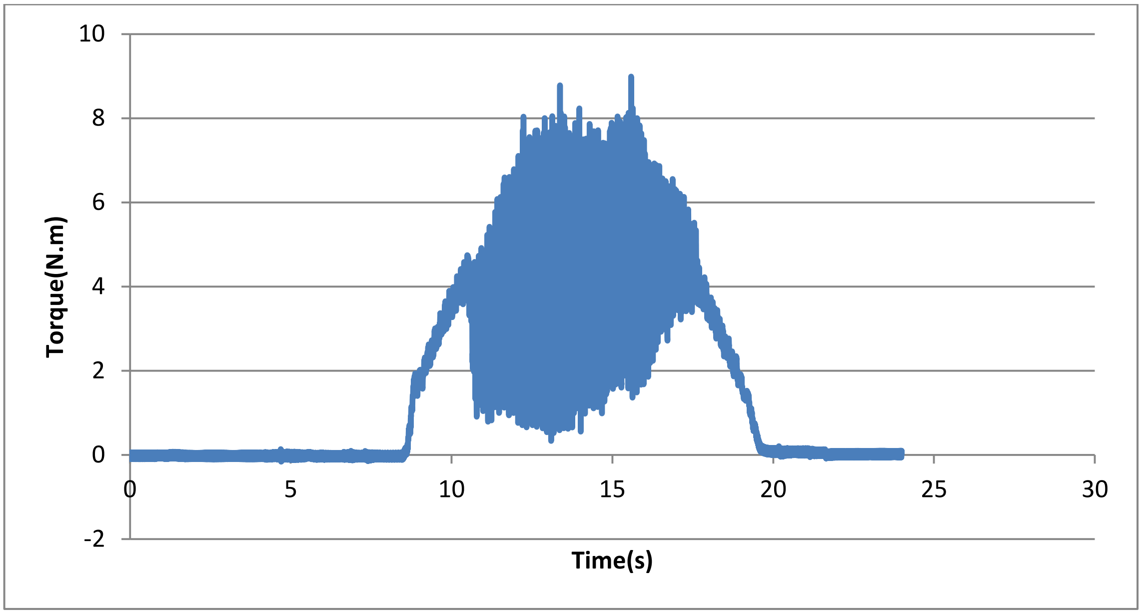
10
8
6
4
2
0
-2
Torque(N.m)
0
5
10
15
20
25
30
Time(s)

b)

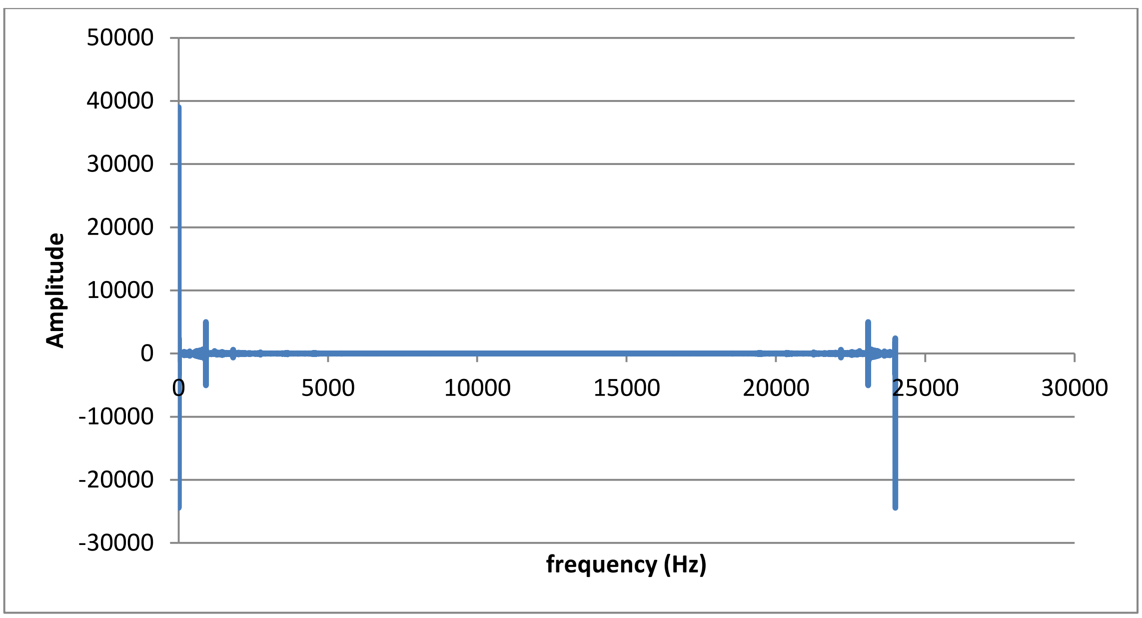
50000
40000
30000
20000
10000
0
-10000
-20000
-30000
Amplitude
0
5000
10000
15000
20000
25000
30000
frequency (Hz)

c)

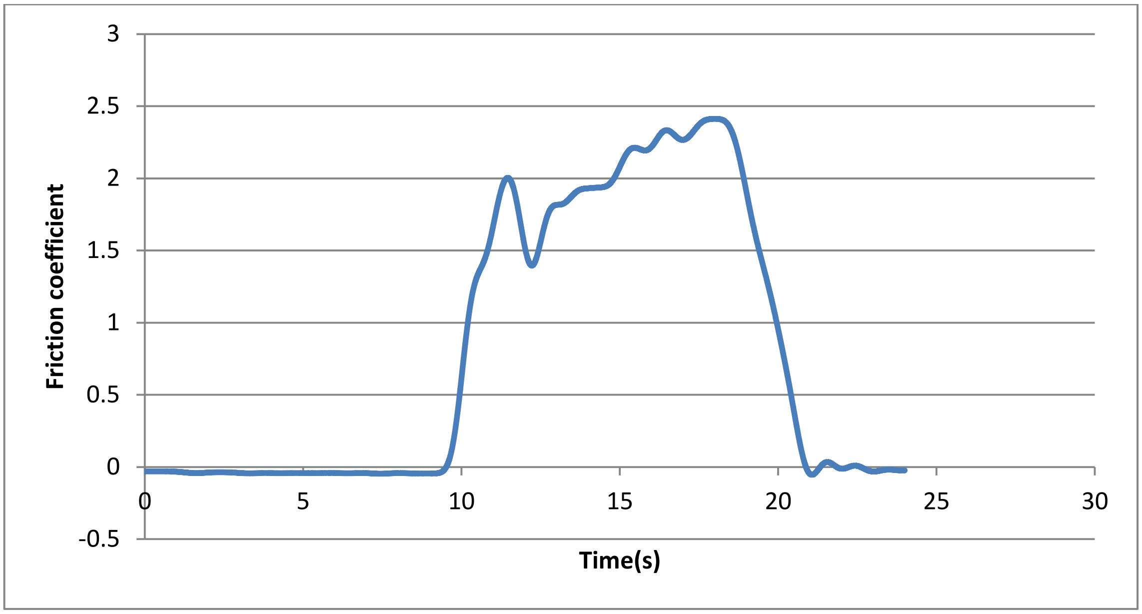

Figure 3-8 A sample (pin on steel disc, normal weight 5 kg, sliding velocity 2 m/s) for the a) raw result, b) applied FFT on it c) the processed result

3.3.4. Rig calibration

It was explained in section 3.3.2 that rig internal friction has effects on the torque reading, and its value needs to be subtracted from the reading to obtain the torque caused by pin and disc friction.This parameter is dependent on the motor specification and the generated torque is different at different velocities. For this purpose the disc was operated on its own with no contact to the pin and the torque reading was recorded. This process was repeated four times and the average was calculated and considered as rig's internal friction. The result is illustrated in Figure 3-9, where by starting the motor it was necessary for power to overcome the motor static phase, and by increasing the velocity the reading decreased slightly. When the motor velocity reached close to its maximum, the torque began to increase, which can be attributed to the disc momentum that causes higher torque value. Therefore, during the experiment, the internal friction was derived based upon disc rotational velocity and the torque reading was subtracted from the internal friction as it was described in Figure 3-9.

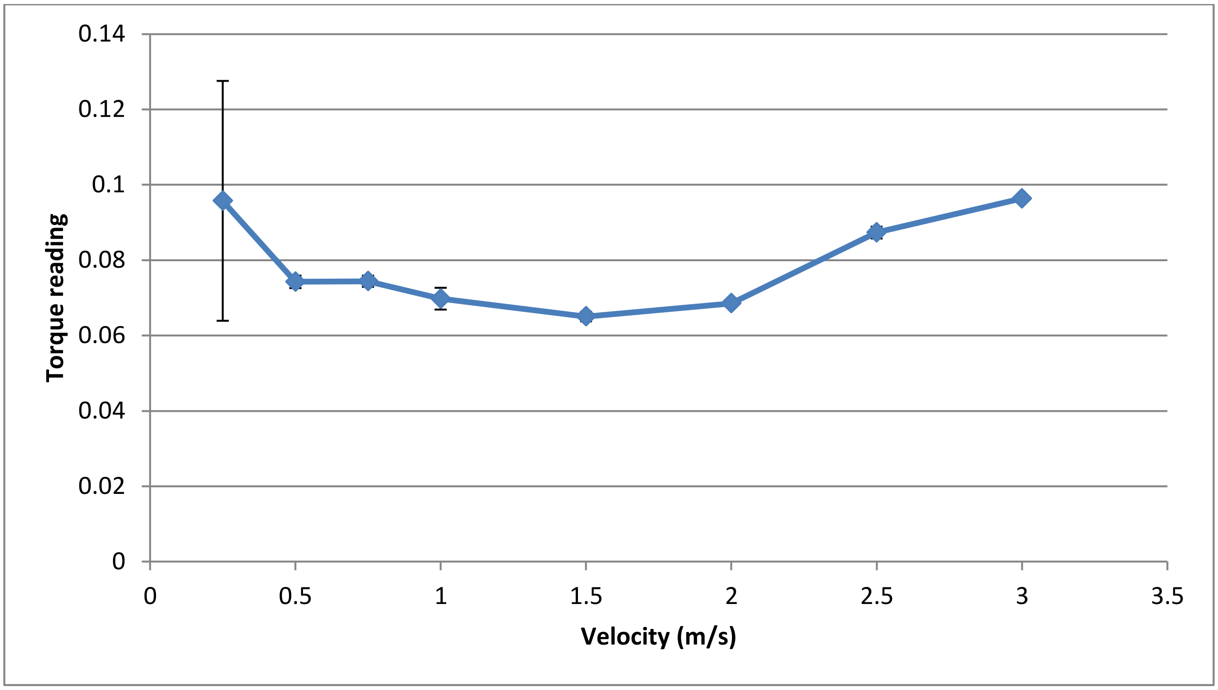

Figure 3-9 Internal torque (N.m) vs. motor velocity

3.3.4.1. *Instrument calibration, measurement accuracy and system error*

It is important for the current study to show that the facility is calibrated and the results are valid for further experiments. The concepts of accuracy and precision were employed in order to confirm the rig's calibration. A facility is defined as precise, when the results are very similar and close to each other though they may not be representing the true value, whereas accuracy is when the readings are close to the expected value, although the result may not be highly reproducible. In order to have a facility calibrated, it is necessary to show it is accurate and precise. Although the torque transducer, which is mounted on this facility, has been calibrated by the manufacturer, it is still required to show the reading is close to the real value and the setup displays the results correctly. Therefore, for this purpose, a simple experiment was designed and conducted. This process is explained in the next section.

3.3.4.2. *Experimental torque measurement*

This test had a simple device similar to a pulley, only with a capability to tolerate high loads without any deformation. A weightless rope was tied around the disc and on the other end it was holding certain amount of loads. Figure 3-10a) shows a general setup of the experiment. A similar method is used by the manufacturer to calibrate their products and this idea was obtained from their technique, Figure 3-10 b) shows their method briefly.

a)

b)

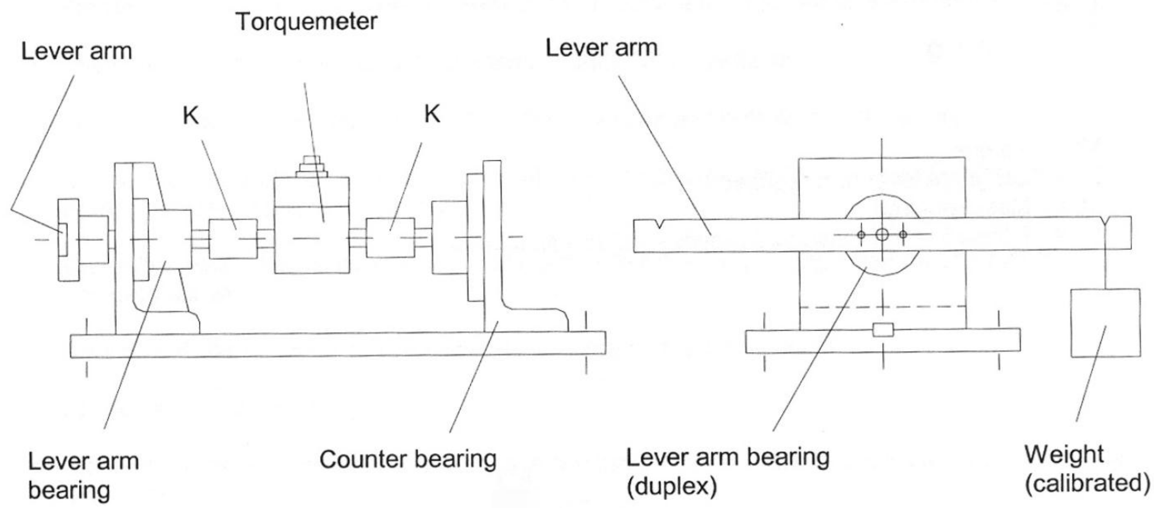

Figure 3-10 a) The setup for the experimental torque measurement- b) Futek method for torque calibration [76]

The experiment was delivered for several ranges of loads (i.e. 1, 1.5, 2, 2.5, 3, 3.5 and 4 kg), Figure 3-11 shows an example for this experiment; the test was repeated three times to show the variation in different tests.

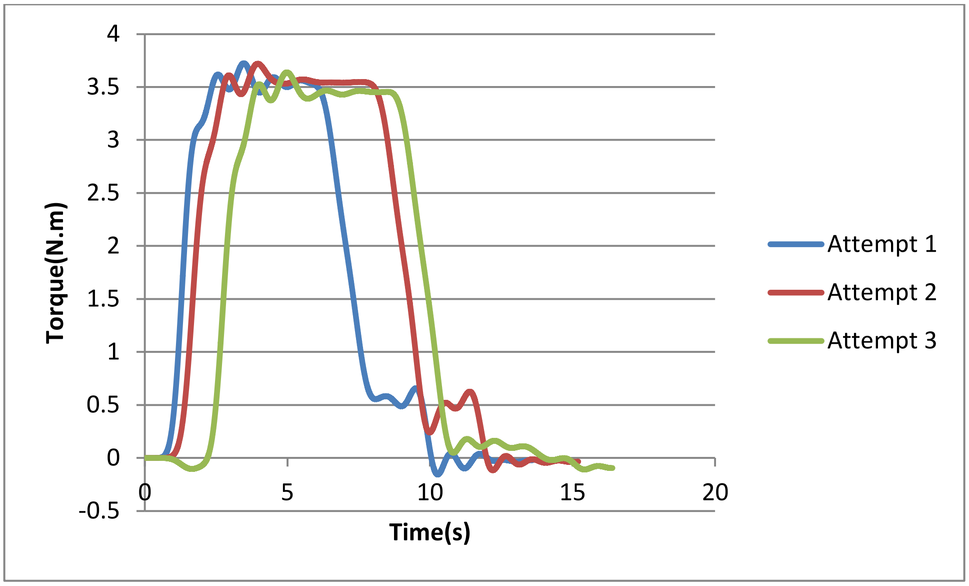

Figure 3-11 An example for torque measurement for three attempts (4 kg)

Figure 3-11 demonstrates that when the motor was lifting the weight the reading torque increased and then reached a constant, which corresponds to the period where the weights were coming up and then when the motor was stopped the reading decreased to zero. Three different tests were conducted and the variation in the results was monitored. In each attempt the average for the constant region was considered as the reading torque and average of all three tests was calculated as the final torque reading for the certain amount of load.

This process was repeated for 7 different loads and the result is shown in Figure 3-12. For each point a confidence interval of 95% is applied, it can be seen on the graph where the results were so similar and the variation was so little where the uncertainties are in a very small range.

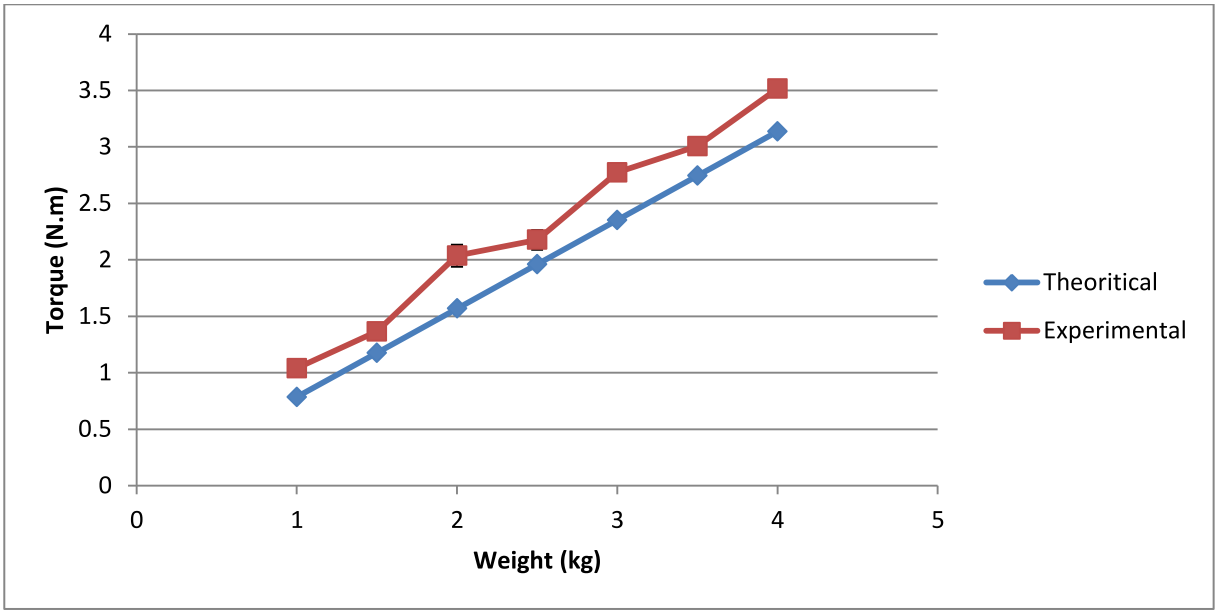

Figure 3-12 Torque measurement vs. mathematical calculation

Figure 3-12 shows that there is a constant difference between expected torque and the torque readings; this shows that the facility's output was higher than the real value by a constant. The value is almost equal to 0.3 N.m; and it was defined as the system error and the torque reading was subtracted from this parameter to make the result reasonable; therefore, Equation 3-2 had to be modified to take the system error into account, and a new equation (Equation 3-5) was generated:

$$Torque_{Friction} = torque\ Reading\ - system\ error \qquad \text{Equation 3-5}$$

In Equation 3-5, frictional torque is obtained by subtracting system error from torque reading. Internal friction is already included in the system error and it does not need to be in this equation. This parameter is created by the friction and it is used for further processing, where it is converted to frictional force and friction coefficient as it is explained further in chapter 4.

3.3.4.3. *Experimental calibration*

An experiment on a PTFE pin against a steel disc was delivered to show that experimental facility provided a valid result. Three PTFE pins were manufactured and examined against a steel disc, cleaning the disc after each test to prevent any wear and corrosion from former tests, which could influence the results. In these experiments the pin was fixed and the disc was rotating with two different sets of speeds, 0.25 m/s and 0.50 m/s. The normal loads, which were applied on the PTFE samples were 2 kg and 3 kg. The PTFE sample was in cylindrical shape, and featured a diameter of 20 mm and a height of 15 mm. Three attempts were made for each test to show the accuracy of the experiment. An example for series of tests is shown in Figure 3-13.

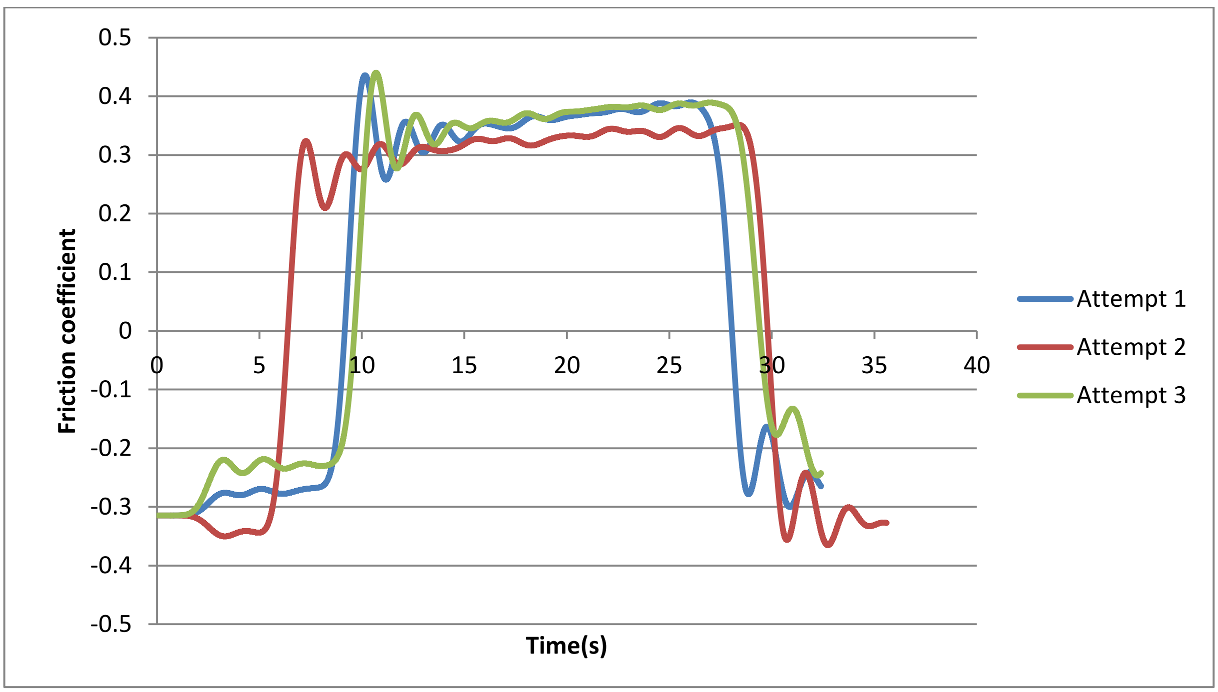

Figure 3-13 An example result for PTFE test, sliding velocity=0.5m/s, normal load=3 kg

Abovementioned figure aims to show an example result for PTFE against steel and the results and processing are described in details in chapter 4. The overall result of the experiment for both ranges of speeds and normal loads is shown in Figure 3-14.

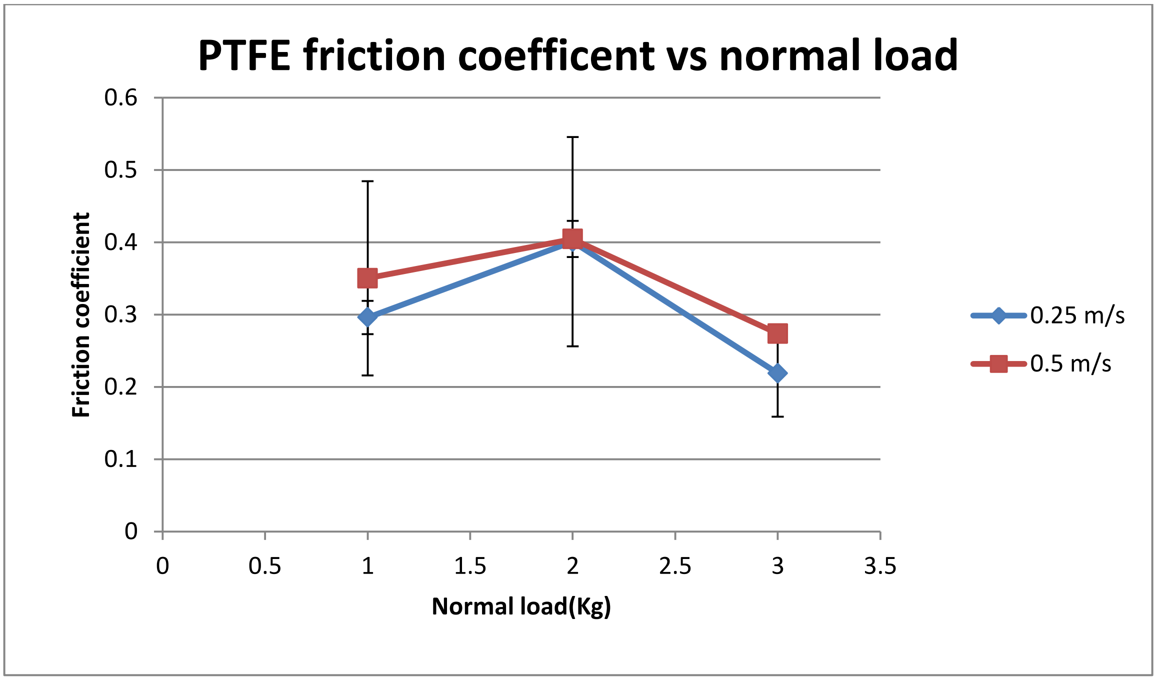

Figure 3-14 Overall friction coefficient for PTFE against steel

Although initially this research was not aiming to investigate the frictional behaviour of PTFE, this experiment proved to be beneficial for the study, as it showed that the obtained result is in the range of expected PTFE friction coefficients. Therefore, it was concluded that the experimental facility provides reasonable results and the outcome for rubber can be considered for further studies.

3.4. Conclusion

This chapter describes the aspects of the two experimental facilities, which have been designed and manufactured for the current research. The limitations of the first rig (pin on disc) were clarified and the description of the adjustments and benefits of second test rig was provided. The design and components of the second tribometer (Rotary pin on disc) were described, the main source of this facility was shown and the modifications were discussed. The experimental setup calibration has been explained and an example was shown. It was shown how a test was delivered for different surfaces and the advantages and disadvantages of the facility clarified during the experimental process were discussed and finally the result processing was described.

In brief it was explained the first experimental facility could not provide the desired result, due to the fact that it was measuring the sliding friction force of rubber and the strain gauges could not provide a steady result due to the stick and slip of rubber, since the obtained data was poor and did not provide a reasonable result, it was not discussed and explained in this research. Therefore, the second setup was designed and manufactured to overcome the problems in the first tribometer, this facility can take two pins and provide precise and accurate results. In this rig, both pin and disc can rotate to show the effect of sliding velocity; various disks with different surface roughness can be mounted to show the wear and friction of sample against several surfaces. This facility was successfully calibrated, and the effect of internal friction and the instruments error were shown. In the next chapter the tests, which were conducted for this study are described in details and operation and outcome of the abovementioned facility is shown.

4. Experimental methodology

4.1. Introduction

In chapter 3 the design, manufacturing and apparatus of the test rig was explained in details, it was mentioned that the aim of this facility is to measure rubber frictional behaviour against sliding velocity and normal load/contact pressure. This chapter elucidates the experimental process, including sample preparation, testing procedure, experimental specifications (i.e. velocity and normal load) and data processing.

4.2. Rubber/Tread samples

The focus of this research is tyre friction modelling; therefore, as discussed earlier, rubber specimen was detached from the tyre contact patch in a form compatible with the experimental facility. For this purpose the tread part of the tyre was separated from the whole tyre, so the rubber samples could be prepared from it easier.

4.2.1. Sample preparation

A specific tool with diameter of 20 mm was made to drill the rubber samples out of the tread, this process allowed to extract rubber pieces from the tread although they were attached to carcass of the tyre. Furthermore, the rubber of tread was separated from the carcass and the rest of the reinforcement of the tyre. In the last step a 3 mm hole was drilled on top of them (i.e. the place they were fixed on the rig) so they can be mounted on the experimental facility. Figure 4-1 shows different steps for pin preparation. Three tyres have been cut for this research to provide enough number of samples for the experiments.

a)

b)

c)

Figure 4-1 Sample preparation progress-a) tread was separated from the tyre sidewalls with grinders-b) a pin sized samples were drilled/punched into the tread c) tread was separated from the reinforcement by hack-saw, so the pin could be extracted

4.2.2. Size

The diameter of the pins for this tribometer was 20 mm (as mentioned in chapter 4) and the pins dimension were measured to be suitable for the experiments as they could have been damaged during the process. Figure 4-2 shows prepared sample for the experiments.

Figure 4-2 Prepared samples

4.3. Test scope

The purpose of this study (as explained before) was to examine the rubber friction dependency on velocity and normal load; therefore the tests were conducted for several ranges of normal load. Sliding velocity in these experiments was defined as the difference between the rotational velocity of the disc and the pin. The tests were divided into two categories: the fixed pin and rotating disc, which is similar to a normal pin on disc tribometer, and pin and disc rotates at the same time, in opposite directions. When the pin is fixed the disc rotational velocity is known as the test rotational velocity. In case where both pin and disc are rotating, the difference of the rotational velocity is defined as sliding velocity, as the disc is rotating with a constant speed and the pin is rotating with a higher velocity against the disc. Since the pin is rotating in the opposite direction of the disc, the value is considered as negative, there the rotational velocity is considered as the sum of both velocities. Next section describes the details of sliding velocity and contact pressure.

4.3.1. Velocity

In different experiments, which examined a wide range of linear velocities, in operation with this test bed, rotational speed (RPM) was used. The mathematical calculation to convert the rotational speed to linear speed is explained below; Equation 4-1 shows the formula that converts the rotational velocity (ω) to linear velocity (v), where r is the radius of the rotation.

$$v = r \times \omega \qquad \text{Equation 4-1}$$

In this equation ω is in rad/s and there is a need to convert this value to rpm for the purpose of the tests. Equation 4-2 shows the formula, which converts ω to rpm (where it is shown with N).

$$N = \frac{60}{2\pi} \times \omega \qquad \text{Equation 4-2}$$

It was mentioned earlier that in this experimental facility, the disc represents velocity of the vehicle and the pin represents the tyre rotational velocity. Normally in quasi-static tyre experiment, the vehicle velocity is assumed to be 10 km/h, therefore for this experiment a series of tests were delivered where the disc is rotating with 10 km/h (2.7 m/s). To show the effect of the disc velocity, two more ranges of speed were examined; the first one when it is assumed to be zero which makes the rig perform like pin on disc tribometer and in the second case it was considered for 5 km/h. In these experiments the pin was rotating with different speeds, which were higher than the disc velocity.

The pin speed was equal to the initial velocity of the disc plus a certain value of velocity, to show the influence of the sliding speed on rubber friction in the current testing device. Therefore, when in this experiment the sliding velocity value is mentioned, it is referred to the difference in value between the pin and the disc rotational velocities. Table 4-1 shows the three ranges of speed for the disc and the range of sliding velocities for the pin. All ranges of sliding velocities were examined for each velocity of the disc, though in some cases when the sliding velocity was low the motors could not move the pin, because the pin and the disc were attached to each other due to high friction, which caused one of the motors to rotate the other one against its rotational direction and in these cases no results could be recorded.

Table 4-1 Ranges of speed for disc and ranges speed for pin (the difference in RPM)

ω_{disc} (RPM)	Sliding velocity (RPM)
	30
	60
	120
0	180
331 (5 km/h, 1.38 m/s)	238
663 (10 km/h. 2.7 m/s)	358
	477
	596

4.3.2. Contact pressure

The experiments were conducted at different contact pressures to show the influence of the normal weight and contact pressure on rubber friction. Since rubber is an expandable material and its contact patch increases by adding normal weight, it was decided to show the value of the contact area for the rubber sample under different loads. For this purpose a FEA model was generated to show the changes of contact area by adding normal weight. However, before considering the FEA model a brief understanding of contact elastomers contact theories is required.

Different theories for calculating the contact area of elastomers against other elastomers or rigid materials have been investigated before based on the requirements of the experiments. For example, Hertz [77] developed a contact theory for fully elastic model, JKR for fully elastic with adhesion [48] and in DMT model (where soft/elastic sphere is in contact with a rigid plane) [78], the contact area was calculated based on the outcome of a FEA model where different normal loads gave the rubber sample area of contact and the contact pressure was calculated based on the obtained contact area. The only possible change of shape, which is shown in Figure 4-3 is the concentration of load on one side of the sample that causes sample deformation. Based on literature if the ratio between width and height of the sample is low, this kind of deformation and buckling does not occur and the pressure is distributed equally. Since in the facility half of the sample is mounted in the pin holder and only about 7 mm of the height is out, and the diameter of the pin is 20 mm, the ratio would be $\frac{7}{20}$ which shows the sample deformation is negligible.

a)

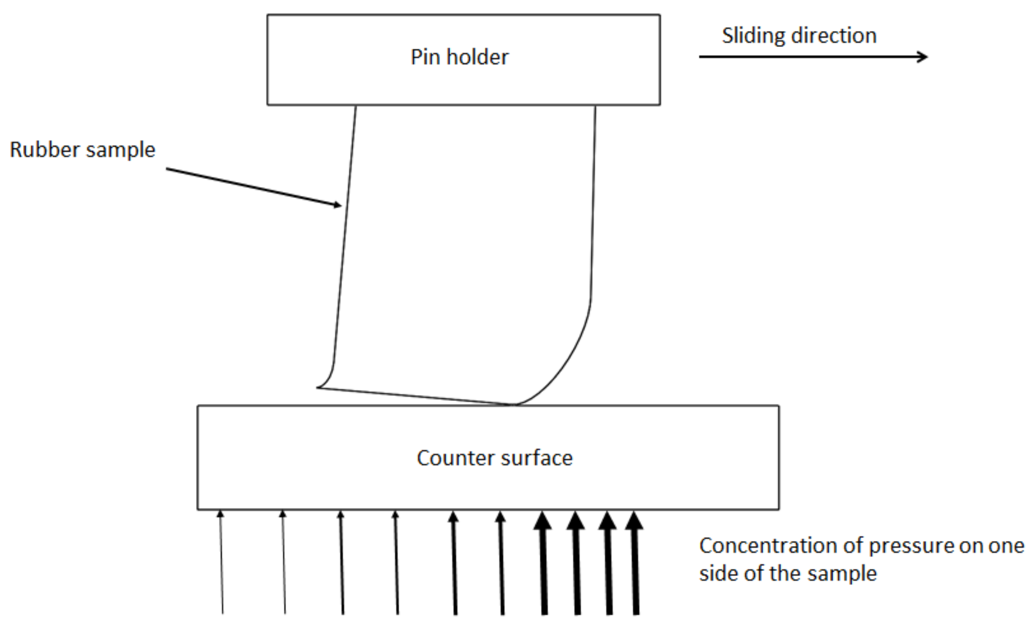

b)

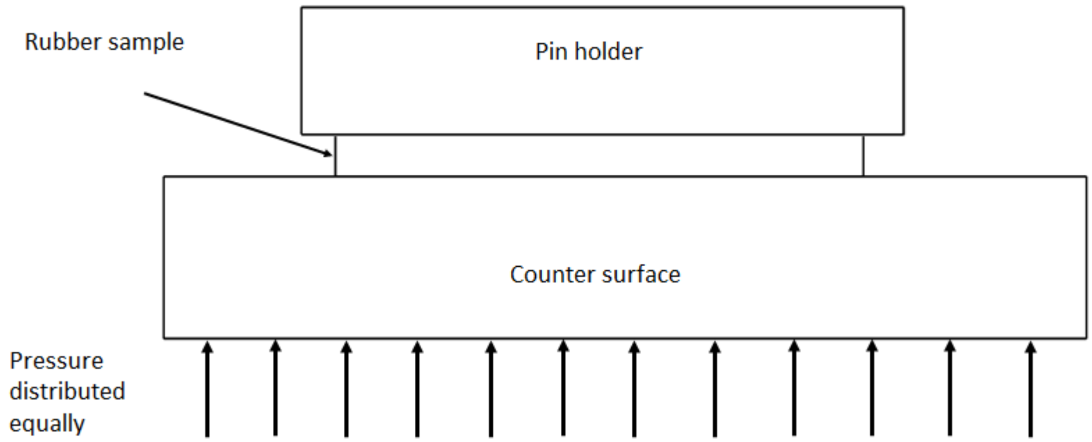

Figure 4-3 a) Shows when the pin is deformed due to the height to width ratio b) pin is not deformed and pressure is equally distributed-Pictures adopted from [79]

a)

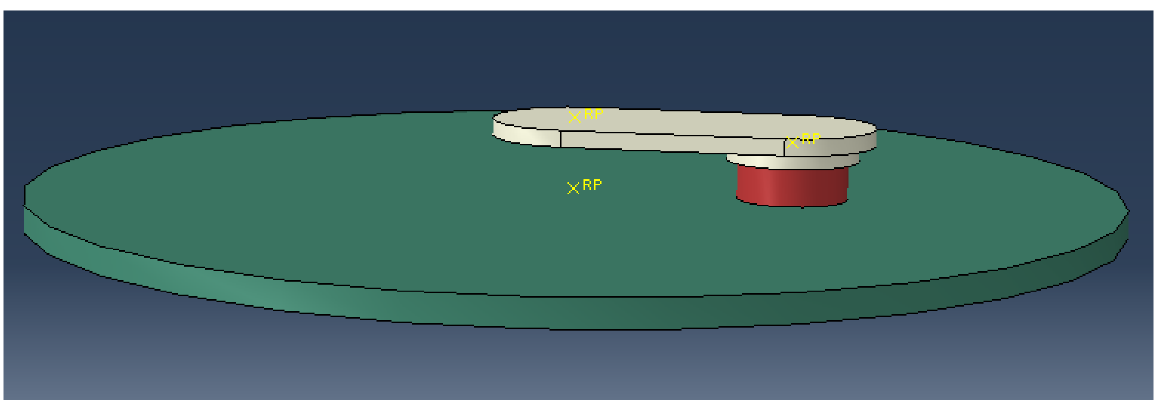

b)

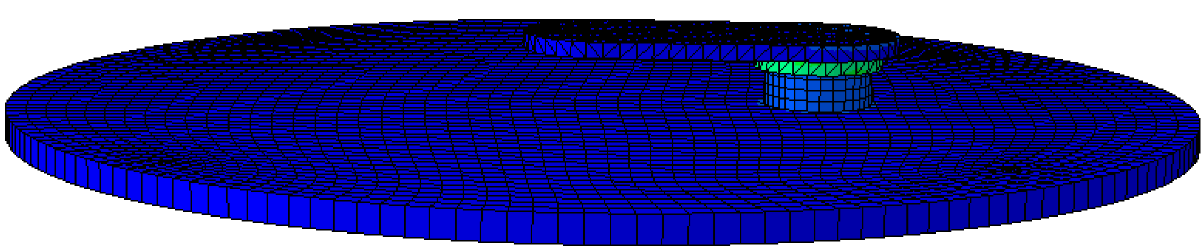

Figure 4-4 FEA Simulation of the pin sample for measuring the contact area

Figure 4-4-a) shows the 3D modelling of the pin and disc in Abaqus and Figure 4-4-b shows the deformation of the sample after the loading. Figure 4-5-a demonstrates the changes in contact area against normal load based on the FEA simulation and Figure 4-5-b illustrates the comparison for contact pressure when the contact area is assumed to be constant and the obtained contact area from the FEA simulation.

a)

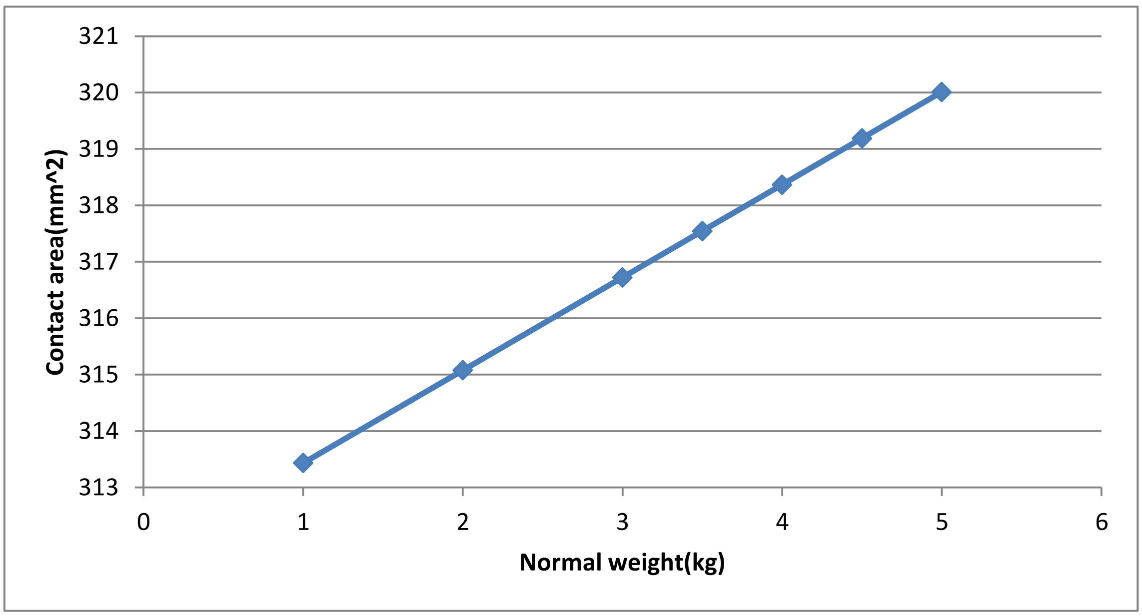

b)

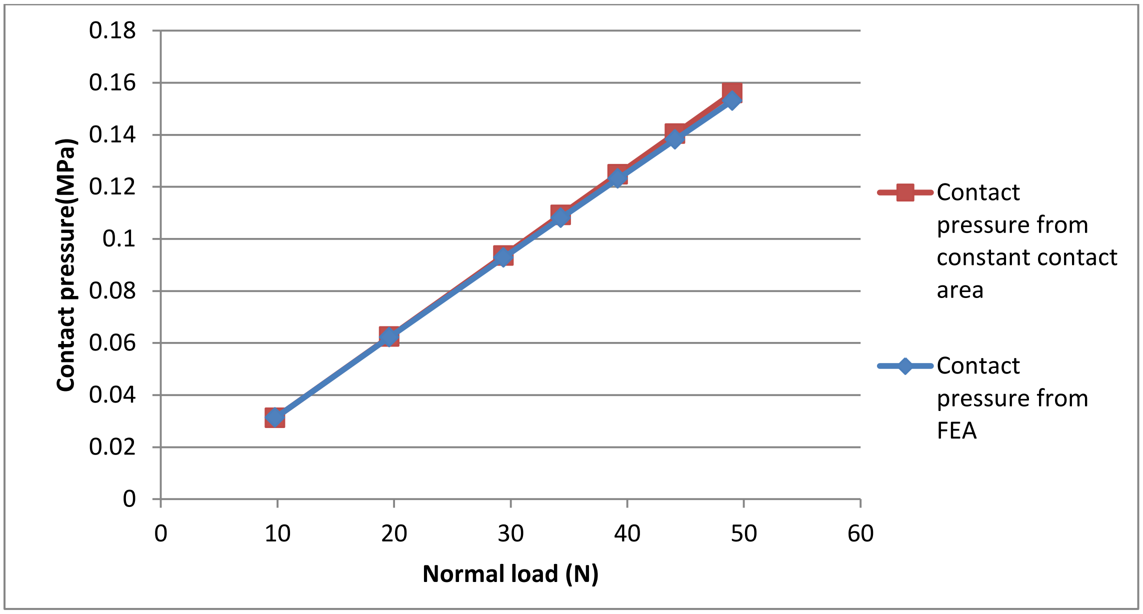

Figure 4-5 a) Rubber contact area against normal load obtain from FEA b) comparison between the contact pressure by considering the pin area as constant or the value from the simulation

4.4. Experimental process

In this section the order of the experiment is described, the obtained raw results are explained based on different tests, and the outcomes of the tests are presented for further discussions. As mentioned in chapter 3, in this facility both of the pin and the disc rotate at different velocities, or the pin could be fixed and the disc rotates and performs as a simple pin-on-disc tribometer.

For the conducted experiments, the values for sliding velocities and contact pressure are explained, also the steps for the test are defined and an example for each test is shown and different stages and regions of results are fully described.

Experiments were conducted at room temperature and for each test the disc was cleaned from any visible rubber particles. Because of the heat generated from the pin sliding on the counter surface, there were gaps between each test to allow the disc to cool down and keep the test condition similar. The time consumed for each test was short as if the test would be performed for a long time, high temperature would cause the rubber to melt down and stick to the disc. The temperature of the disc was recorded by laser thermometer, and it was varying between 18-20 ^{o}C, whereas if the test was running for one minute, the temperature was increasing to about 60 ^{o}C. In addition, the sensor (as explained in chapter 3) was connected to a data logger to record the result, data recording frequency was 1 KHz, in order to cover all the asperities of the surface and provide the result which contain most of the contact of the pin and the counter-surface. In each test, the experiment was repeated for several times (from 3 to 7 times) to make the result statistically rigorous. The average value of the attempts was shown as final result and a 95% confidence interval was used for each point.

The raw results were processed using a Matlab code, in which a low pass filter was applied to remove the noise in the raw results and convert the torque reading to friction force by considering internal friction and system error; then the value was divided by the normal load to show the friction coefficient. (Internal friction and system error was explained in details in chapter 3, calibration section). The result process displays the whole duration of the test, though only a specific region in the obtained data refers to the contact between the pin and the counter-surface. The code enables the operator to choose an interval of the processed result, which is the period where the pin was sliding on disc. This process is explained thoroughly in the following sections based on experiment condition.

4.4.1.1. *Fixed pin on rotating disc*

It was shown in Table 4-1 that the experiments were conducted based on three cases of disc velocity, since the rig is designed in the way that the sensor is located on the disc rotating shaft, it is not possible to fix the disc and rotate the pin, where would be no reading from the transducer. To perform the experiment, the pin was fixed instead and the disc was rotating with different rotational velocities. The lowest speed, where the motor provides a smooth rotation was 120 RPM (0.5 m/s).

The experimental process is performed in following steps:

- Mount the pin and fix in the holder
- Check if the disc contains any particle residue from previous tests
- Adjust the disc (and the pin if it was rotating) velocity
- Run the data logger to record the data
- Apply normal load on the weight holder plate
- Start rotating the disc
- Wait for 10-20 seconds to let the rubber slide on the counter-surface
- Stop the motor
- Stop the data logger from recording data
- Clean the surface, give it time to cool down and change the pin for the next test

The recorded result was processed using a Matlab code; Figure 4-6 shows an example for a raw data before (a) and after the processing (b). This example illustrates fixed rubber sliding on steel, when normal load is 4 kg and sliding velocity is 1m/s (238 RPM). In Figure 4-6-c, all the attempts for this experiment are shown; in total 6 attempts were assessed and attempt 4 was presented in Figure 4-6-b. All the tests are following the same trend, but the attempts 3 and 5 deviate from the rest, therefore considered as outliers and removed from the statistical calculation (i.e. average, standard deviation and confidence interval). The removal of these two attempts was as can be seen in the graph they were following the similar pattern as the rest of the tests, also some of the results were removed because the samples deflected or damaged during the experiment.

a)

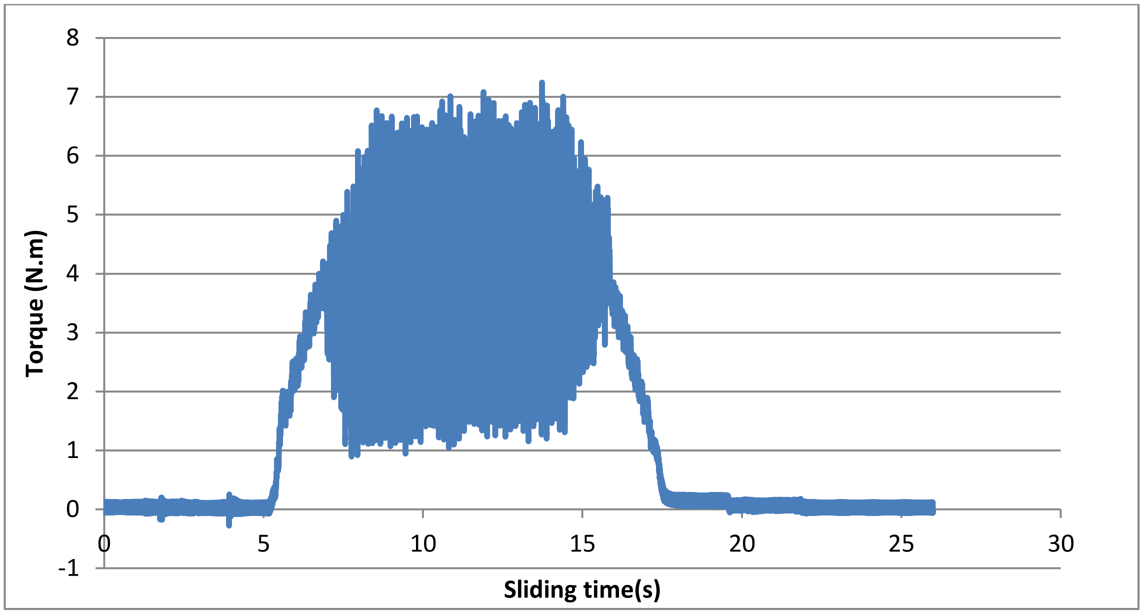
Torque (N.m)
8
7
6
5
4
3
2
1
0
-1
0
5
10
15
20
25
30
Sliding time(s)

b)

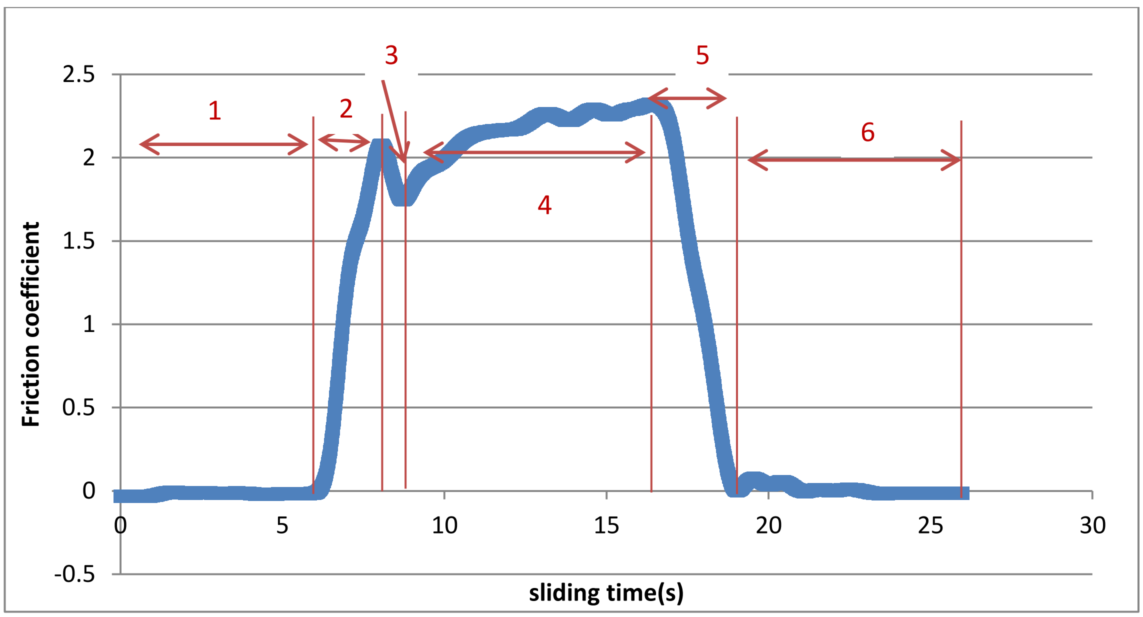
Friction coefficient
2.5
2
1.5
1
0.5
0
-0.5
0
5
10
15
20
25
30
sliding time(s)
1
2
3
4
5
6

c)

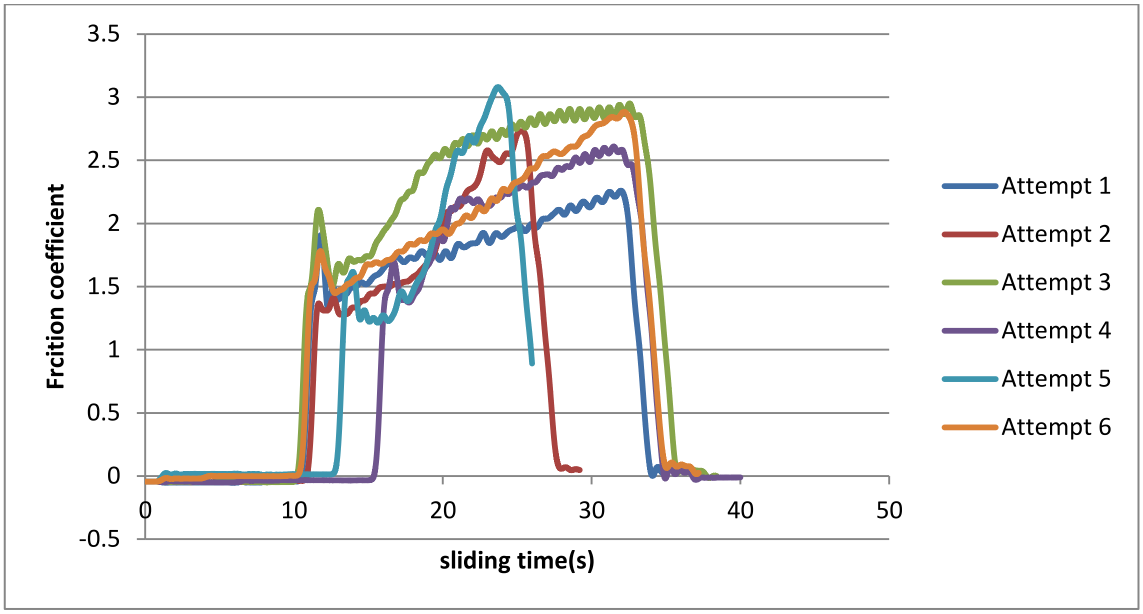

Figure 4-6 Data gathered for fixed rubber sample sliding against a steel disc with a normal of 4 Kg and 1 m/s sliding velocity a) collected data before processing (torque, N.m) b) procecessed data (friction coefficient) c) friction coefficient for 6 different samples

4.4.1.1.1. *Recorded data specification*

In Figure 4-6-b) the test result is presented, it is shown that at the first period (1), the torque is zero as there is no motion in the facility and during this period the loading is happening. Then the increase occurs (2), which is the moment where the motor initializes. Since the torque sensor is gathering data due to the torsion of its shaft, and in the first step there is not motion on one side of it and the other end started to rotate, there is peak, which decreases (3). After this point the result from the rubber sliding on the disc was recorded (4), and ultimately, the motor is turned off and the torque was decreased back to zero (5 & 6). It was described earlier that a MATLAB code enables the operator to choose the duration of contact and calculate the average for the desired period. This value is outcome for friction coefficient of a single test. It should be noted that each test was repeated between 4 to 7 times with different rubber samples to make the result statistically rigorous.

4.4.1.2. *Rotary pin and disc*

In this experiment, the disc is rotating in opposite direction to the pin and with lower speed. The test process is mainly similar to fixed pin on rotating disc, the difference is that the motor velocity has to be adjusted and the effect of starting the motor before running the pin and turning it off after turning off the pin are visible in the recorded data.

In these tests, the disc velocity was chosen as 5 km/h; the pin was rotating with a range of velocities superior than the disc speed as it is shown in Table 4-1, and for each set of velocity, the variety of normal weight were examined. During the rotary tests, there was a hazard of the rubber sample deformation and loosing the surface contact with counter-surface, and if this occurred the experiment was stopped and repeated to obtain a valid result. An experimental result is presented in Figure 4-7 as an example.

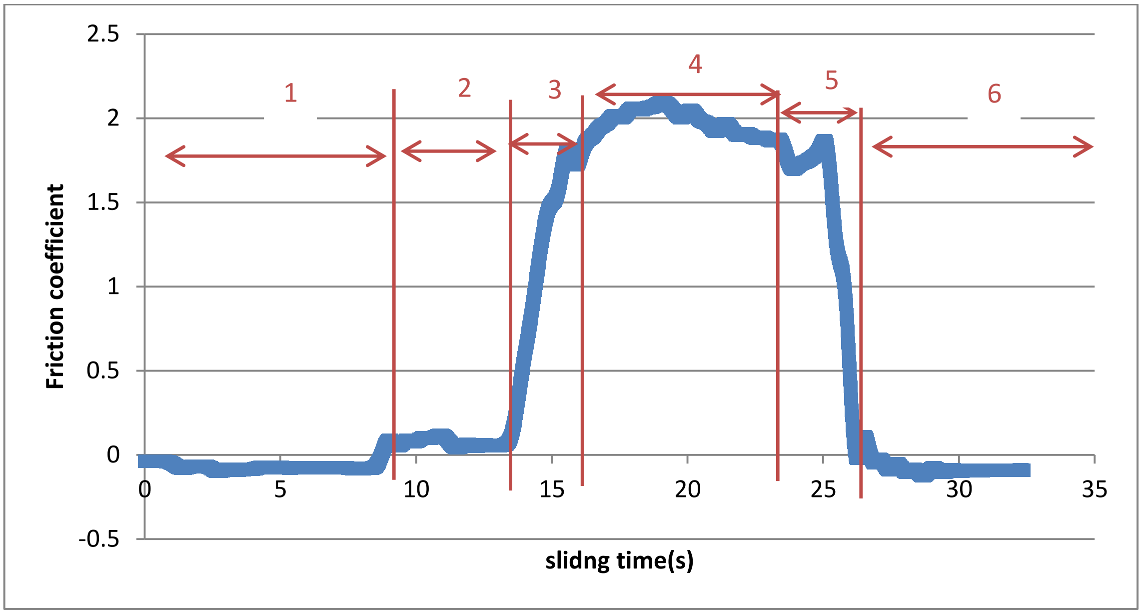

Figure 4-7 Rotating rubber pin against rotating steel disc, normal load =4 kg, disc veloicty=1.38 m/s,pin velocity=2.38 m/s

4.4.1.2.1. *Recorded data specification*

In Figure 4-7 the processed result from an experiment is presented, again, it is shown that in region 1 the reading value is zero, and by running the first motor there is a slight increase in the reading (2). In region 3 the value starts to peak as the second motor begins to rotate the pin. Section 4 is the main focus of this test, corresponding to the pin sliding on the counter-surface; the average of this part has been used as the friction coefficient of the test. By turning off the second motor, the reading has dropped (5) and the last division (6) shows that the first motor is off and value dropped to zero. It should be noted that the internal friction and system error has been subtracted from processed result, therefore, region 1 and 6 are slightly below zero.

4.4.1.2.2. *Same rotational direction tests*

In all the experiments, the disc and pin were rotating against each other to represent the resistant to the motion of rubber as it is defined in the definition of friction. However, when the disc and pin are rotating in the same direction with different speed, a friction exists in the contact patch. Therefore, a series of experiments were delivered to show the friction coefficient in the abovementioned condition.

For these series of tests the wiring of the motors were changed to make the disc rotate in the opposite direction. The pin was rotating with higher rotational speed than the disc and the disc was rotating with a fix speed. During the experiment there was a problem in conducting tests, due to the pin inability to rotate in low ranges of sliding velocity, thereby a the motor controllers could not provide enough power to rotate the pin and the test was stopped. Consequently, the tests were conducted when the disc was rotating with 5 km/h and the pin was rotating with 7.5 and 10 km/h. The normal loads which applied in this experiment were 1, 2, 3, 3.5, 4, 4.5, 5, 5.5, 6 kg. Figure 4-8 shows an example result for this experiment.

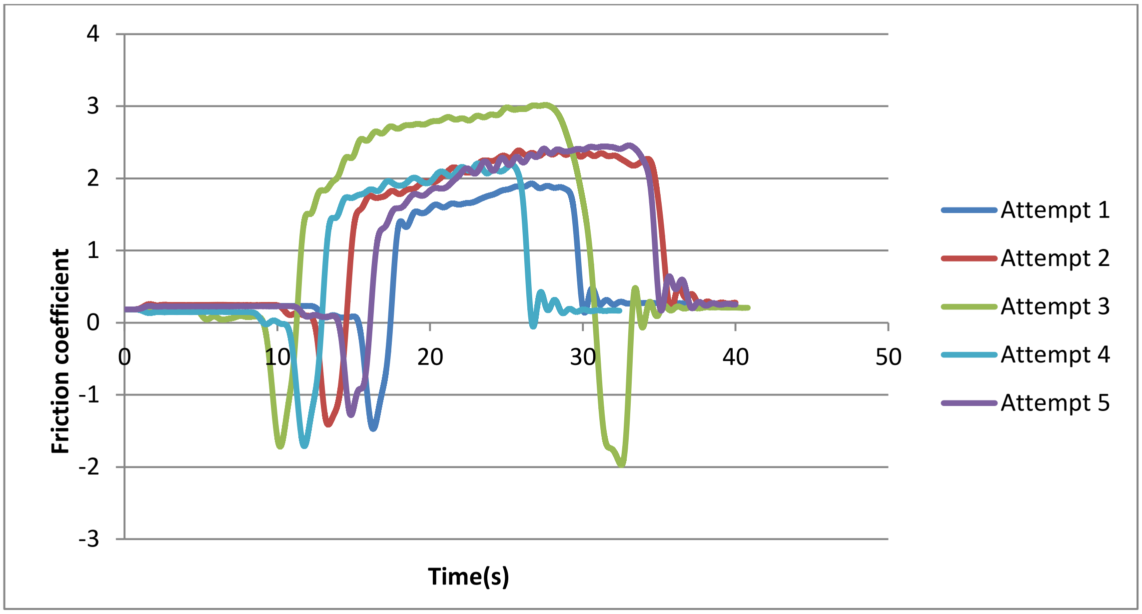

Figure 4-8 Friction coefficient recorded during a same rotational direction test, disc velocity=5 km/h and pin velocity=10 km/h normal load=5kg

The trends in the results for this test is similar to the other steel disc, the main difference in the trend and shape of the recorded data is the drop in the readings when the second motor started to rotate and produced a high torsion in the main shaft. Similar to the other steel disc the result from this test is investigated for further discussion.

4.4.1.3. *Sandpaper test*

Similar to steel disc process, two counter-surfaces with sandpaper were examined (i.e. grit 120 and 400), the only main difference in the obtained result from the sandpaper compared to the steel disc, is the region considered as the rubber/sandpaper friction coefficient. Sandpaper cause abrasion of a rubber samples and the abraded parts prevent the rubber pin to contact the counter-surface properly and these large abraded rubber particles play a crucial role in the decay in the reading. Therefore, only a few initial seconds of sliding region were collected giving the appropriate value and this region is shown in Figure 4-9. Each test for sandpaper was repeated no more than two to three times, as further testing was not possible since, a sample after the test was completely worn out and further repetition of the experiment was unfeasible as would require extensive recourses and further sample preparation. In Figure 4-10, three attempts of a sandpaper test are shown.

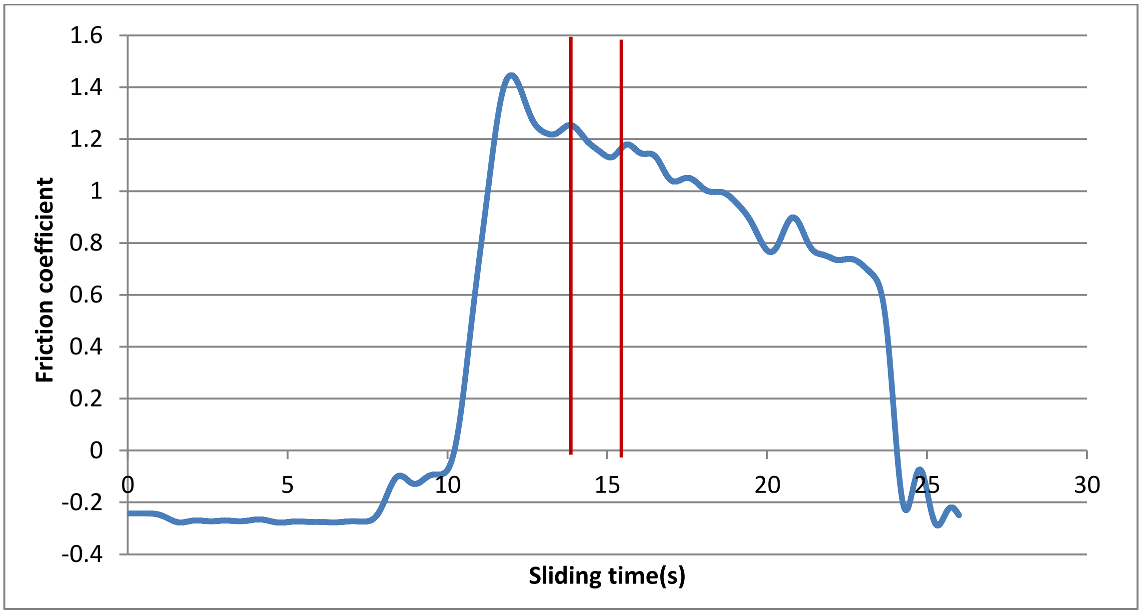

Figure 4-9 Rubber/sandpaper (grit 120), pin velocity=3.7 m/s, disc velocity= 2.7 m/s, normal load=4 kg

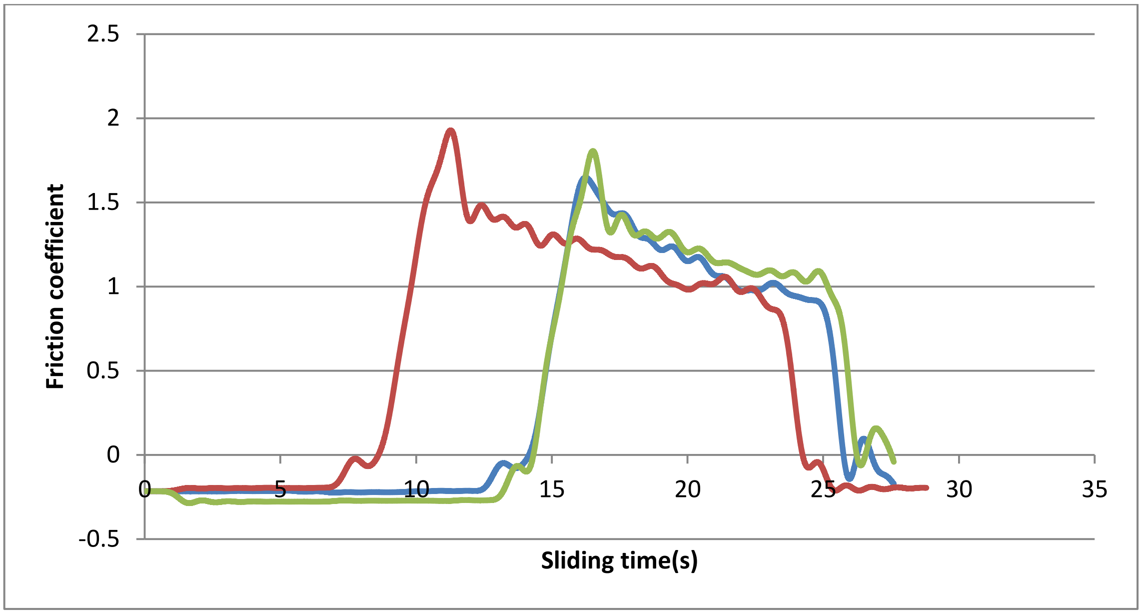

Figure 4-10 Test attempts for rubber/sandpaper (grit 120), pin velocity=3.7 m/s, disc velocity= 2.7. m/s, normal load=4.5 kg

4.4.1.4. *Glass disc*

Rubber frictional behaviour against glass has been investigated for a long time, to make a brief comparison and obtain a better understanding of the tests; a pin on disc test for a glass disc was conducted. The disc was rotating in with the speed of 0.5 and 2 m/s and several normal loads. Rubber tests are very dependent on the surface structure of rubber samples, (reviewed in chapter 5), however this dependency is very understandable for smooth surfaces such as glass. Therefore in this experiment (when the disc was rotating with 2 m/s) 5 rubber samples were selected and each of them was examined twice, thus for each case of normal load 10 attempts were recorded. In Figure 4-11 the results for two different samples are demonstrated; the attempt results for a single sample are very similar, however for different samples result varies, therefore the reproducibility is poor.

a)

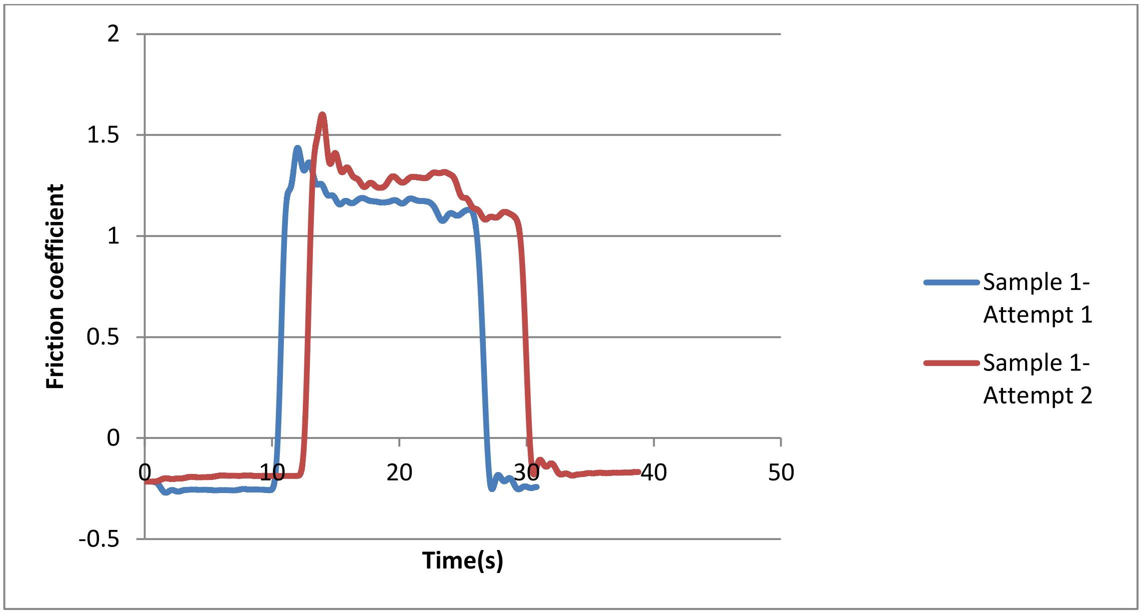

b)

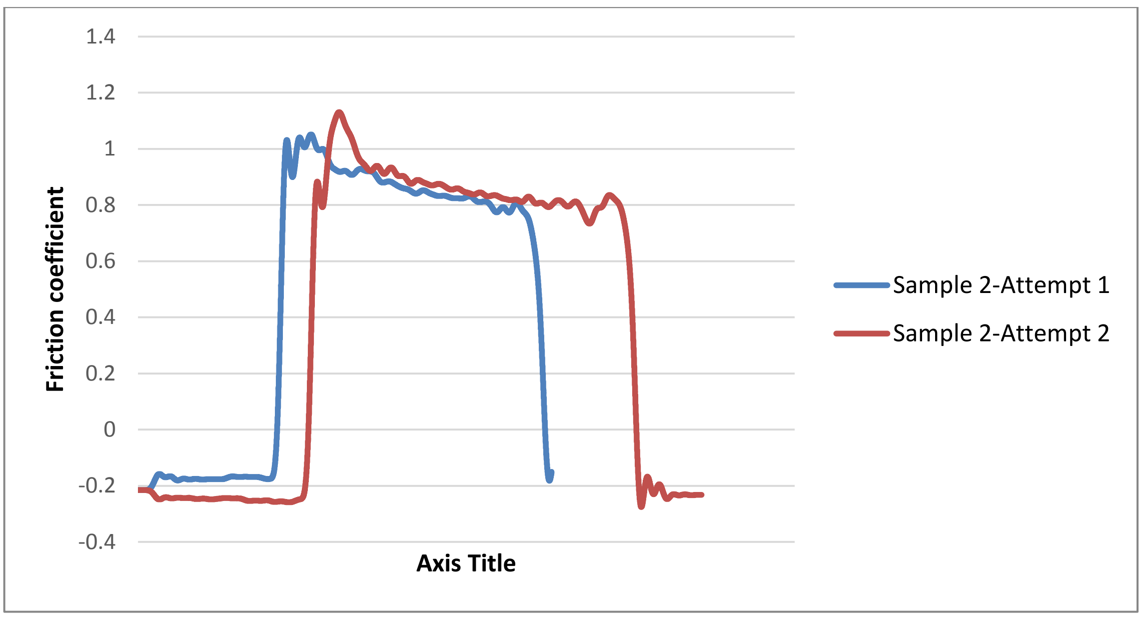

Figure 4-11 Result for two sample of rubber (a & b) in the same condition, each sample has been examined twice, sliding velocity 2 m/s and normal load=4 kg,

4.5.Data processing

In the first series of experiments, rubber friction was examined against steel, in each case of normal load and velocities, tests were repeated several times to present statistically robust results. During this steel experiment each sample was used few times, before the samples surface deformed significantly. It is important to note that using a new sample for each test would make a more accurate and precise result, however due to the high number of experiments and the difficulty in preparing the rubber samples, this was not feasible. Since in sandpaper tests, the pins wear out, it was not possible to use them again for any other experiments.

In order to obtain a friction coefficient value for a case of normal load and sliding velocity, the average of the attempts was calculated. To show the range of error of the result, the standard deviation and a standard error of 95% were calculated. These values were used for further steps in reviewing rubber frictional behaviour and modelling.

Table 4-2 Attempts for each test and the total number of tests

Experiment	Valid results
Steel fixed disc	167
Steel 5km/h disc	169
Steel 10 km/h disc	174
Same disc rotation	82
Glass	120
Sandpaper 120 fixed disc	27
Sandpaper 120- 5 km/h disc	31
Sandpaper 120-10km/h disc	30
Sandpaper 400	43
Total	843

Various numbers of tests were conducted, Table 4-2 shows the number of attempts which provide valid results where has been used for the research, it is necessary to consider more number of tests were delivered to provide the valid results, for instance the steel discs, were repeated three times, the first couple sets of experiments provided invalid results as the experiments had to be adjusted precisely.

The obtained valid results were processed in the following steps:

- The torque was obtained from the sensor
- Low pass filter was applied on the torque and the internal friction and system error were further subtracted to show torque, which results from rubber friction

- The torque was converted to friction force by considering the radius from centre of the pin to the centre of the rotation
- Coulomb-Amontons law was applied to obtain the friction coefficient by dividing the friction force by the normal load

Therefore, the friction coefficient/friction force variations were observed against normal load/contact pressure and the sliding velocities. The results are discussed in the chapter 5 in detail.

4.6. Conclusion

In this study, rubber samples were extracted from the tread and prepared for the experiments, then samples were inspected and proved to be similar, therefore the results follow a similar pattern. The method for testing and recording result was established. The experiment test scope was described and the ranges for velocity and contact pressure were shown and discussed. Tests were divided into three cases based on the velocity and the sliding velocities. All tests were delivered when the disc was rotating in opposite direction to the pin, however another set of tests was conducted to show the difference in the results if both rotate in the same direction. The difference between counter-surfaces was shown and their result processing was described.

5. Experimental results and discussion

5.1. Introduction

In this chapter the outcome of the experiments is reviewed for each case of fixed pin and rotating discs and then the results for different surfaces are compared. The variability of the results is justified and the effects of the surface roughness and sliding velocity are addressed.

5.2. Steel disc experiments

As addressed earlier, rubber friction was measured against a steel disc in three different cases: in the first the pin is fixed and the disc is rotating with different sliding velocities, in second the disc rotates with 5 km/h (331 rpm) and finally, with 10 km/h (663 rpm)and the pin is rotating with higher sliding velocities.

5.2.1. Fixed pin rotating on steel disc

Figure 5-1-a) shows an example of pin on disc result, when the sliding velocity is 0.5 m/s and the normal load is 2 kg. An interval, in which the rubber was sliding on the disc is marked by lines; this part is displayed separately in Figure 5-1-b).

a)

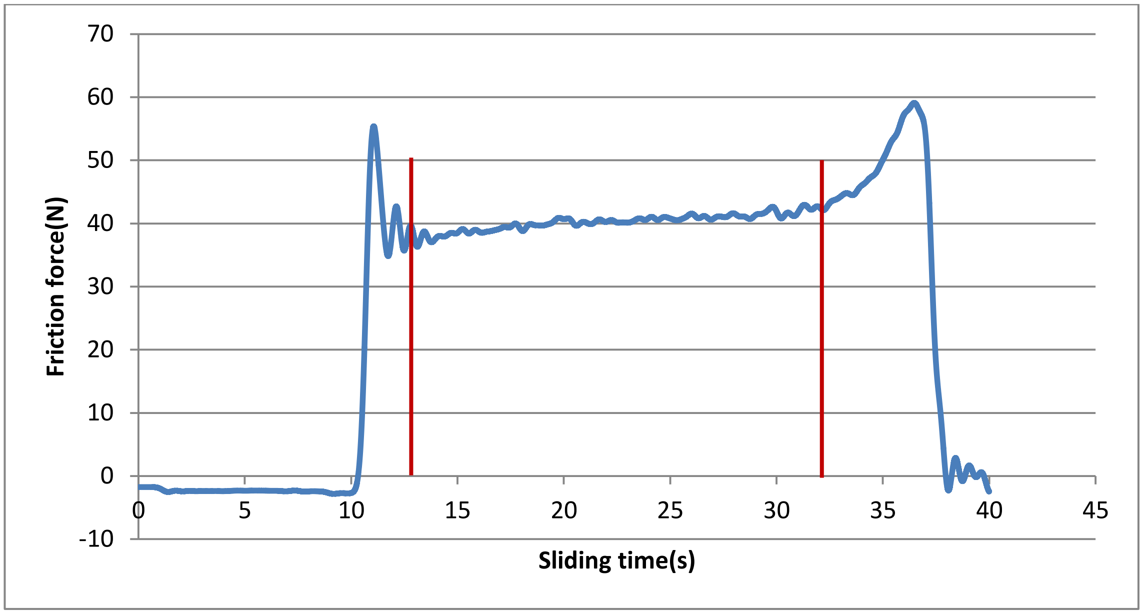

b)

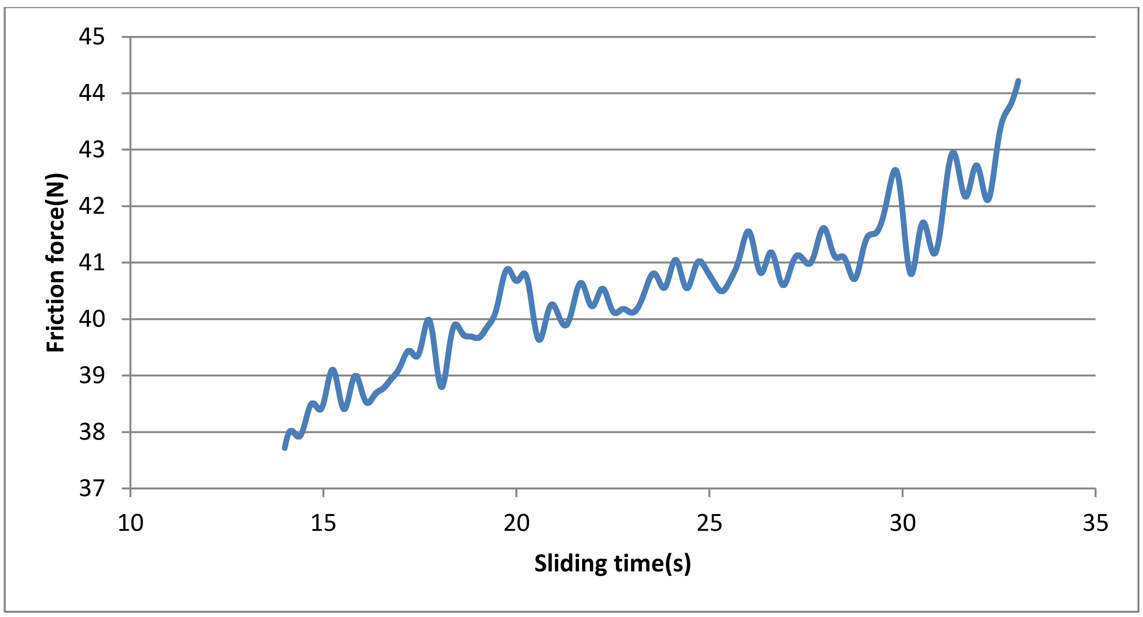

Figure 5-1-a) An example friction for fixed pin on disc - b) the selected range which has been considered for observation (sliding velocity=0.5 m/s, normal load=2kg)

Since in this test the rotational velocity was 120 rpm (0.5 m/s), each second the disc has been rotated for two times. During the time when rubber slides on surface, stick and slip occurs, and a thin layer of rubber is detached from the sample and attaches to the counter surface. Therefore, when rubber is sliding on the surface, which has small particles of rubber sample, the stick is increased and it causes higher friction force. This phenomenon can be observed in Figure 5-1-b), where the friction force is slightly increasing and the variation in the force is caused by stick and slip of rubber. Schallamach has defined a rubber string, which makes a bond with a surface and elongates during sliding, then is separated and creates a new bond; this theory is still generally accepted [37, 57]. Similar to this data, another example can be observed for the same sliding velocity, but with a higher normal load. Figure 5-2 shows the similar condition to abovementioned one, however the normal load is 3 kg.

a)

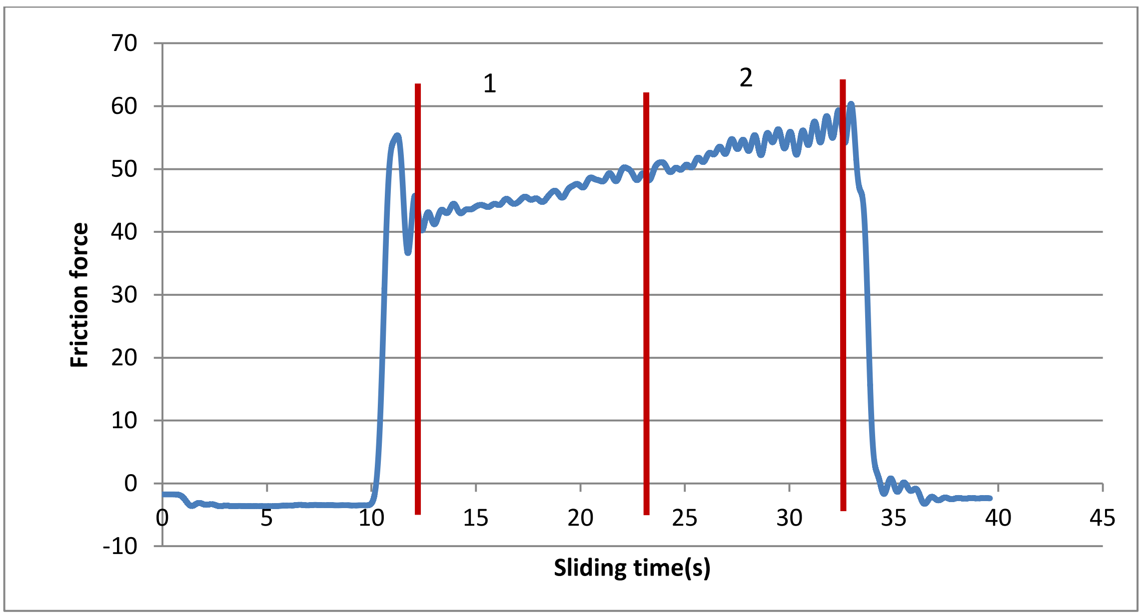

b)

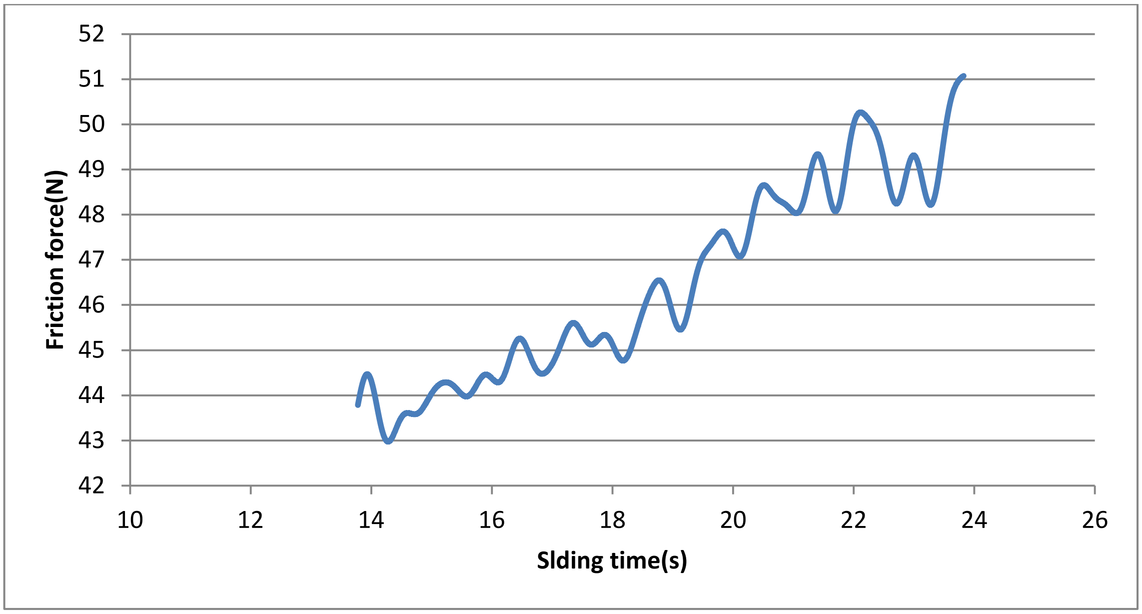

Figure 5-2-a) An example friction for fixed pin on disc - b) the selected range (1) which has been considered for observation (velocity =0.5 m/s, normal load=3 kg)

As it is expected by increasing the normal load, the friction force is increasing. If the period during which the contact occurs is considered, it can be determined where the friction force is increasing with higher rate (part 1 in Figure 5-2). In time the variation in the result is getting higher (part 2 in Figure 5-2-a) due to the fact that the rubber particles, which are attached to the surface are not distributed equally; therefore, rubber samples accumulate the particles and get separated, what causes higher fluctuations.

The average resultant friction forces (calculated from the average of abovementioned period on the graph) for steel disc against fixed pin are shown in the Figure 5-3.

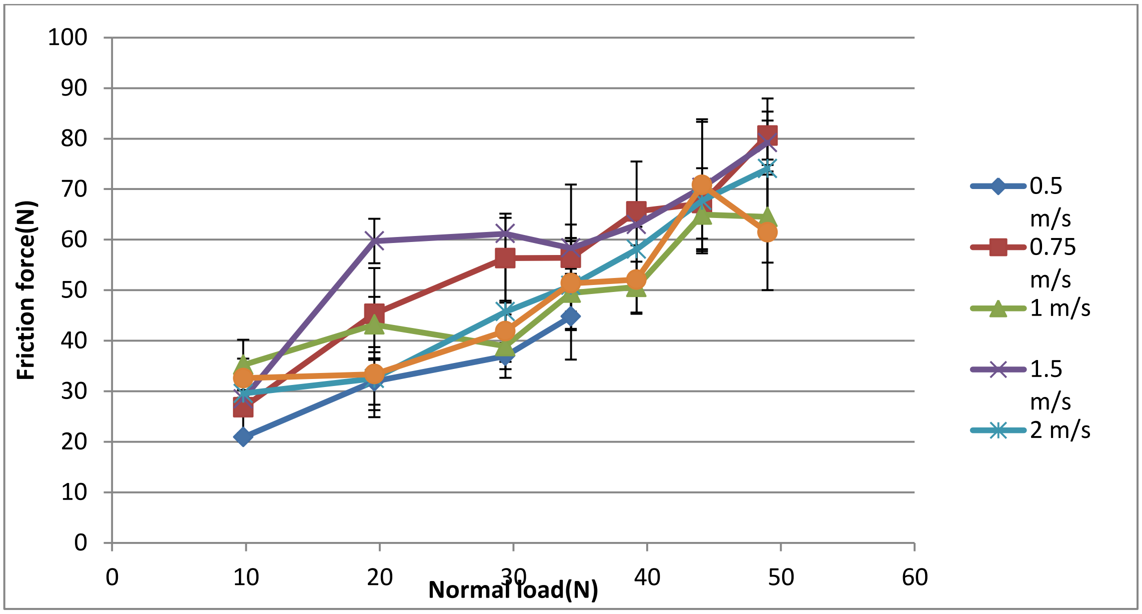

Figure 5-3 Friction force results vs. normal loads for different sliding velocities for fixed pin on disc

In Figure 5-3 there is a clear trend in friction force, which increases as the normal load is added, though it appears show that the velocity does not have a definitive effect on the result. Friction coefficient allows grasping the relation of the forces in an excellent manner and shows the system condition; therefore the results from the experiments will be presented as friction coefficients. Moreover, the aim of this research is to present the friction results in a way to be applicable on tyres; normal loads do not show the pressure on a tyre, therefore instead of normal loads, contact pressure is considered.

The friction coefficient against contact pressure is demonstrated in Figure 5-4, which shows that the friction coefficient is decreasing by increasing the contact pressure. In addition, by increasing the contact pressure the changes in friction coefficients values for different sliding velocities are decreased. It was explained earlier that at contact pressure higher than 0.1 MPa rubber friction coefficient converge to a constant value [51]. Figure 5-4 demonstrates that similar pattern occurs for the contact pressure in this study. Moreover, there are differences in the friction coefficients for different velocities and by increasing contact pressure all the curves converge to the same value.

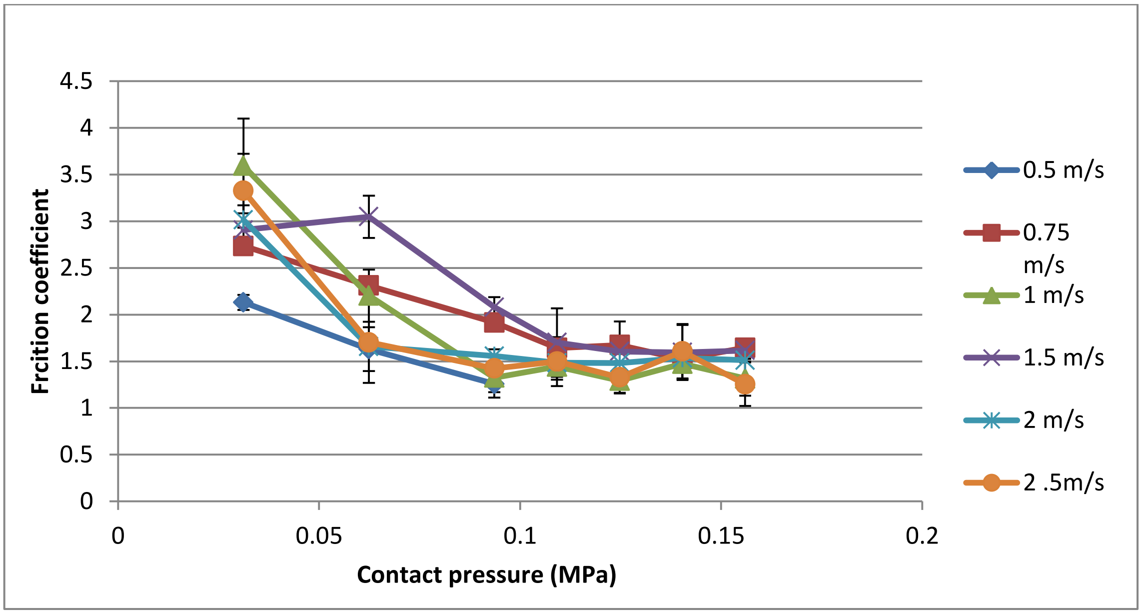

Figure 5-4 Pin on disc friction coefficient against contact pressure

5.2.2. Steel disc rotating with 5 and 10 km/h (331 and 663 rpm)

In this section the results for rubber friction coefficients, when the disc is rotating with 5 and 10 km/h, are demonstrated and discussed. Because in these tests the disc was rotating with initial velocity, more ranges of rotational velocities were considered for the pin; Figure 5-5 shows the result for both cases.

a)

b)

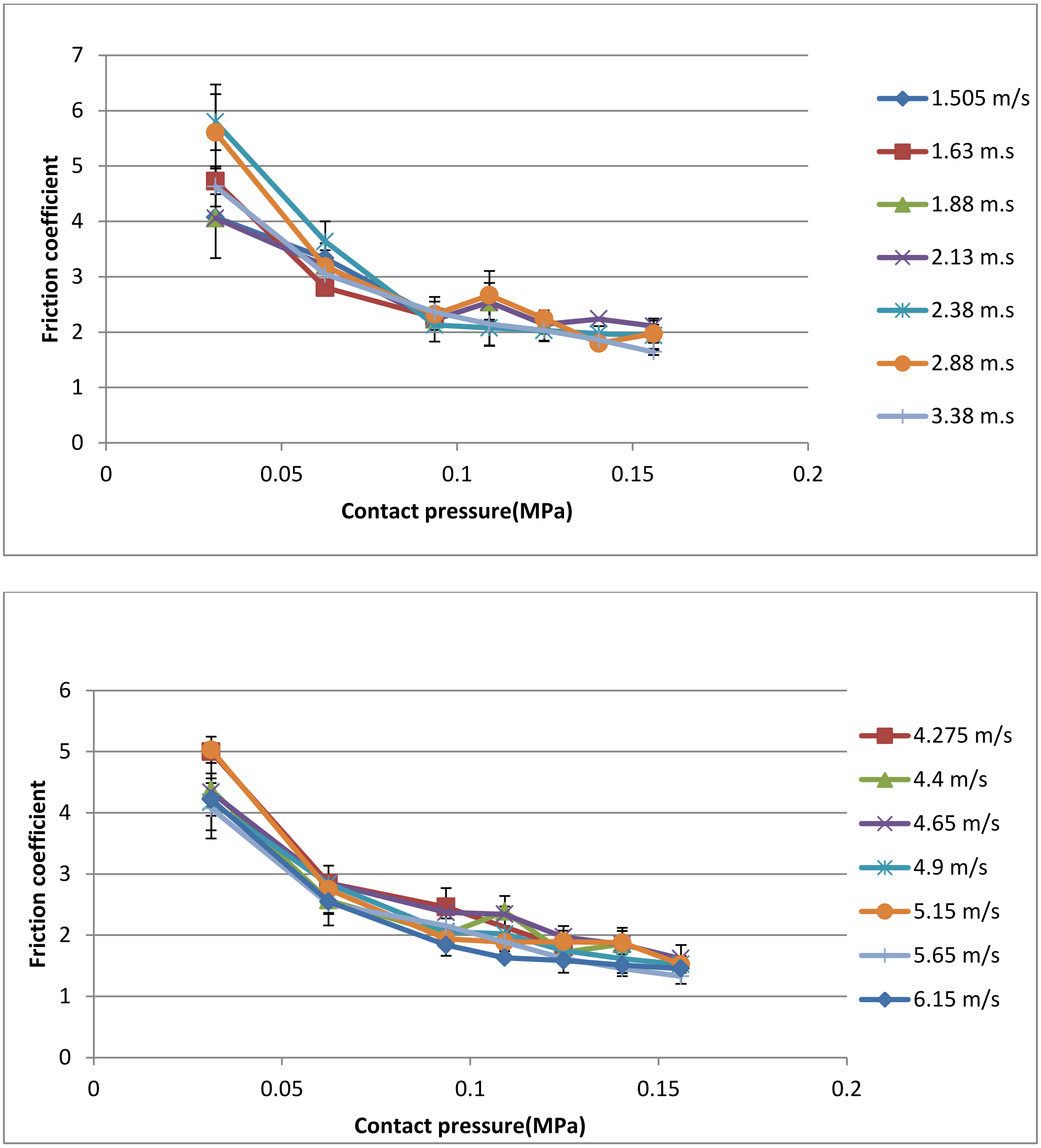

Figure 5-5 Rubber friction coefficient against contact pressure-a) disc velocity 5 km/h (1.38 m/s) b) disc velocity 10 km/h (2.7 m/s)

In Figure 5-5 the friction coefficient against contact pressure is shown, it is apparent that different sliding velocities have very little effect on friction coefficient specifically in the examined speed ranges. Similar to fixed pin result, friction coefficient does not change when the contact pressure reaches approximately 0.1 MPa.

5.2.3. Pin and disc rotation in same direction

All the previous tests in this research were conducted in a way that the pin was rotating in the opposite direction to the disc, and the sliding velocities were calculated based on this relative motion. However, it was unclear if there are any differences when the pin rotates in the same direction as the disc. The ranges of velocities and normal loads for these tests were fully explained in same direction of rotation section. Figure 5-6 shows the results obtained from these experiments, where different sliding velocities do not affect friction coefficient and all the previous statements for contact pressure are valid for this test.

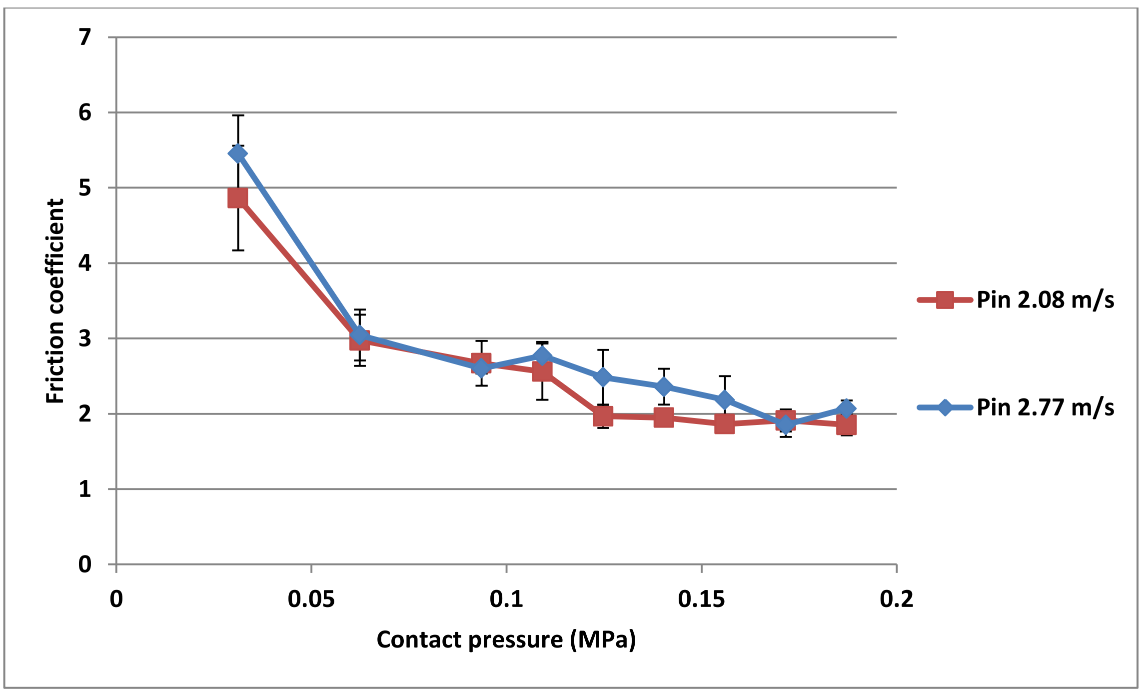

Figure 5-6 Friction coefficient against contact pressure, disc and pin rotating in same direction (disc velocity=5 km/h, pin velocities= 7.5 km/h (2.08 m/s) and 10 km/h (2.77 m/s))

5.2.4. Steel disc overall comparison

The results between all four cases (Fixed pin, disc velocity=5 km/h, 10 km/h and the same rotational direction) are comparable. It is apparent that the results do not vary in a significant way and the outcome of all the experiments depends on contact pressure. This is in agreement with observations from earlier researches, and friction coefficient only changes in low sliding velocities, thereby it is not possible to obtain results in that range [56].

5.3. Sandpaper experiments

Rubber samples were examined against a 120 grit sandpaper to show the effect of the surface roughness on the result. Since it was proven that the ranges of disc velocities when the pin is fixed and the ranges of pin velocities when disc is fixed do not affect the result, the ranges of sliding velocities were reduced. Only one range of speed was examined for all the contact pressures and in another range three contact pressures were examined to show that the sliding velocity does not affect the friction coefficient in this experiment even on a rough surface.

5.3.1. Fixed pin on rotating sandpaper 120 disc

Two examples for fixed rubber pin sliding on sandpaper are shown in Figure 5-7. In this figure the friction force is recorded against the sliding time, where in case (a) the normal load is 34.4 N and in case (b) the normal load is 53.9 N. The pin does not move until the motor provides enough power to rotate the sample. It is observed in Figure 5-7-b that the recorded friction force is decreasing with sliding time, which is due to higher normal load in comparison to the case (a).

a)

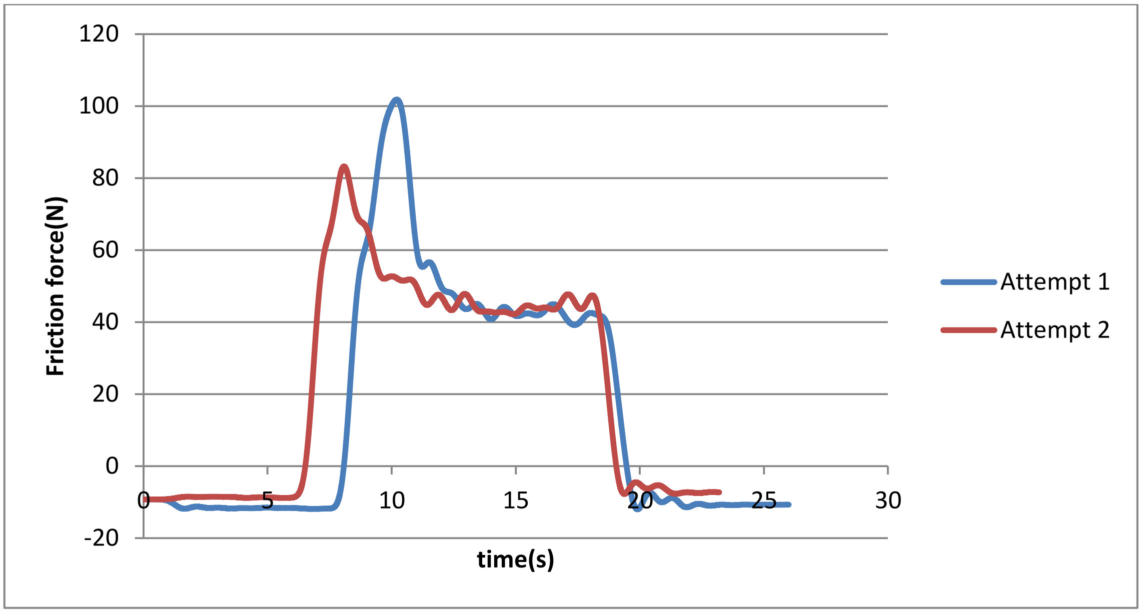

b)

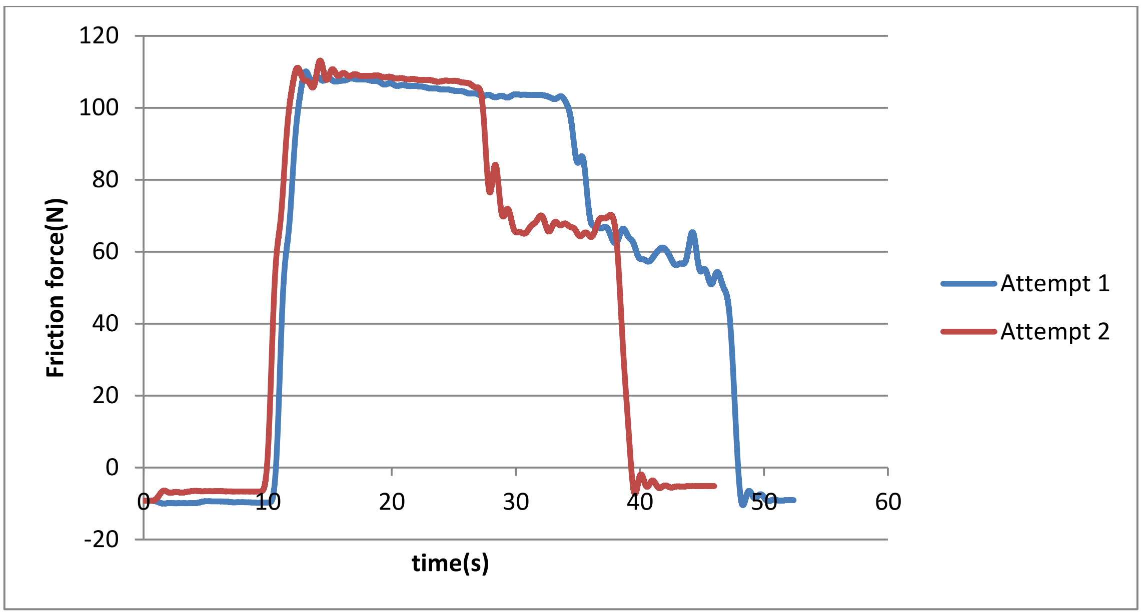

Figure 5-7 Friction force (N) vs. time(s) for rubber against fixed sandpaper, sliding velocity 1 m/s normal load for a) 34.3 N-3.5 kg normal load b) 53.9 N-5.5 kg

As already mentioned the tests were conducted in one range of velocities for the all contact pressures and in another sliding velocity few points were examined to show friction force/coefficient depends on velocity in this facility; Figure 5-8 shows the outcome for the obtained data. The first range of sliding velocity for the experiment was 1 m/s and the test was repeated for three points of contact pressure when the sliding velocity was 2 m/s. Similar to abovementioned conditions (i.e. steel disc), the friction coefficient decrease with increasing normal load and it converges to constant value when the contact pressure has reached 0.1 MPa.

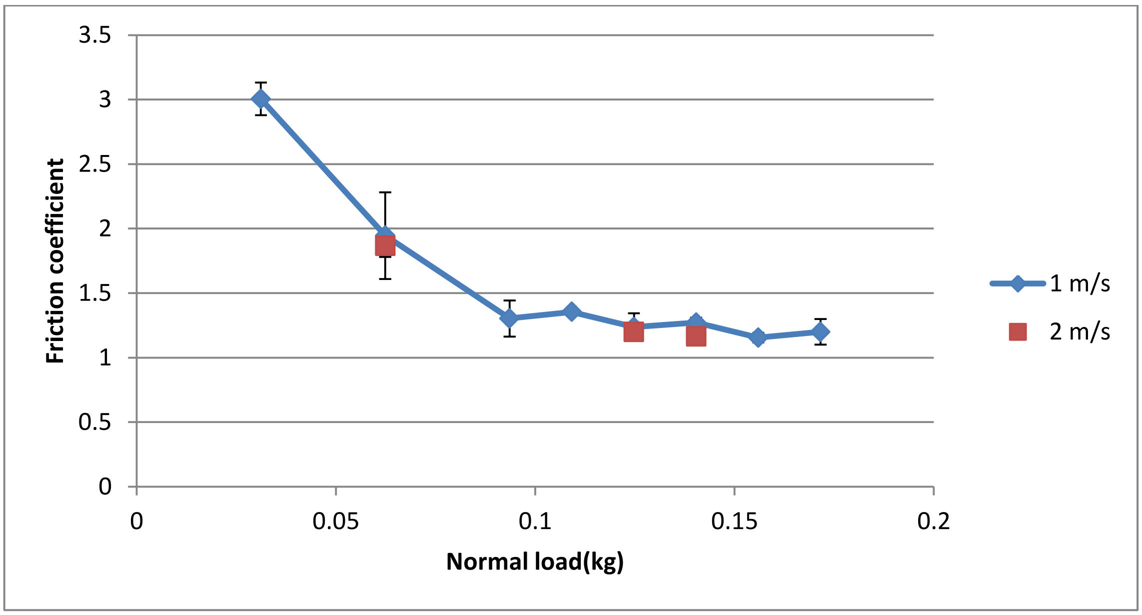

Figure 5-8 Friction coefficient against contact pressure (MPa)-fixed pin on sandpaper disc, test for sliding velocities of 1 m/s and 2 m/s

5.3.2. Experiments with rotating sandpaper 120 disc

The experiments were carried out in the conditions where the sandpaper disc was rotating with 5 and 10 km/h and the pin was rotating with a higher velocity in opposite direction to the disc. Experiments in both cases were conducted for two ranges of speeds. The friction results are presented in Figure 5-9; and the justification for the previous results is also valid for these examples.

a)

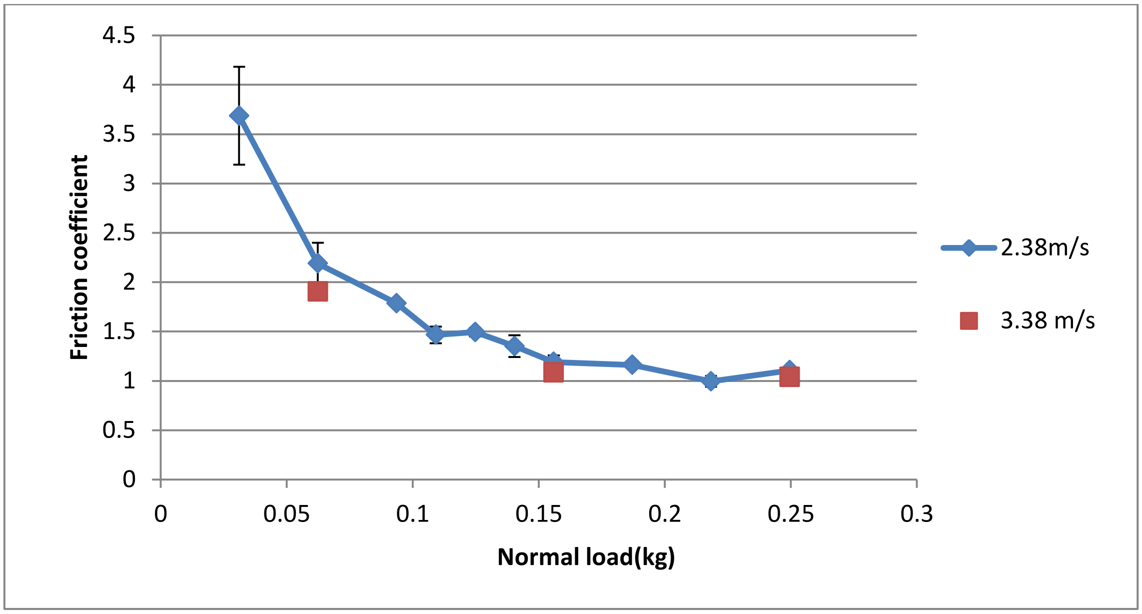

b)

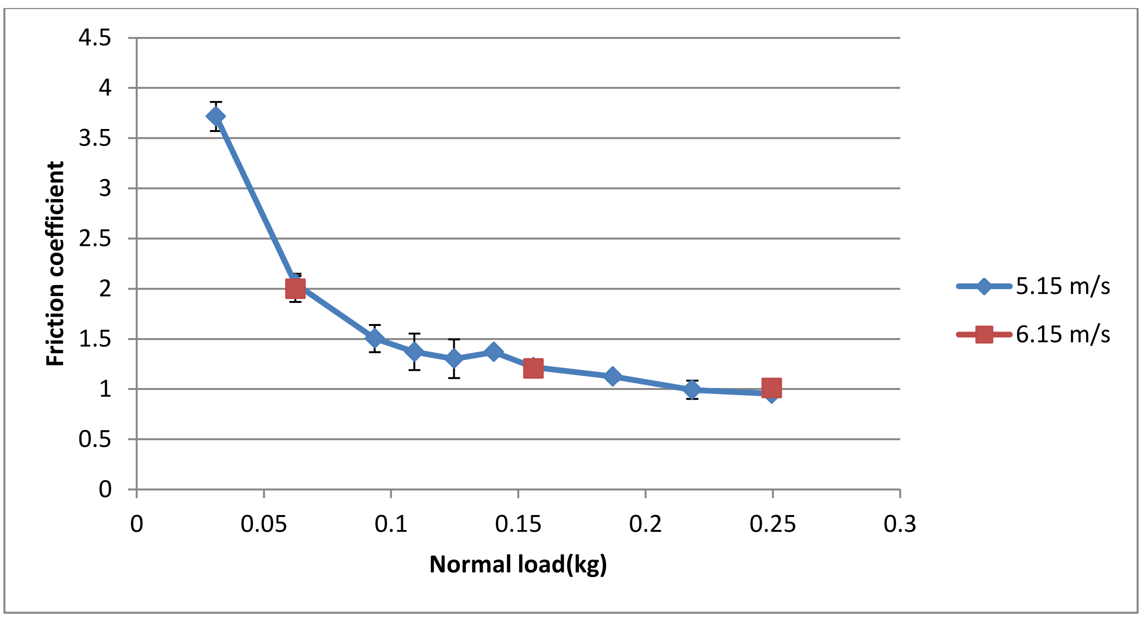

Figure 5-9 Friction coefficient against contact pressure, a) disc rotates with 5 km/h (1.38) - b) disc rotates with 10 km/h (2.7)

5.3.3. Overview of the friction results (sandpaper 120)

Figure 5-10 shows the result for all three experimental cases, and although the sliding velocities are different it can be seen that the results are similar and follow the same trend. The range of error bars decreased when the normal load has increased, which indicates that by increasing the contact pressure, stronger bonds are made with the contact surface and the friction result becomes more reproducible.

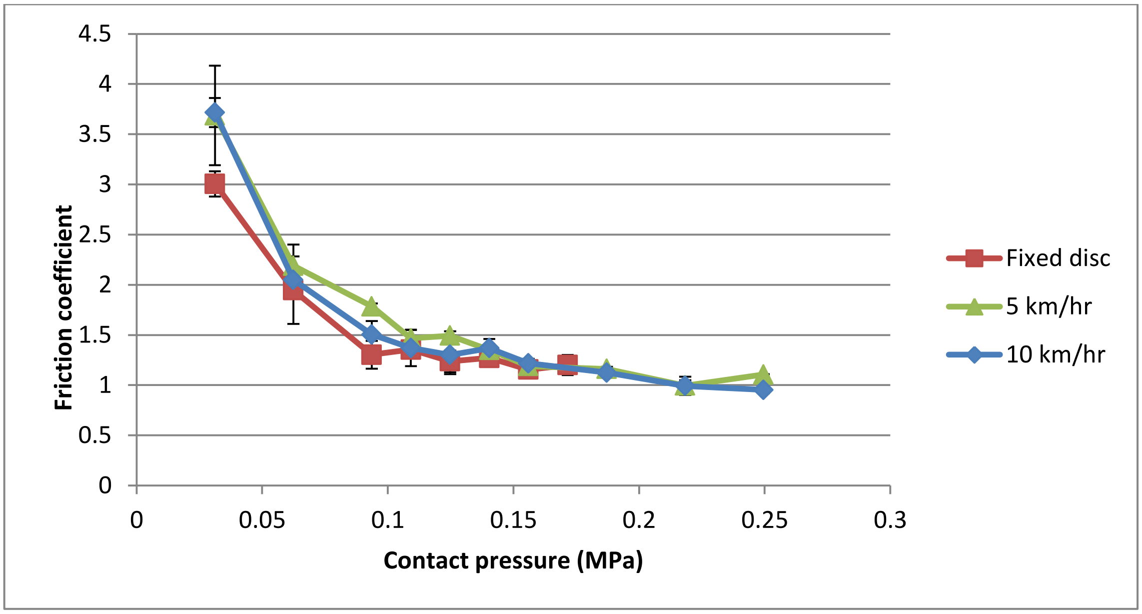

Figure 5-10 Friction coefficient vs. contact pressure for all the three cases, sandpaper 120

5.3.4. Sandpaper experiment (grit 400)

In previous experiments rubber friction against fine surface (steel) and rough surface (Sandpaper 120) was examined. In addition, another surface with roughness between the two aforementioned surfaces was used to show the friction coefficient of rubber. The experiments for this surface were only delivered in one range of speed in each case of disc velocity. Figure 5-11 shows an example for the fixed rubber pin against sandpaper 400, where the normal load is 6 kg and sliding velocity is 1 m/s. The graph in Figure 5-11 represents the region where the pin is sliding on sandpaper; the friction force is slightly dropping, which is due to wear of the sample. The decrease rate is less than sandpaper 120, which is reasonable because of the lower surface asperities.

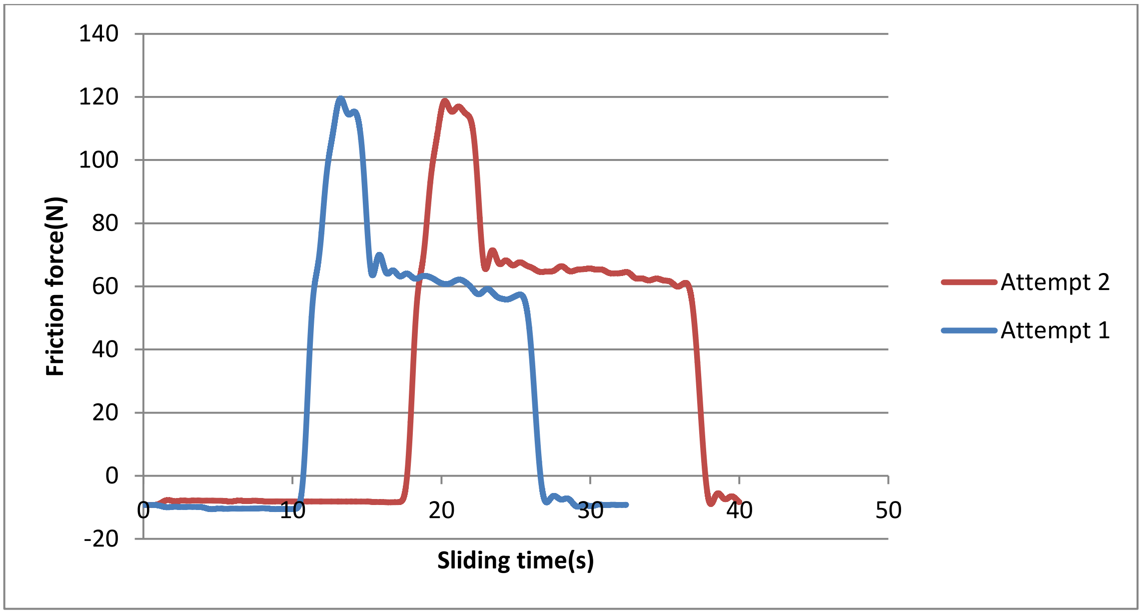

Figure 5-11 An example for fixed rubber against sandpaper400, sliding velocity 1 m/s & normal load=6 kg

The overall result for this experiment is demonstrated in Figure 5-12 for all three cases of disc velocities. In this result the sliding velocities of the pin were different, but the outcome is similar. When the pin was fixed the disc was rotating with 1 m/s, and when the disc was rotating with 1.38 and 2.7 m/s, pin velocity was 2.38 and 5.15, respectively. Similar to other surfaces and conditions the rubber friction coefficient showed less variation when the contact pressure reached 0.1 MPa.

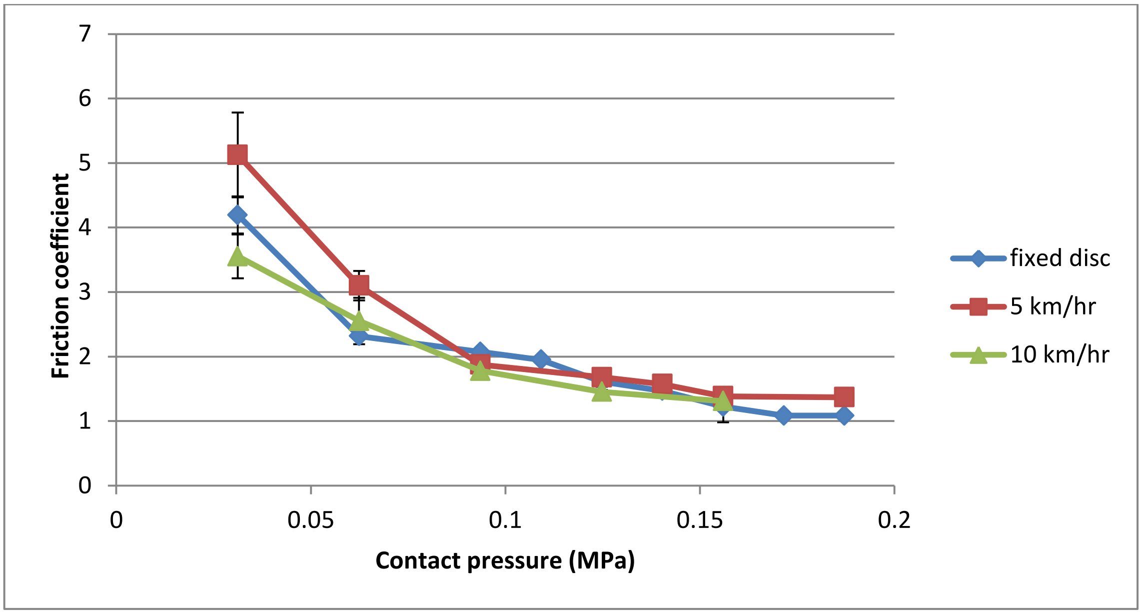

Figure 5-12 Overall results for friction coefficient against sandpaper 400, in three cases of disc velocity

5.4. Overall surface comparison

In sections 5.2 and 5.3 the results for steel disc and sandpaper disc were shown individually and the rubber friction coefficient was assessed. In this section the results based on surfaces in each case has been compared and discussed. Figure 5-13 shows the differences in friction coefficient in three cases: fixed pin (a), disc rotates with 1.38 m/s (b) and disc rotates with 2.7 m/s (c). In all three cases, friction coefficient varies in a similar pattern. The majority of fluctuations in friction coefficient occurred when there was a small amount of contact pressure between the rubber and the disc. The results from the sandpaper 120, as shown in Figure 5-13, in all three cases have significantly lower friction coefficient, the rubber sliding on sandpaper 400 provides higher values of friction coefficient, followed by the steel, which has the highest result. This is due to adhesion between the surfaces when rubber sliding on smooth surfaces, therefore increasing the surface roughness reduces the adhesion and the friction coefficient declines. Another intriguing subject is the convergence of the results for all three surfaces, by increasing the normal load, when friction coefficient is approaching a constant value, the reason for this converge is the mainly the high temperature at that point, since the temperature is so high in that amount of contact pressure, it is the main factor which cause the friction coefficient to decrease. In similar experiments for rubber against different surface roughness similar results were presented [80, 81].

a)

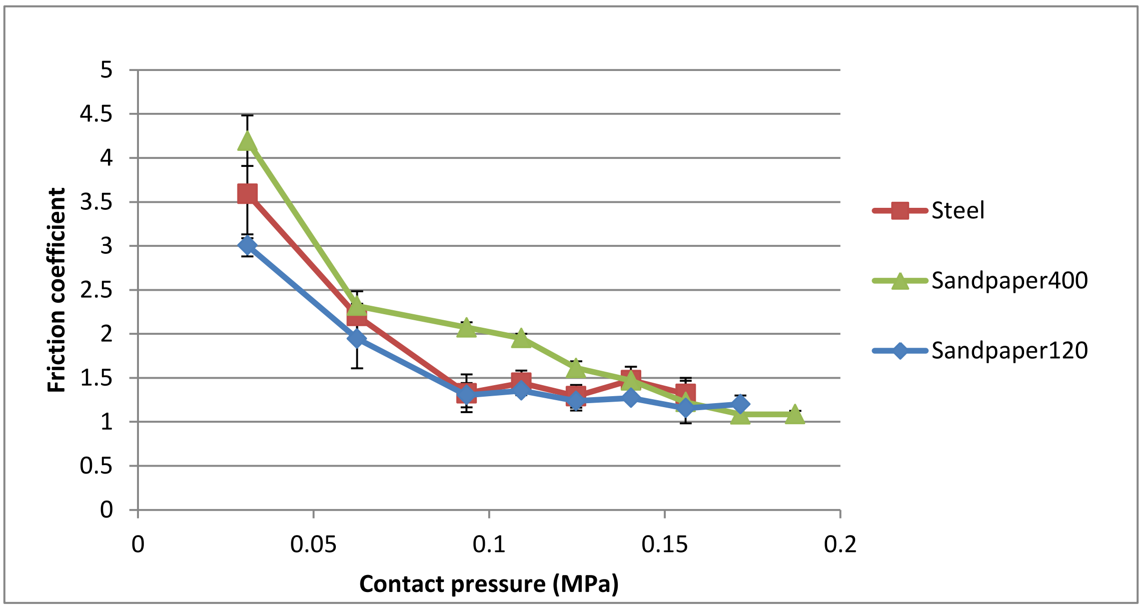

b)

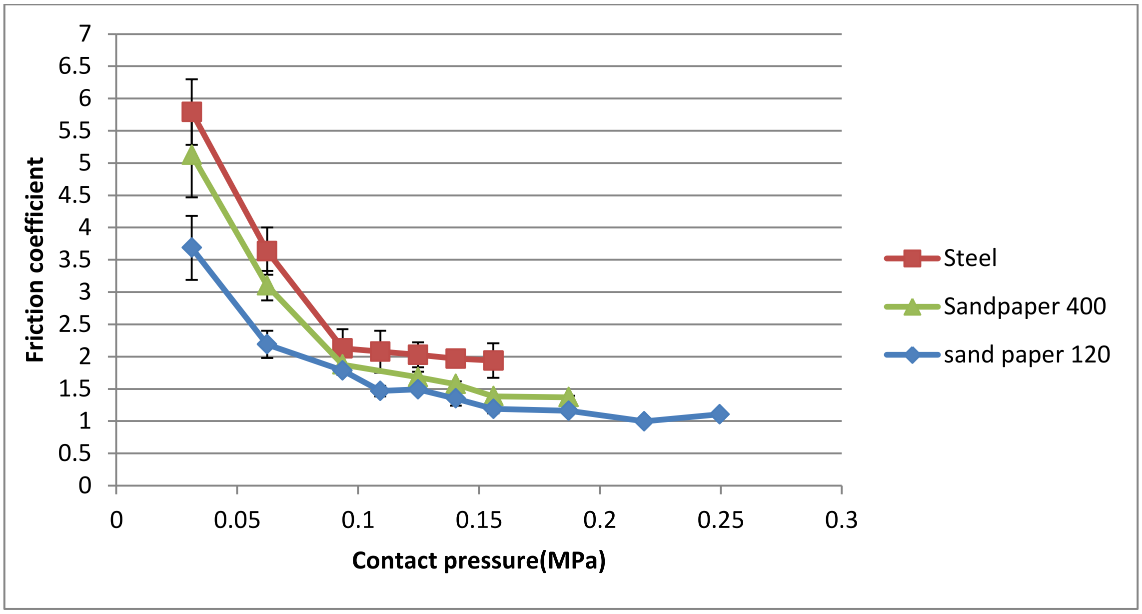

c)

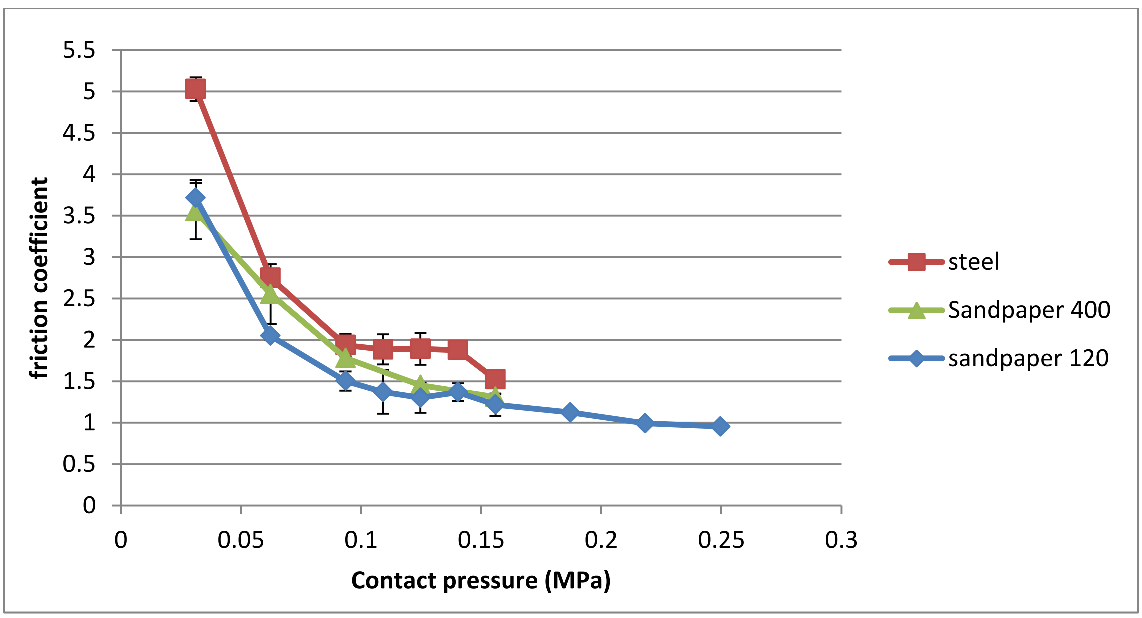

Figure 5-13 Surface comparison in three cases; a) fixed pin b) disc rotates 1.38 m/s c) disc rotates 2.7 m/s

5.5. Glass disc experiment

In sandpaper and steel experiments the effect of adhesion and surface roughness was discussed and shown in detail. It was stated that rubber friction is dependent on the rubber sample surface structure and different samples provide diverse results. Therefore, a brief experiment on rubber against glass was conducted with the aim to show the rubber surface structure dependency. The experiment for rubber was delivered when the pin was fixed and the glass disc was rotating with different sliding velocities and the sliding velocities were 0.5 and 2 m/s.

In the test, where the sliding velocity was 0.5 m/s, several rubber samples were examined and friction coefficients were investigated. Friction coefficient varied in a wide range, and the reproducibility was poor. The test was repeated with a higher sliding velocity and 10 rubber samples were selected for this experiment, in each case of normal load each sample was examined twice to achieve a better understanding of rubber samples. Figure 5-14 shows the obtained friction coefficient for rubber sliding against glass for both sliding velocities. Load dependency is not observable when rubber slides against a smooth surface like glass. However, the results became more reasonable undergoing a slight decrease when the test for 2 m/s was conducted and the number of attempts was increased to 10.

a)

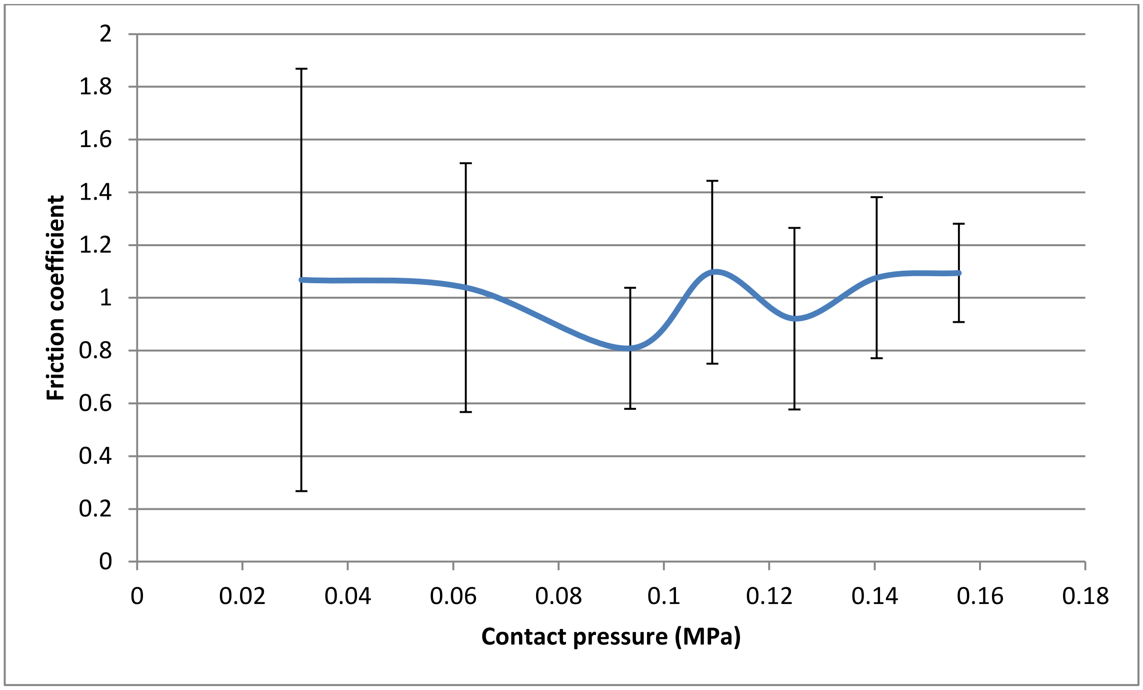

b)

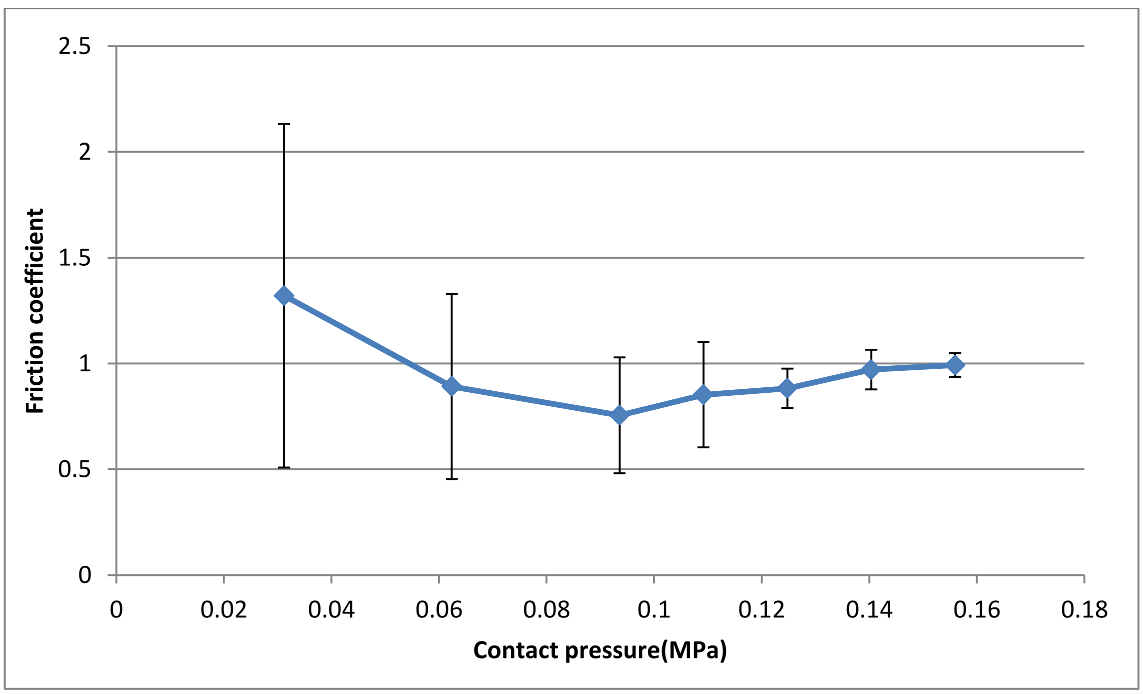

Figure 5-14 Friction coefficient for rubber against glass, sliding velocity=2 m/s

In glass test the sliding velocity was 2 m/s, 5 samples were examined with two attempts for each; Figure 5-15 shows the result for the two different samples. It was observed that each sample showed diverse results, although repeating the test with the same sample for the second time provides a similar result.

a)

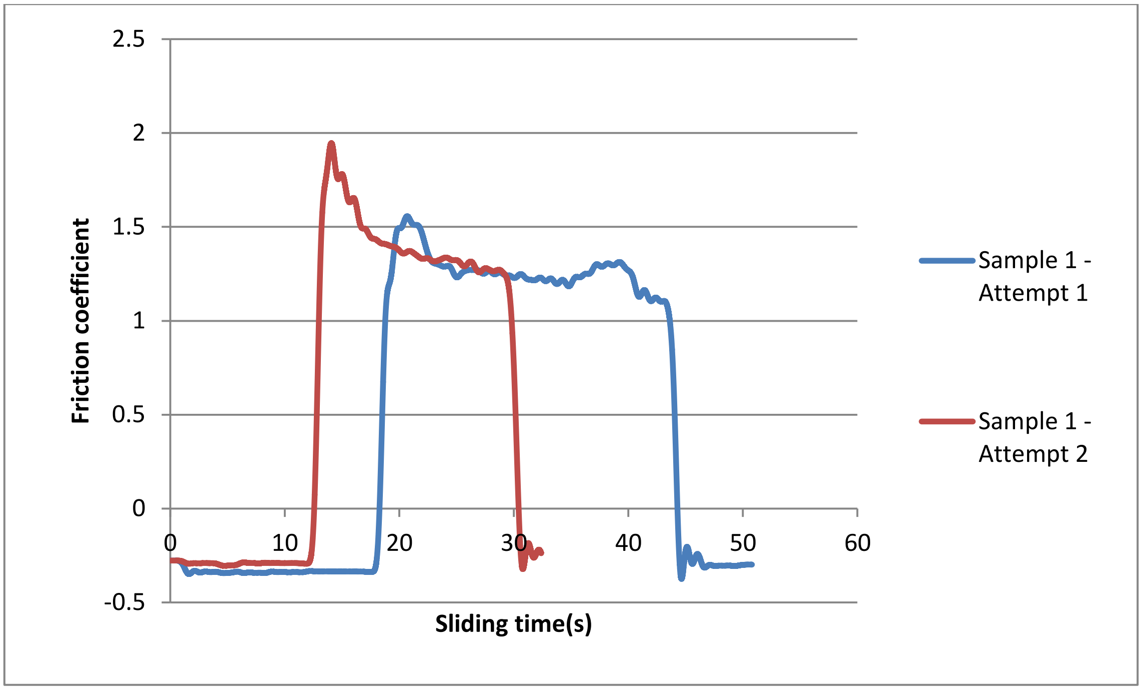

b)

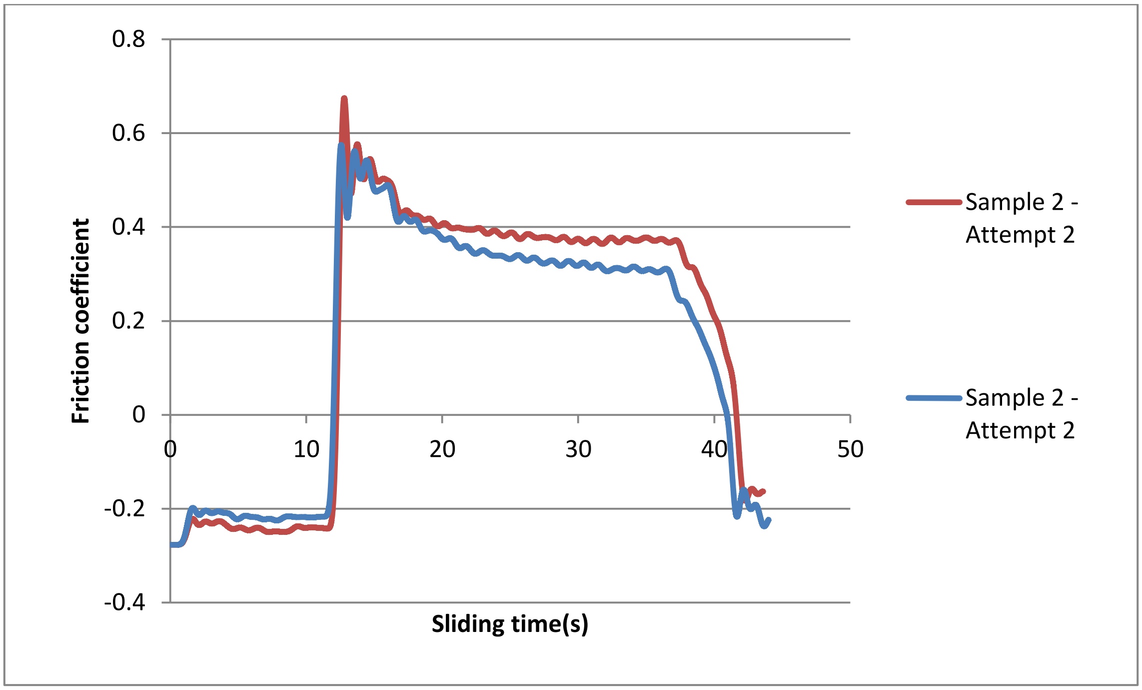

Figure 5-15 Friction coefficient for two different samples (a & b) that each sample examined two times

Although initially in this study it was not planned to measure rubber friction coefficient against glass, and the outcome of it is not as expected, the glass test shows that rubber surface roughness has an important role in rubber friction coefficient. This has been observed by several researchers and there were attempts to use coarse rubber and abraded rubber to avoid heavy adhesion between rubber and the counter-surface [82].

5.6. An overview of the results

It was shown in the results that the pin changes and the pin velocity have no effect on the friction coefficient. The disc velocity has no effect in high contact pressure and there are minor changes in the friction for lower range of contact pressure. Although the rubber surface roughness has an influence on the results, it is mostly the case for smooth surfaces. The main effect of rubber surface structure was visible during the steel disc experiments (as it is considered a fine surface in comparison to sandpaper) and it was attempted to balance this effect by using several samples and increasing the test replications. The results can be divided into two categories: 1) rubber sliding against a fine surface (steel) and 2) rubber against rough surfaces (sandpapers). This type of categorizing the data is useful for modelling friction coefficient dependence on contact pressure and the disc velocity. In the next section friction coefficient modelling is explained in details.

5.7. Friction coefficient modelling

It was stated that modelling friction coefficient is a challenging process, thus there is no model, which can provide a result to cover all the requirements and shortcoming of the other friction models and techniques. Linear regression is the most well-known method, which can present a model based on experimental results when more than one value is affecting the results. This method provides 2nd and 3rd polynomial order equations and provides a squared residual (R^2) value for each correlation. The squared residual shows the accuracy of the correlation if it is close to 100%. As explained in section 5.6, the results were divided into two parts; steel and sandpaper; therefore, two correlations (2nd and 3rd) for each surface are derived and the R^2 value for each of them is calculated. It is evident that a 3rd order equation covers a higher range and is more accurate than 2nd order but this adds complexity to the model and increases the coefficients. To calculate the linear regression for this model engineering software was used called Engineering Equation Solver (EES). In EES the data are imported as look-up table and it enables the operator to choose the order of the polynomial equation and provides the constants of the equation in a table with evaluated squared residual.

a)

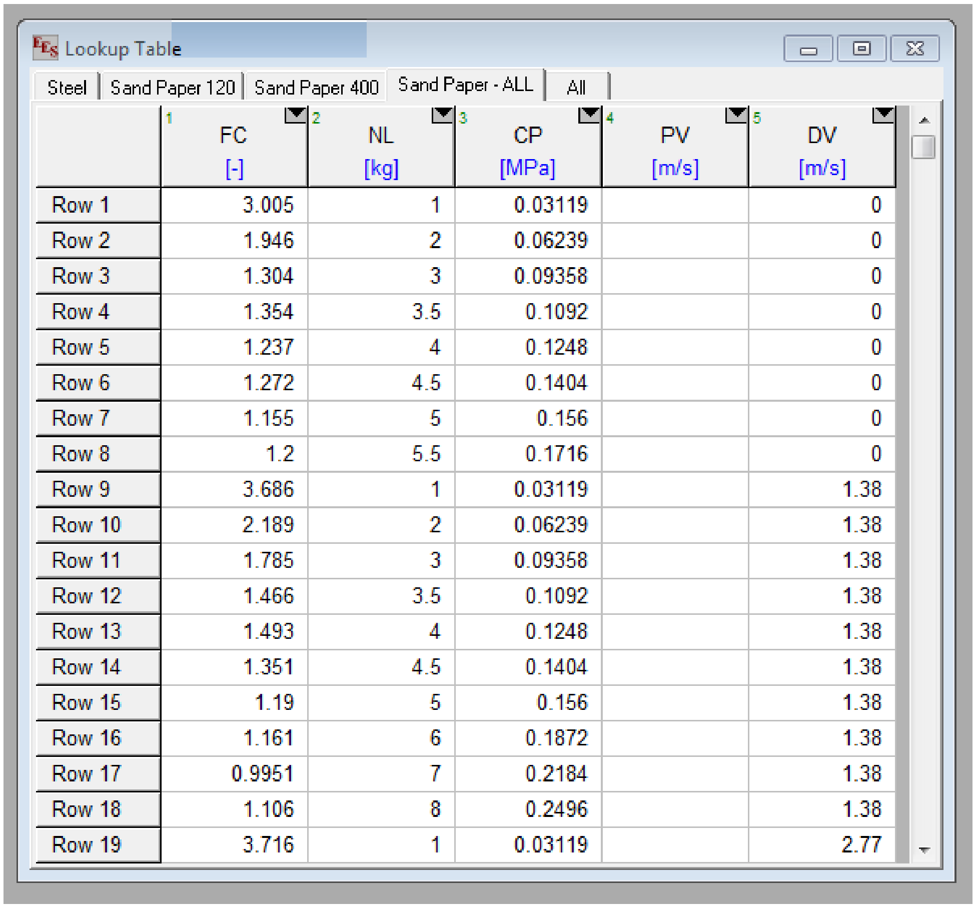

Lookup Table

Steel | Sand Paper 120 | Sand Paper 400 | Sand Paper - ALL | All

	FC [-]	NL [kg]	CP [MPa]	PV [m/s]	DV [m/s]
Row 1	3.005	1	0.03119		0
Row 2	1.946	2	0.06239		0
Row 3	1.304	3	0.09358		0
Row 4	1.354	3.5	0.1092		0
Row 5	1.237	4	0.1248		0
Row 6	1.272	4.5	0.1404		0
Row 7	1.155	5	0.156		0
Row 8	1.2	5.5	0.1716		0
Row 9	3.686	1	0.03119		1.38
Row 10	2.189	2	0.06239		1.38
Row 11	1.785	3	0.09358		1.38
Row 12	1.466	3.5	0.1092		1.38
Row 13	1.493	4	0.1248		1.38
Row 14	1.351	4.5	0.1404		1.38
Row 15	1.19	5	0.156		1.38
Row 16	1.161	6	0.1872		1.38
Row 17	0.9951	7	0.2184		1.38
Row 18	1.106	8	0.2496		1.38
Row 19	3.716	1	0.03119		2.77

b)

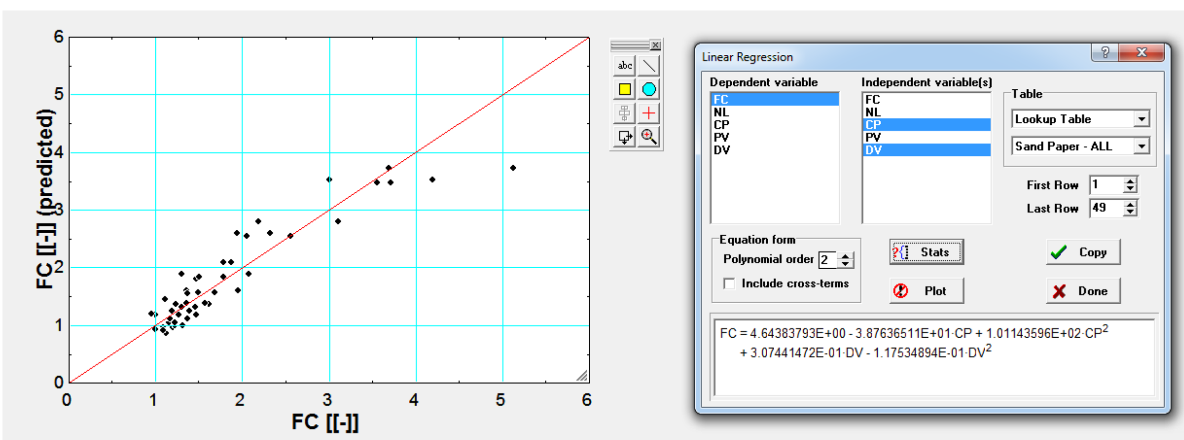

c)

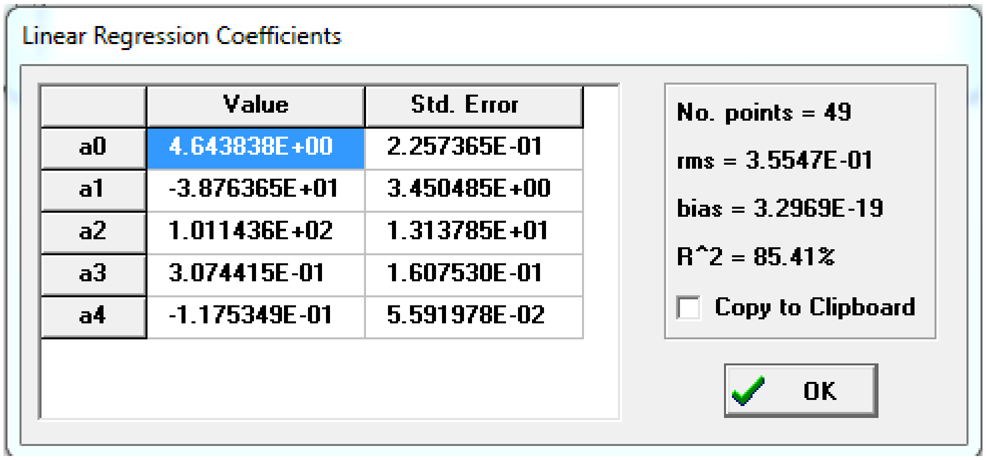

	Value	Std. Error
a0	4.643838E+00	2.257365E-01
a1	-3.876365E+01	3.450485E+00
a2	1.011436E+02	1.313785E+01
a3	3.074415E-01	1.607530E-01
a4	-1.175349E-01	5.591978E-02

Figure 5-16 An example for linear regression with EES; a) data imported in look up tables b) evaluating the correlation based on the polynomial order c) the coefficients of the correlation provided in table and the R^2 is shown next to it

5.7.1. Friction coefficient correlations

The calculated correlations with the R^2 are presented here; and even though the 3rd order polynomial has more complexity in comparison to the 2nd order correlation, it provides a higher R^2 meaning higher accuracy. As friction results are divided into two categories; steel and sandpaper results, the general equation for 2nd and 3rd order equations are provided and the constant coefficients are presented in tables according to each model. Equation 5-1 and Equation 5-2 show the general form of the 2nd and 3rd polynomial equations, respectively, where *c.p* is the contact pressure and V is the disc velocity.

$$\mu(V,P) = a_0 + a_{1*}c.p + a_2 * c.p^2 + a_3 * V + a_4 * V^2 \qquad \text{Equation 5-1}$$

$$\mu(V,P) = a_0 + a_{1*}c.p + a_2 * c.p^2 + a_3 * c.p^3 + a_4 * V + a_5 * V^2 + a_6 * V^3 \quad \text{Equation 5-2}$$

The constants coefficients for the 2nd degree friction correlation (Equation 3-1) and squared residual values are presented in Table 5-1 for each disc results. Furthermore, in Table 5-2 coefficients and the squared residuals are presented for the 3rd degree friction correlation; each surface is accompanied by the average number of friction coefficients, upon which the model was developed. Although a higher R^2 represent a more accurate model, this number is affected by the number of friction coefficients, which were used for calculation. Therefore, a model can be selected, based on surface roughness (fine, rough or combination of both) and also the complexity (2nd or 3rd order) of the proposed models.

Table 5-1 2nd degree coefficients for the correlations

Coefficients	Steel (126)	Sandpaper (49)	All (175)
a_0	5.18E+00	4.64E+00	4.54E+00
a_1	-5.92E+01	-3.88E+01	-3.84E+01
a_2	2.20E+02	1.01E+02	9.91E+01
a_3	1.05E+00	3.07E-01	8.27E-01
a_4	-3.03E-01	-1.18E-01	-2.44E-01
R^2	85.58 %	85.41 %	79.97 %

Table 5-2 3rd degree coefficients for the correlations

Coefficients	Steel (126)	Sandpaper (49)	All (175)
a_0	6.28E+00	5.73E+00	5.73E+00
a_1	-1.08E+02	-7.65E+01	-8.19E+01
a_2	8.09E+02	4.31E+02	5.05E+02
a_3	-2.09E+03	-8.18E+02	-1.07E+03
a_4	1.58E-01	-4.37E-02	1.74E+00
a_5	6.69E-01	2.84E-01	-1.22E+00
a_6	-2.35E-01	-9.70E-02	2.33E-01
R^2	86.64 %	89.64 %	84.11 %

5.1. Conclusion

The resultant force and friction for each surface and counter-surface was extensively described and the effects of normal load/contact pressure, disc velocities and surface roughness were compared. It was shown that the pin velocity does not affect the result in any of the experiments therefore only one range of speed can be considered for its velocity and thus different velocities are not necessary. The disc velocity had some effect on the results in low contact pressures though they were not significant. The influence of surface roughness was explained and shown. It is concluded that rubber structural surface significantly affect the friction force and a test against smooth surface (glass) was conducted to show whether there is a wide range of variation in the result.

Based on the obtained result from steel and sandpapers, several models were developed by linear regression technique and due to the complexity of condition and the necessity of accuracy a model can be selected for predicting friction coefficient dependent on velocity and contact pressure.

6. Tyre Finite element analysis

6.1. Introduction

Finite element analysis (FEA) in tyre modelling is an aid to engineering for manufacturing and design. It is an ultimate goal to make tyre FEA simulations as accurate and close to real tyre behaviour as possible to reduce the cost of tyre testing [83]. The aim of this research was to obtain friction results dependant on contact pressure and velocity to make the outcome of the simulation accurate and similar to the realistic tyre performance. In this chapter preparation of a tyre 3D model is described in brief and the obtained friction coefficients are applied on the tyre. Furthermore, the imported friction coefficient and the constant friction coefficient are compared. The process of obtaining the friction results for rubber against different contact pressure and velocities was fully described earlier. In the literature review the friction models, which were previously applied on tyres and simulated the dynamics were discussed. The focus of this research was to compare between the outcome of constant friction coefficient and the obtained friction coefficients. ABAQUS provides a commercial method for Tyre modelling, which is the most common technique to model tyre vehicle dynamics. In this method, a 2D cross-section of a tyre is imported into ABAQUS, the 2D model was obtained from the image-processing presenting reinforcements co-ordination and rebar materials. In this study the rubber samples were collected from a tyre, which has already been modelled at the University of Birmingham, therefore this tyre model was used to observe the effect of the friction models [84].

6.2.Friction coefficients implementation

The friction coefficients, which have been obtained from the experiments, were converted into a look-up table as μ (friction coefficient) against the contact pressure. The models did not show any significant dependency on velocity, therefore only their variation against contact pressure was modelled.

Three tables containing the results of the steel, sandpaper 120 and sandpaper 400 were presented and imported in to FEA package. In ABAQUS a subroutine (i.e. FRIC and VFRIC) has to be prepared to show the friction result effect; however it is possible to import the friction coefficient in the software's interface or in the simulation inp codes (input files), therefore in this simulation the friction coefficients were added to the inp codes. To show the comparison between these models and a constant friction coefficient, the same tyre model was developed with two constant friction coefficients; 0.9 and 1. The specifications, which have been varied in the model, to observe the changes and variations are as below:

- 5 Friction coefficients: Steel, sandpaper 120, sandpaper 400, constant friction coefficients; 1 and 0.9
- Normal loads: 2, 2.5, 3, 3.5, 4, 4.5, 5, 5.5, 6 and 6.5 kN
- Slip angle: 1, 2 and 3 Degrees

6.3. Tyre finite element analysis process

Modelling tyre in ABAQUS includes several steps: preparing a 2D model in the software interface, adjusting the rubber and the reinforcements regions, allocating the material properties, and defining the constraints between rubber and the reinforcements. Moreover, defining the surface for the inflation pressure and the contact to the road is involved in this stage of the modelling. Figure 6-1 shows the 2D sketch of the tyre and reinforcement of the tyre, the details of the modelling of this tyre has been explained in details in main article [84].

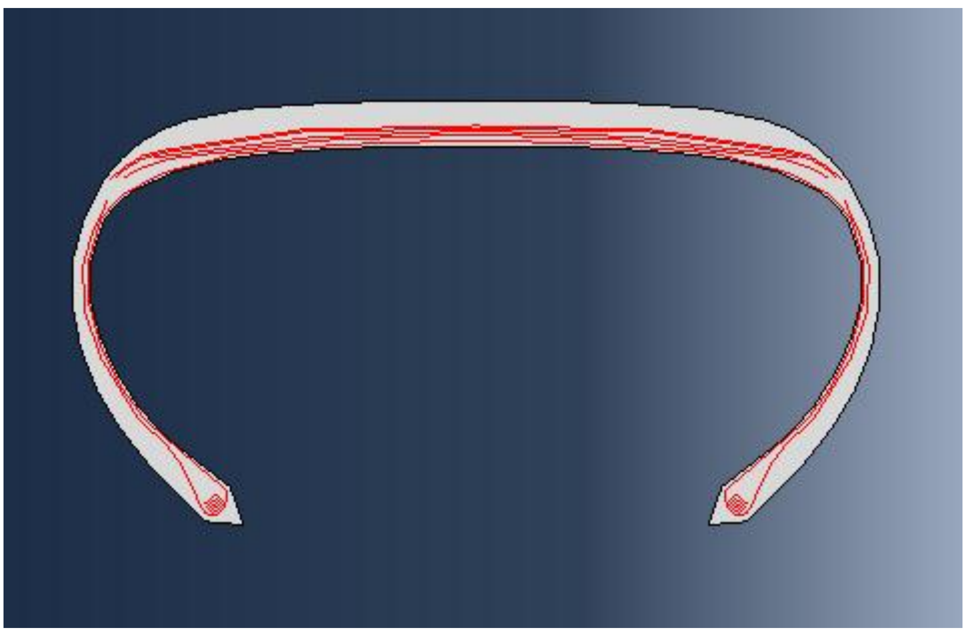

Figure 6-1 2D sketch of a tyre with the reinforcement

In this simulation the tyre is inflated in a 2D geometry and with an inp code it is converted into a 3D geometry. In this step the contact between the tyre and the road is adjusted and the amount of normal load is applied. Then the model goes through two more codes to reach free rolling condition (slip = 0), and the friction coefficients are applied in the primary code (known as brake-traction). In the first code, a wide range of rotational velocity (rad/s) for tyre was selected. The amount of longitudinal force against the rotational velocity was considered for the models output. The velocity, at which longitudinal force equals zero (which means rolling resistance equal to zero, therefore slip is zero, although in reality there is rolling resistance in free rolling but since this value is so small, it is neglected in the simulations) was selected as the free rolling velocity. In the second code, a smaller range of rotational velocities was selected to make the free rolling velocity more accurate. Then another code is used to simulate cornering on the tyre; in this code the free rolling velocity is applied on the tyre and the velocity of the road is calculated for each slip angle; V_x and V_y were the components of velocity in x and y directions. The tyre lateral force is defined as the cornering force, which is the main focus of this research. Figure 6-2 shows a brief diagram of tyre modelling in Abaqus.

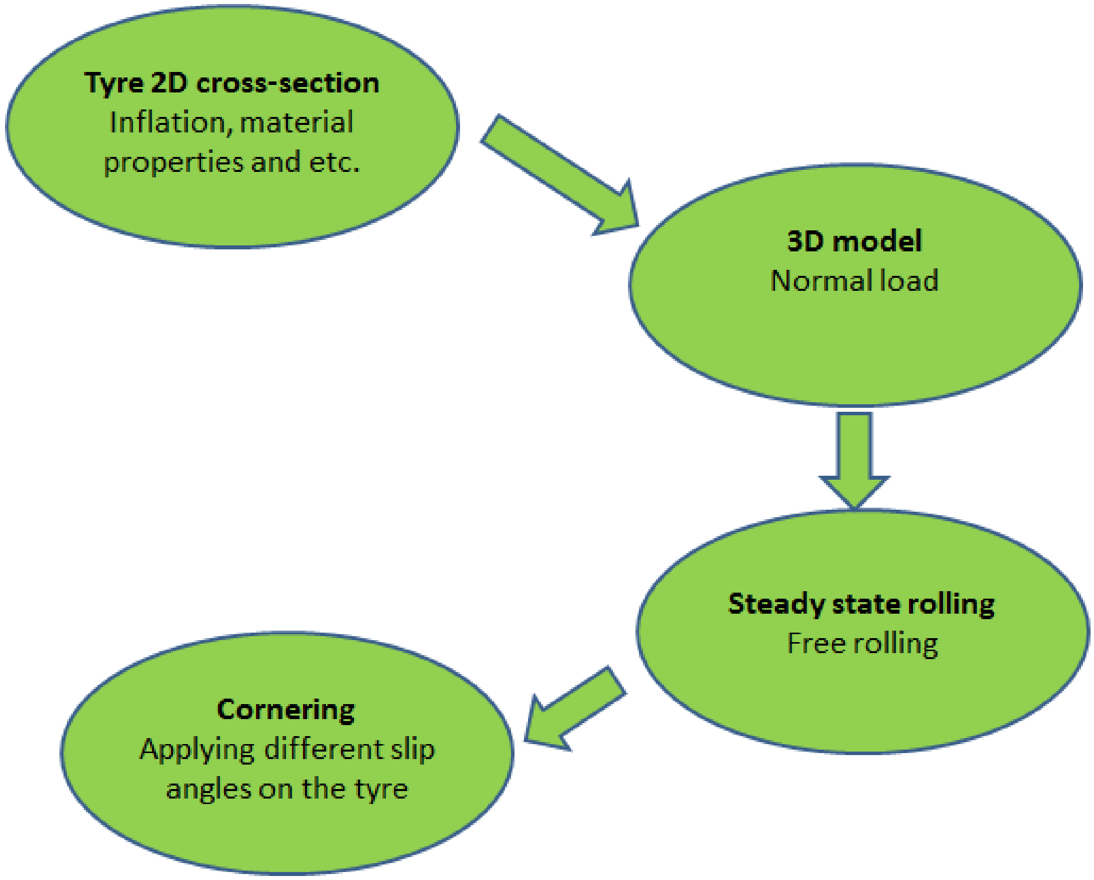

Figure 6-2 A diagram to show tyre FEA modelling

6.3.1. Modelling

The inflation pressure in tyre was 0.22 MPa, Figure 6-3 shows the tyre cross-section before and after inflation. Then the tyre was converted into 3D model and normal loads from 2 to 6.5 kN with the increments of 0.5 kN were applied on the tyre. The deflection and the vertical stiffness of the tyre is not the topic to discuss in this research and their variations are not demonstrated. The simulation carries brake and traction code, in the inp files, the friction coefficients were applied, since in this model the road was moving with 10 km/h, the friction coefficients were from the tests in which the disc was rotating with 10 km/h speed. In each case of normal load and friction coefficient the free rolling velocity were varying although the changes were minor, however the ranges in all simulations were measured, in general the free rolling velocity was 8.3 rad/s and it was increasing by increasing the normal load. Table 6-1 shows the range of normal loads and minimum and maximum of the rotational velocity for each case, during the brake-traction simulations.

a)

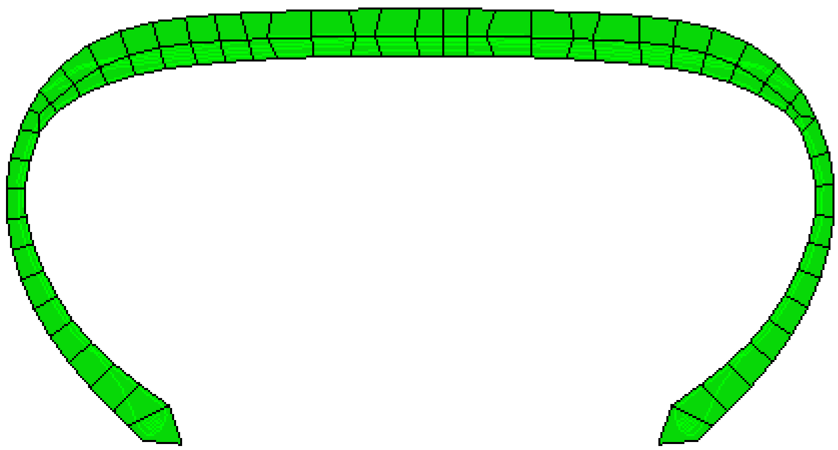

b)

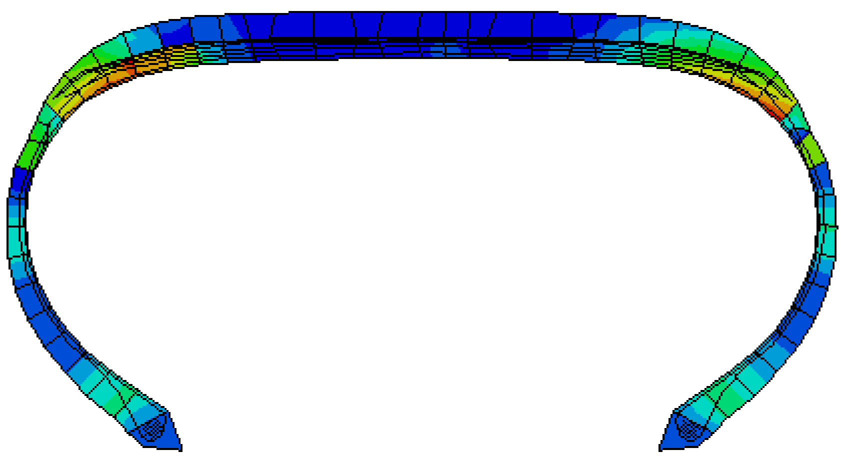

Figure 6-3 a) The tyre profile before inflation b) tyre after inflation, 0.22 MPa

Table 6-1 Range of normal loads where the model was working and maximum and minimum rotational velocity in each range

µ	Range of Normal load (kN)	Min rotation velocity (rad/s)	Max rotation velocity (rad/s)
0.9	2-6	8.37	8.44
1	2-6	8.37	8.42
steel	2-4.5	8.37	8.41
Sandpaper 120	2-5.5	8.39	8.43
Sandpaper 400	2-4.5	8.37	8.41

6.3.2. Cornering results

In this section the results for the cornering forces against different normal loads for with each friction coefficients are compared and discussed. Unfortunately the simulations for the cornering forces did not entirely converge due the shortage of computer resources. The results for cornering force against different slip angles are demonstrated, the results are shown for each set of friction coefficients.

a)

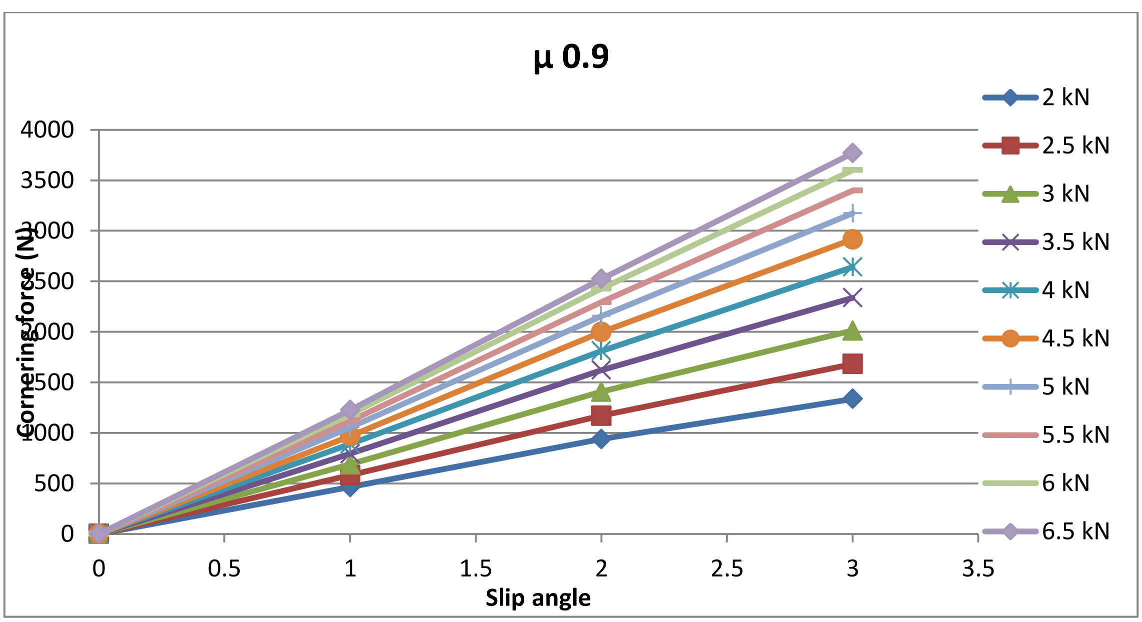

b)

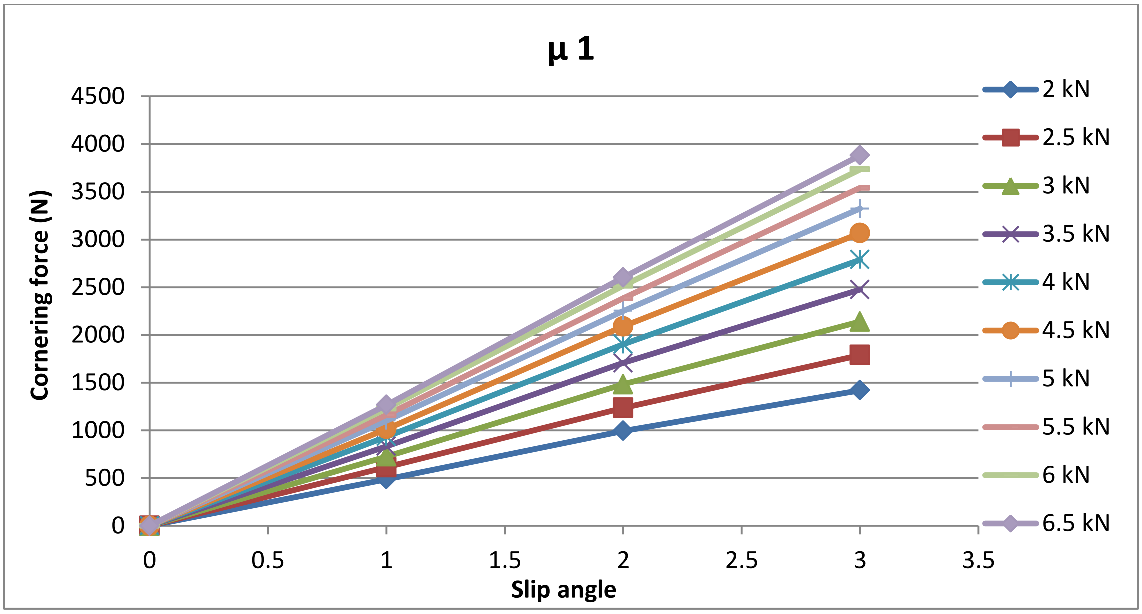

μ 1
Cornering force (N)
Slip angle
2 kN
2.5 kN
3 kN
3.5 kN
4 kN
4.5 kN
5 kN
5.5 kN
6 kN
6.5 kN

c)

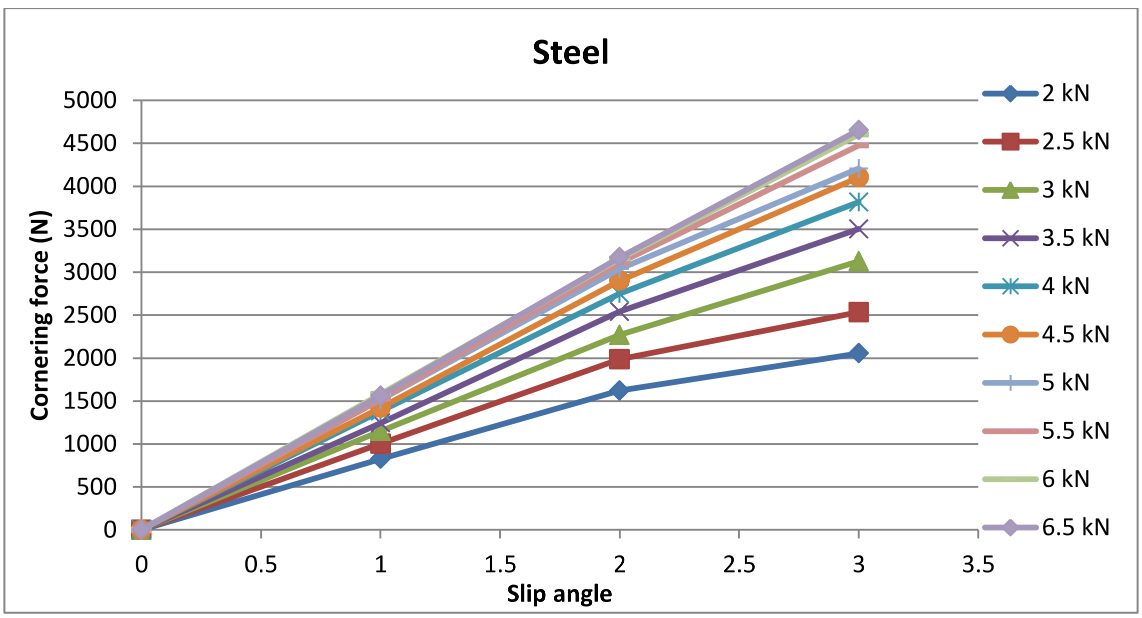

Steel
Cornering force (N)
Slip angle
2 kN
2.5 kN
3 kN
3.5 kN
4 kN
4.5 kN
5 kN
5.5 kN
6 kN
6.5 kN

e)

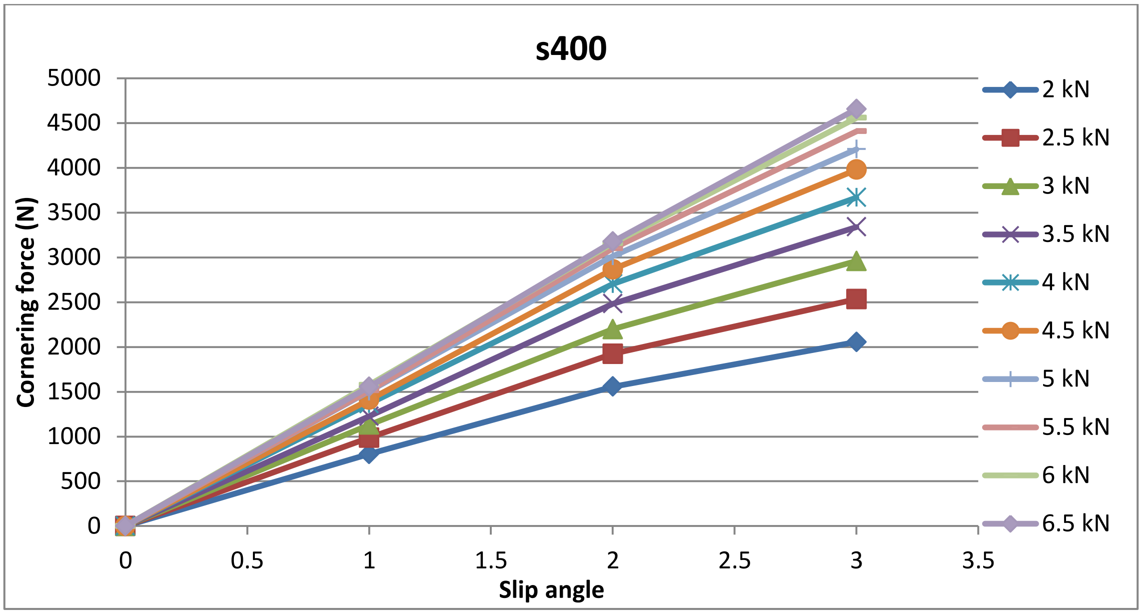

f)

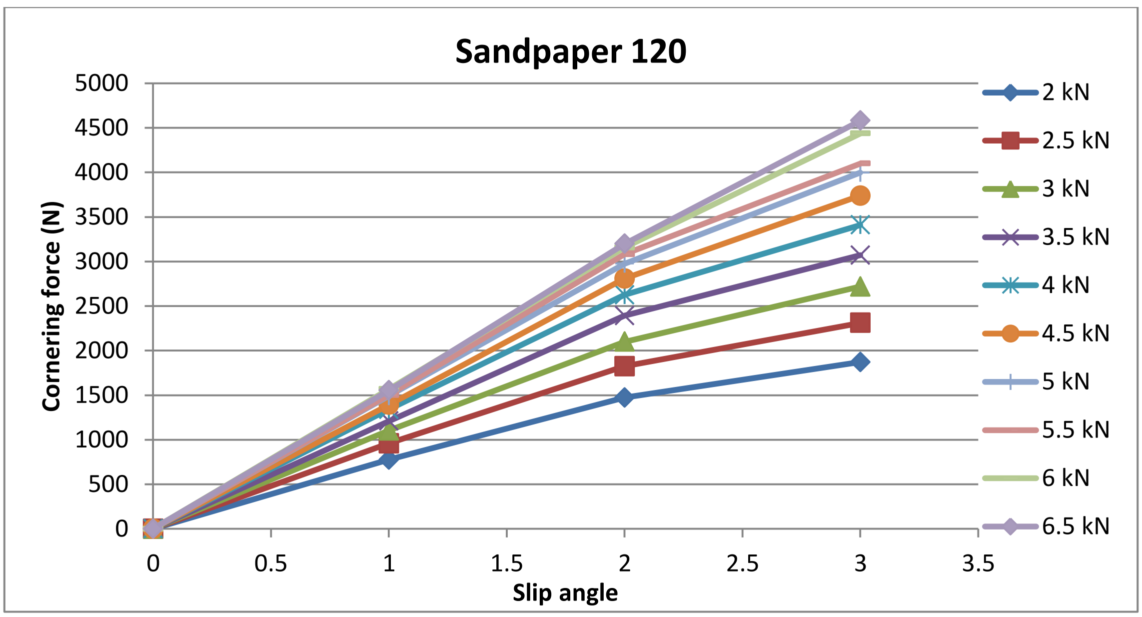

Figure 6-4 Cornering forces vs. slip angle for different friction coefficients: a) constant 0.9 b) constant 1 c) steel friction coefficients e) sandpaper 400 friction coefficients f) sandpaper 120 friction coefficients

6.3.3. Cornering stiffness

Cornering stiffness is defined the most important parameter when a tyre is steering [85]. They are more significant as the vehicle is moving in high speeds and since lateral force can control the direction of the vehicle. Cornering stiffness is mainly affected by two parameters, normal load and the tyre inflation [86]. From the cornering forces obtained from the above-mentioned simulations, the cornering stiffness was calculated. Figure 6-5 shows the result for the cornering stiffness. It can be observed in the simulations with constant friction coefficient the cornering stiffness is increasing though in the simulations which the experimental friction coefficients (sandpaper 120 and sandpaper 400) were applied, it increases to a certain load and reaches a steady value, as it is expected in reality. The calculated values of cornering stiffness are shown in Table 6-2 for each case of normal load and friction model. The result for the model with rubber/steel friction coefficient did not proceed to a higher normal load values, this is due to the fact that the rubber/steel friction coefficient is slightly higher than the other models.

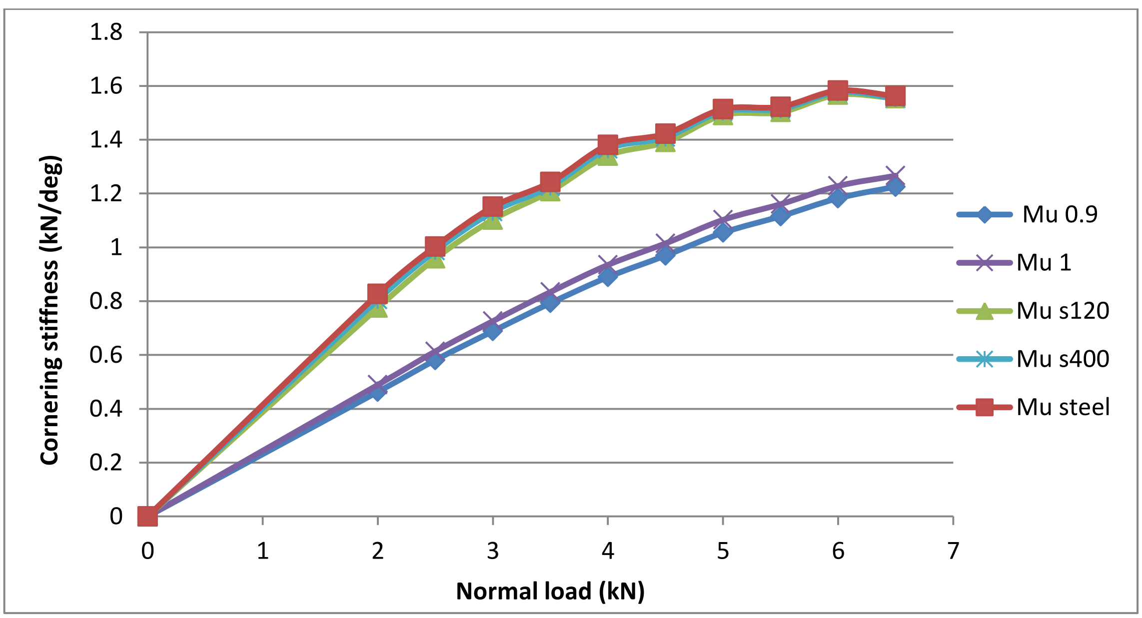

Figure 6-5 Cornering stiffness (kN/degree) Vs. normal load (kN)

Table 6-2 Cornering stiffness (kN/deg) Vs. normal load for different friction values

	Cornering stiffness (kN/Deg)				
Normal load (kN)	0.9	1	S120	S400	Steel
2	0.463	0.489	0.826	0.776	0.805
2.5	0.581	0.613	1.003	0.959	0.987
3	0.688	0.726	1.151	1.103	1.132
3.5	0.793	0.834	1.242	1.209	1.226
4	0.890	0.935	1.380	1.341	1.366
4.5	0.969	1.015	1.422	1.391	1.409
5	1.055	1.102	1.514	1.491	1.505
5.5	1.116	1.161	1.522	1.502	1.514
6	1.183	1.228	1.583	1.567	1.576
6.5	1.226	1.266	1.562	1.554	1.555

In Table 6-2 and Figure 6-5 the values and results for cornering stiffness are shown, it is clear that in the cases where constant friction coefficients were applied the cornering stiffness was increasing and where the friction values dependent on contact pressure were applied, cornering stiffness increases and after reaching a certain amount of normal load, decreases (the values are highlighted in Table 6-2).

6.4. Conclusion

The tyre which has been used for this study was modelled in ABAQUS and a range of normal loads was applied on it, the model was developed for different friction coefficients. Tyre was simulated in steering and different values of slip angle were compared. Eventually cornering stiffness was compared. As it was expected the cornering stiffness increases with increasing the normal load. This increase was continuous in model with constant friction coefficient, in the other models it reaches a certain value and started to decrease and this shows the validity of the proposed models.

7. Conclusion and future work

7.1. Conclusions

In this research rubber frictional behaviour was discussed, it was mentioned that rubber is a main component in a tyre and therefore, it has a major role in tyre modelling. Prediction of the frictional behaviour is divided into two categories: 1) rubber friction modelling and 2) tyre friction modelling. The examples of both techniques were discussed and advantages and drawbacks of each model were described. To this day there is no friction model, which can predict all the aspects of frictional rubber behaviour and which can be universally applicable in tyre modelling. Every single model, whether derived mathematically or obtained experimentally, has deficiencies.

The main parameters, which affect rubber friction, are normal load and velocity, whereas friction coefficient is a convenient way to demonstrate the relation of forces in a system and varies in different situations. To obtain a friction coefficient dependent on normal load and contact pressure a pin on disc tribometer was designed and manufactured. The main deficiency of this facility was the fact that the pin condition was stationary; therefore the friction result for it was the sliding friction coefficient. Moreover, the pin was not large enough to show the bonds between rubber and contact-surface, and the sensor, which was used in it, could not provide high resolution steady results, therefore, they were not shown and discussed in this research. Furthermore, another modified tribometer (rotary pin on disc) was designed; in this facility the pin was rotating around the same axis as the disc, and it was possible to control the velocity of the motors to provide different slip ratio and sliding velocities. Several ranges of speed and numerous contact pressures were examined and rubber friction was measured against different surfaces. The results showed that rubber friction did not vary in the range of velocities, which this facility can manoeuvre. As it was expected, friction force increased with increasing normal load, while friction coefficient decreased. Moreover, the disc velocity had minor effect in low contact pressures, however in general the results did not differ considerably. Friction coefficients were obtained for rubber against steel and two kinds of sandpaper. Since in this facility the rubber was sliding against the counter-surface, adhesion was the main reason of friction between the contacts. Therefore, steel disc provided a higher friction coefficient than sandpapers, and amongst sandpapers the one, which had a lower surface roughness delivered a higher friction coefficient.

Rubber surface structure has a significant effect on the friction force; in order to show the validity of this theory in this research and justify the changes in the results for abovementioned surfaces a test against glass disc was conducted. Glass has a smooth surface and the friction results from examining rubber against glass provide understating of the adhesion. The high range of uncertainties from rubber against glass test from all the condition of test showed that the variation were mostly due to the difference in rubber samples, though a rubber sample provided a similar results when it was examined two times.

To express a friction coefficient as a function of contact pressure and velocity, models for different surfaces were developed with linear regression. Linear regression is the technique, which can replace curve-fitting when there are more than one dependent variable in the system condition. Proposed models were divided to three categories: a model based on steel disc results, another for sandpapers and one based on the all results (steel and sandpapers). The correlations were in 2^{nd} and 3^{rd} degree of polynomial order; model involving 3^{rd} degree of polynomial order is more complicated although more accurate and a correlation is selected based on consideration of the squared residual of the model.

The friction results were used in tyre finite element analysis, the process of tyre modelling was briefly described and the effects of the friction values in cornering were reviewed. A comparison between the constant friction coefficients and the experimentally derived friction values was provided. Cornering forces and cornering stiffness were the main focus of the simulation, since cornering stiffness is the parameter to show vehicle handling property. In FEA cornering stiffness increases proportionally, whereas in experimental conditions cornering stiffness reaches a steady value after normal load has increased to a certain point and then decrease gradually. Therefore, it is concluded that the experimental friction values obtained in this study can be used for future work and benefit tyre modelling. Additionally, several problems and obstacles, which were encountered in this research, can be investigated in the future as it is explained further.

7.2. Future work

The friction results from this research did provide a model for tyre simulations, however there are still gaps to be considered and scientifically reviewed. The future steps involve several stages including experimental facility, friction model and the FEA tyre model.

7.2.1. Experimental setup future work

In this setup the provided results were precise and accurate, though the friction force, which has been measured, is in longitudinal direction and in cornering the friction force could be in two directions, which can vary with different angles. It is assumed that by changing the centre of rotation of the pin, the friction between the sample and the disc changes by the position of the pin over the disc; however manufacturing this facility and adjusting the distance for rotation centres has its own complexity. Therefore, to show the variation in the friction force a FEA model (Figure 7-1) for the proposed experimental setup was developed to represent a general idea of the friction force. The result from this model is under investigation.

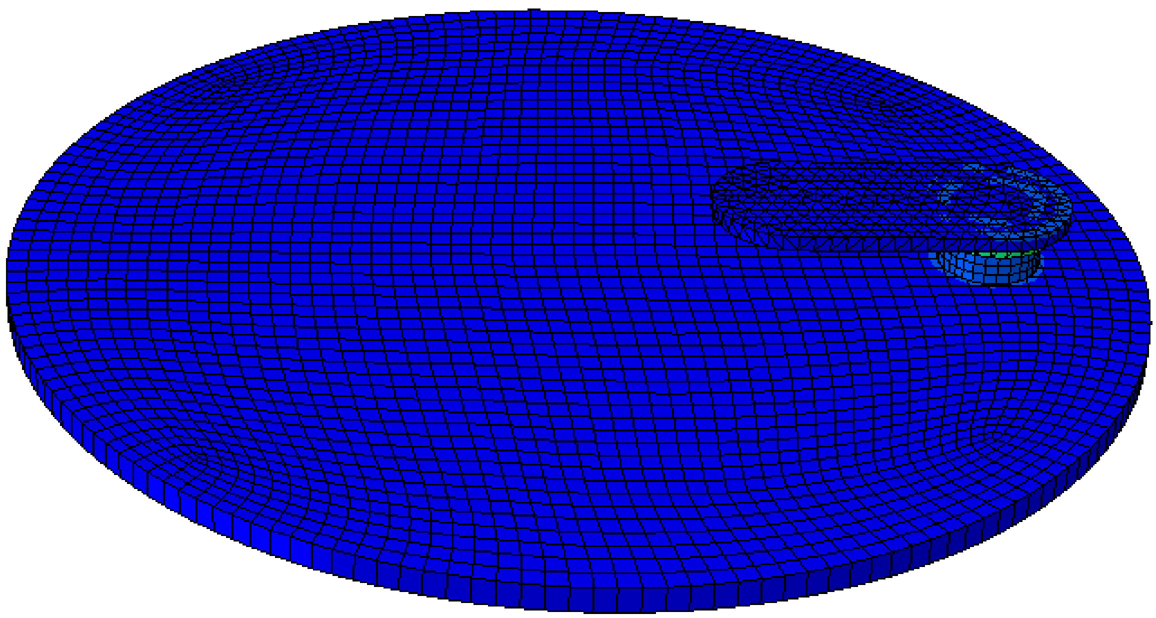

Figure 7-1 tribometer when pin is not co-centric to the disc

7.2.2. Further experiments

The obtained results for rubber against glass allow comprehending rubber surface effects in a better manner. Therefore, rubber samples with different surface roughness grits can be provided and examined against glass in order to achieve a better understanding of the adhesion between rubber and the disc. Although similar experiments have been performed by other researchers, it can nevertheless show more aspects of the rubber adhesion.

7.2.3. Rubber friction modelling

In this study friction coefficients were represented as a function of contact pressure and velocity; in these models contact pressure was calculated by dividing the normal load over the contact area. Although the changes in contact area were negligible, there were researchers who showed the expansion of different rubber samples during loading and these contact pressure modelling can be replaced in the proposed models.

7.2.4. FE tyre model future work

In this research, only a tyre in cornering was simulated and the results were compared, though full braking is important in tyre behaviour, and the effect of the friction models on braking can be observed and simulated. For this purpose the braking force of the tyre has to be measured against the slip ratio and the outcome can be compared to constant friction coefficient models.

8. References

1. Dictionary, C., *Cambridge Advanced Learner's Dictionary*. 2008, PONS-Worterbucher, Klett Ernst Verlag GmbH.
2. Andrzejewski, R. and J. Awrejcewicz, *Nonlinear dynamics of a wheeled vehicle*. Vol. 10. 2006: Springer Science & Business Media.
3. Bowden, F.P. and D. Tabor, *Friction: an introduction to tribology*. 1973: RE Krieger Publishing Company.
4. Gohar, R. and H. Rahnejat, *Fundamentals of tribology*. 2012: World Scientific.
5. Salomon, G., *Application of systems thinking to tribology.* ASLE TRANSACTIONS, 1974. **17**(4): p. 295-299.
6. van Geffen, V., *A study of friction models and friction compensation.* DCT, 2009. **118**: p. 24.
7. Rajapakshe, M., M. Gunaratne, and A. Kaw, *Evaluation of LuGre Tire Friction Model With Measured Data on Multiple Pavement Surfaces.* Tire Science and Technology, 2010. **38**(3): p. 213-227.
8. Korunović, N., M. Trajanović, and M. Stojković, *Finite element model for steady-state rolling tire analysis.* Journal of the Serbian Society for Computational Mechanics/Vol, 2007. **1**(1): p. 63-79.
9. Dorsch, V., A. Becker, and L. Vossen, *Enhanced rubber friction model for finite element simulations of rolling tyres.* Plastics, rubber and composites, 2002. **31**(10): p. 458-464.
10. Blau, P.J., *Friction Science and Technology: From Concepts to Applications, Second Edition*. 2008: CRC Press.
11. Bhushan, B., *Introduction to tribology*. 2013: John Wiley & Sons.
12. Moore, D. and W. Geyer, *A review of adhesion theories for elastomers.* Wear, 1972. **22**(2): p. 113-141.
13. Van Der Steen, R., I. Lopez, and H. Nijmeijer, *Experimental and numerical study of friction and. giffness characteristics of small rolling tires.* Tire Science and Technology, 2011. **39**(1): p. 5-19.
14. Schallamach, A., *The velocity and temperature dependence of rubber friction.* Proceedings of the Physical Society. Section B, 1953. **66**(5): p. 386.
15. Roth, F.L., R.L. Driscoll, and W.L. Holt, *Frictional properties of rubber.* Rubber Chemistry and Technology, 1943. **16**(1): p. 155-177.

16. Denny, D., *The influence of load and surface roughness on the friction of rubber-like materials.* Proceedings of the Physical Society. Section B, 1953. **66**(9): p. 721.
17. Bauer, K., D. Garbe, and H. Surburg, *Ullmann's encyclopedia of industrial chemistry.* Ullmann's Encyclopedia of Industrial Chemistry, 1988. **11**.
18. Clark, S.K., *Mechanics of pneumatic tires*. 1981: US Department of Transportation, National Highway Traffic Safety Administration.
19. Grosch, K. *The relation between the friction and visco-elastic properties of rubber*. in *Proceedings of the Royal Society of London A: Mathematical, Physical and Engineering Sciences*. 1963. The Royal Society.
20. Williams, M.L., R.F. Landel, and J.D. Ferry, *The temperature dependence of relaxation mechanisms in amorphous polymers and other glass-forming liquids.* Journal of the American Chemical society, 1955. **77**(14): p. 3701-3707.
21. Gabriel, P., *Investigation and modelling of rubber friction*. 2010.
22. Roberts, A., *Theories of dry rubber friction.* Tribology International, 1976. **9**(2): p. 75-81.
23. Schallamach, A., *How does rubber slide?* Wear, 1971. **17**(4): p. 301-312.
24. Bartenev, G. and A. El'Kin, *Friction properties of high elastic materials.* Wear, 1965. **8**(1): p. 8-21.
25. Savkoor, A., *Dry adhesive friction of elastomers*. 1987, Dissertation, Delft University of Technology.
26. Bulgin, D., M. Walters, and G. Hubbard, *Road and laboratory studies of friction of elastomers*. 1962.
27. Ludema, K. and D. Tabor, *The friction and visco-elastic properties of polymeric solids.* Wear, 1966. **9**(5): p. 329-348.
28. Roberts, A. and A. Thomas, *The adhesion and friction of smooth rubber surfaces.* Wear, 1975. **33**(1): p. 45-64.
29. Briggs, G. and B. Briscoe, *How rubber grips and slips Schallamach waves and the friction of elastomers.* Philosophical Magazine A, 1978. **38**(4): p. 387-399.
30. Greenwood, J. and D. Tabor, *The friction of hard sliders on lubricated rubber: the importance of deformation losses.* Proceedings of the Physical Society, 1958. **71**(6): p. 989.
31. Denny, D., *Time effects in the static friction of lubricated rubber.* Wear, 1959. **2**(4): p. 264-272.

32. Moore, D.F., *The friction and lubrication of elastomers*. Vol. 9. 1972: Pergamon.
33. Roberts, A., *Looking at rubber adhesion.* Rubber Chemistry and Technology, 1979. **52**(1): p. 23-42.
34. Wu-Bavouzet, F., et al., *Stick-slip: wet versus dry.* The Journal of Adhesion, 2007. **83**(8): p. 761-784.
35. Thirion, P., *Les coefficients d'adherence du caoutchouc*. 1946.
36. Schallamach, A., *The load dependence of rubber friction.* Proceedings of the Physical Society. Section B, 1952. **65**(9): p. 657.
37. Schallamach, A., *A theory of dynamic rubber friction.* Wear, 1963. **6**(5): p. 375-382.
38. Barquins, M., *Adherence, friction and wear of rubber-like materials.* Wear, 1992. **158**(1): p. 87-117.
39. Briggs, G. and B. Briscoe, *The dissipation of energy in the friction of rubber.* Wear, 1975. **35**(2): p. 357-364.
40. Persson, B., *Theory and simulation of sliding friction.* Physical review letters, 1993. **71**(8): p. 1212.
41. Roberts, A.D., *New rubber friction testing machine.* Rubber World, 1994. **209**(4): p. 16-18.
42. Pfalzner, P., *On the friction of various synthetic and natural rubbers on ice.* Canadian Journal of Research, 1950. **28**(12): p. 468-489.
43. Hample, W., *Friction Study of Aircraft Tire Material on Concrete.* 1955.
44. Bowden, F. and D. Tabor, *Action of extreme pressure lubricants.* The Friction and Lubrication of Solids, Oxford Classic Texts in the Physical Sciences, Oxford Classic Series, New York, 2001: p. 228-246.
45. Yap, T., et al., *Friction Performance Analysis of Waste Tire Rubber Powder Reinforced Polypropylene Using Pin-On-Disk Tribometer.* Procedia Engineering, 2013. **68**: p. 743-749.
46. Xu, F., K.-i. Yoshimura, and H. Mizuta, *Experimental Study on Friction Properties of Rubber Material: Influence of Surface Roughness on Sliding Friction.* Procedia Engineering, 2013. **68**: p. 19-23.
47. Mofidi, M., et al., *Rubber friction on (apparently) smooth lubricated surfaces.* Journal of Physics: Condensed Matter, 2008. **20**(8): p. 085223.
48. Johnson, K.L. and K.L. Johnson, *Contact mechanics*. 1987: Cambridge university press.

49. Bo, L.C. and D. Pavelescu, *The friction-speed relation and its influence on the critical velocity of stick-slip motion.* Wear, 1982. **82**(3): p. 277-289.
50. Pinnington, R., *Rubber friction on rough and smooth surfaces.* Wear, 2009. **267**(9): p. 1653-1664.
51. Park, K.-S., et al., *An improved friction model and its implications for the slip, the frictional energy, and the cornering force and moment of tires.* Journal of mechanical science and technology, 2006. **20**(9): p. 1399-1409.
52. Manual, A.U., *Version 6.13-2.* Dassault Systémes Simulia Corp., Providence, Rhode Island, USA, 2013.
53. Huemer, T., et al., *A 3D finite element formulation describing the frictional behavior of rubber on ice and concrete surfaces.* Engineering Computations, 2001. **18**(3/4): p. 417-437.
54. Heinrich, G. and M. Klüppel, *Rubber friction, tread deformation and tire traction.* Wear, 2008. **265**(7): p. 1052-1060.
55. Wriggers, P. and J. Reinelt, *Multi-scale approach for frictional contact of elastomers on rough rigid surfaces.* Computer Methods in Applied Mechanics and Engineering, 2009. **198**(21-26): p. 1996-2008.
56. Persson, B.N., *Theory of rubber friction and contact mechanics.* The Journal of Chemical Physics, 2001. **115**(8): p. 3840-3861.
57. Persson, B.N., *Rubber friction: role of the flash temperature.* Journal of Physics: Condensed Matter, 2006. **18**(32): p. 7789.
58. Persson, B., et al., *On the nature of surface roughness with application to contact mechanics, sealing, rubber friction and adhesion.* Journal of Physics: Condensed Matter, 2005. **17**(1): p. R1.
59. Bielsa, J.M., et al., *Application of finite element simulations for data reduction of experimental friction tests on rubber–metal contacts.* Tribology International, 2010. **43**(4): p. 785-795.
60. Gent, A. and T. Walter, *The pneumatic tire national highway traffic safety administration [R].* Washington DC: US Department of Transportation, 2005.
61. Kummer, H. and W.E. Meyer, *Rubber and tire friction*. 1960, DTIC Document.
62. Pacejka, H.B., *Chapter 4 - Semi-empirical tyre models*, in *Tyre and Vehicle Dynamics (Second Edition)*, H.B. Pacejka, Editor. 2006, Butterworth-Heinemann: Oxford. p. 156-215.

63. Germann, S. and A. Daiß. *Monitoring of the friction coefficient between tyre and road surface*. in *Control Applications, 1994., Proceedings of the Third IEEE Conference on*. 1994. IEEE.
64. Burckhardt, M., *Fahrwerktechnik: Radschlupf-Regelsysteme.* Vogel-Verlag, Germany, 1993: p. 16.
65. Kiencke, U. and A. Daiss, *Estimation of tyre friction for enhanced ABS-systems.* JSAE Review, 1995. **16**(2): p. 221-221.
66. Canudas-de-Wit, C., et al., *Dynamic friction models for road/tire longitudinal interaction.* Vehicle System Dynamics, 2003. **39**(3): p. 189-226.
67. Gustafsson, F., *Slip-based tire-road friction estimation.* Automatica, 1997. **33**(6): p. 1087-1099.
68. Aguilar-Martínez, J. and L. Alvarez-Icaza, *Analysis of tire-road contact area in a control oriented test bed for dynamic friction models.* Journal of Applied Research and Technology, 2015. **13**(4): p. 461-471.
69. Castillo, J., et al., *An optical tire contact pressure test bench.* Vehicle System Dynamics, 2006. **44**(3): p. 207-221.
70. Bird, K. and J. Martin, *The calspan tire research facility: design, development, and initial test results*. 1973, SAE Technical Paper.
71. Ginn, J.L. and R. Marlowe, *Road contact forces of truck tires as measured in the laboratory*. 1967, SAE Technical Paper.
72. Hays, D., *The physics of tire traction: theory and experiment*. 2013: Springer Science & Business Media.
73. United, S., et al., *Mechanisms of Solid Friction. Edited by P.J. Bryant and M. Lavik ... and G. Salomon. (Conference on the Fundamental Mechanisms of Solid Friction held at Midwest Research Institute, Kansas City, on September 16, 17 and 18, 1963, sponsored by the Air Force Materials Laboratory, Research and Technology Division.) [With illustrations.]*. 1964, Amsterdam: Elsevier Publishing Co.
74. Pérez, A.T., et al., *A model of friction for a pin-on-disc configuration with imposed pin rotation.* Mechanism and Machine Theory, 2011. **46**(11): p. 1755-1772.
75. Standard, A., *Standard Test Method for Wear Testing with a Pin-on-Disk Apparatus.* Annual Book of ASTM Standards, G99-05, 2000. **3**.
76. Futek

Operating Manual-Futek Rotary Torque Sensors TRD, TRH & TRS Series.

77. Hertz, H., *Über das Gleichgewicht schwimmender elastischer Platten.* Annalen der Physik, 1884. **258**(7): p. 449-455.
78. Derjaguin, B.V., V.M. Muller, and Y.P. Toporov, *Effect of contact deformations on the adhesion of particles.* Journal of Colloid and interface science, 1975. **53**(2): p. 314-326.
79. Maegawa, S., F. Itoigawa, and T. Nakamura, *A role of friction-induced torque in sliding friction of rubber materials.* Tribology International, 2016. **93**: p. 182-189.
80. Hutchings, I. and P. Shipway, *Tribology: friction and wear of engineering materials*. 2017: Butterworth-Heinemann.
81. Archard, J. *Elastic deformation and the laws of friction*. in *Proceedings of the Royal Society of London A: Mathematical, Physical and Engineering Sciences*. 1957. The Royal Society.
82. Le Gal, A. and M. Klüppel, *Investigation and modelling of rubber stationary friction on rough surfaces.* Journal of Physics: Condensed Matter, 2007. **20**(1): p. 015007.
83. Olatunbosun, O. and O. Bolarinwa, *FE simulation of the effect of tire design parameters on lateral forces and moments.* Tire science and Technology, 2004. **32**(3): p. 146-163.
84. Wei, C. and O.A. Olatunbosun, *Transient dynamic behaviour of finite element tire traversing obstacles with different heights.* Journal of Terramechanics, 2014. **56**(Supplement C): p. 1-16.
85. Vorotović, G.S., et al., *Determination of cornering stiffness through integration of a mathematical model and real vehicle exploitation parameters.* FME Transactions, 2013. **41**(1): p. 66-71.
86. Gillespie, T.D., *Fundamentals of Vehicle Dynamics. Warrendale PA: SAE*. 1992, Inc.